ENANTIOMERIC SEPARATIONS BY HPLC: TEMPERATURE, MOBILE PHASE, FLOW RATE AND RETENTION MECHANISM STUDIES

by

Robert Cragg Klute

Dissertation submitted to the Faculty of the
Virginia Polytechnic Institute and State University
in partial fulfillment of the requirements for the degree of

DOCTOR OF PHILOSOPHY

in

CHEMISTRY

APPROVED:

Harold M. McNair, Chairman

Mark R. Anderson

Neal Castagnoli

Gary L. Long

Joseph Merola

March, 1993

Blacksburg, Virginia

LD
5655
V856
1993
K588
c.2

c.2

ENANTIOMERIC SEPARATIONS BY HPLC: TEMPERATURE, MOBILE PHASE, FLOW RATE AND RETENTION MECHANISM STUDIES

by

Robert Cragg Klute

Committee Chairman: Harold M. McNair
Chemistry

(ABSTRACT)

The effects of changes in temperature, mobile phase composition, flow rate, and stationary phase upon the enantiomeric separation of several racemic mixtures are investigated. The changes in capacity factor (k'), selectivity (α), and efficiency (N) and enantiomeric resolution (R), are explored. Resolution is then shown to be controlled by the specific combination of chiral stationary phase (CSP), solute, mobile phase and temperature.

The key to optimizing chiral resolution lies in understanding the retention mechanism(s) for a given CSP. The proposed retention mechanisms for the two CSPs used in the optimization studies are evaluated using chromatographic/thermodynamic data. Inferences are made which support the well-characterized "Pirkle"-type R-dinitrobenzoylphenylglycine retention mechanism, which depends solely on attractive-repulsive interactions to establish two diasteriomeric complexes having unequal internal energy, and therefore eluting at different times from the chromatographic system. For comparison, a more complicated CSP composed of a tris cellulose(3,5-dimethylphenylcarbamate) coated to a silica gel support is also examined. For this CSP

the proposed mechanisms, which include both attractive-repulsive interactions and inclusion complex types, are evaluated according to the chromatographic optimization data, and compared to similar data for the single-mechanism "Pirkle" CSP.

In contrast to the above"macromolecular"-level inferences about retention mechanisms drawn from chromatographic data, a second study was initiated using a model CSP attached to a 1000-Å gold surface, with Fourier-Transform Infrared Spectrometry in a Reflectance-Absorbance mode, to probe the specific molecular interactions which make possible the diasteriomeric complex. This *in situ* experiment, in contrast to previous *ex situ*, stationary phase work, is designed to show that hydrogen bonding is, as predicted, a principal force holding the complexes together, and that a measurable difference exists between the weaker R-trifluoroanthrylethanol (TFAE) and the stronger S-TFAE complexes due to their different stereo-geometry.

A further experiment to characterize the difference in mechanisms between the "Pirkle" and cellulose CSPs involves relating their chromatographic retention behavior to their structure, known as Qualitative Structure Retention Relationships (QSRR). Some structure-specific physical-organic chemistry parameters are determined using an EPA-developed computer program and correlations are made between retention on a given CSP and some of the parameters.

ACKNOWLEDGMENTS

I wish to thank Dr. Harold McNair and all past and present members of our research group for their understanding, help and encouragement. Dr. Mark Anderson and his group were valuable in helping me complete the difficult surface chemistry involved in the model stationary phase work. Former McNair group members, including Doctors. Vince Remcho, Chris Palmer, Lisa Goebel, and Henrik Rasmussen provided a wealth of scientific motivation and knowledge not available in any textbook. Present group member Maha Khaled was always ready to make time to hear problems or ideas. Undergraduate Britt Langston was very helpful in spending many afternoons helping me finish the temperature studies. Dr Mike Henry of the J. T. Baker company and a former group member was extremely generous in donating the many expensive chiral columns used in this research. The entire graduate school experience would not have been possible without the backing of my wife Carol, her parents and my own father. Their irrepressible encouragement and support has been wonderful. Finally, I owe my basic chemistry education and interest in chemical research to Mr. Ivan Whitesel, chemistry teacher at Richmond Senior High School, Richmond, Indiana.

TABLE OF CONTENTS

Abstract			ii
Acknowledgements			iv
Table of Contents			v
List of Figures			viii
List of Tables			ix
Chapter	I.	Introduction	1
1.1		Importance of Chirality	1
1.2		Research Objectives	5
1.3		Initial Optimization Studies	7
1.4		Sub-Zero Optimization Studies	13
1.5		Mobile Phase Studies	14
1.6		Retention Mechanism Studies	16
1.7		Summary	18
Chapter	II.	Historical	19
2.1		Early Attempts At Chromatographic Chiral Resolution	19
2.2		Non-Chromatographic Methods	21
2.3		Indirect Chromatographic Methods	23
2.4		Direct Chromatographic Methods, (CSPs)	26
2.5		Previous Optimization Research: Temperature, Flow rate	

	and Mobile Phase Effects	39	
2.6	Chiral Retention Mechanism Studies	55	
Chapter	III. Theory		62
3.1	Diasteriomeric Complex Formation	62	
3.2	Generalized Chiral Separation	76	
3.3	Role of Temperature	77	
3.4	Other Theoretical Method Optimization Considerations	82	
3.5	Specific Mechanisms Suggested for DNBPG and Cellulose CSPs	87	
3.6	Model Stationary Phase Studies via Self-Assembled Monolayers	94	
	3.6.1 Self-Assembled Monolayer Theory	94	
	3.6.2 Summary of Organic Reactions	99	
	3.6.3 FTIR-Reflectance Absorbance (IRRAS)	100	
	3.6.4 FTIR-Polarization Modulation (PM-IRRAS)	102	
Chapter	IV. Experimental		105
4.1	Early Optimization Studies	105	
4.2	Sub-Zero Optimization Studies	112	
4.3	Mobile Phase Studies	114	
4.4	Model CSP Experiments	117	
	4.4.1 Substrate Material and Surface Preparation	117	
	4.4.2 Liquid Phase Reactions	118	
	4.4.3 Vapor Phase Reactions	119	
	4.4.4 Analytical Procedures	122	
	4.4.5 Spectroscopic and Other Analytical Techniques	123	

Chapter V. Results and Discussion 137

5.1 Initial Optimization Studies 137

5.1.1 TFAE on DNBPG 137

5.1.2 TFAE and t-Stilbene Oxide on Chiralcel OD 145

5.2 Sub-Zero Optimization Studies 162

5.3 Mobile Phase and Solute Studies 175

5.3.1 Mobile Phase Study Background 175

5.3.2 Alcohol Mobile Phase Studies 176

5.4 Quantitative Structure Retention Relationships 186

5.5 Application Studies 191

5.5.1 Acetylacetamide Cinnamic Acid Methyl Ester 191

5.5.2 4-Fluoroglutamic Acid 194

5.6 Model Stationary Phase Modification of a Gold Surface 197

Chapter VI. Conclusions 203

Literature Citations 205

Vita 215

LIST OF FIGURES

Figure 1	(R)-3,5-dinitrobenzoylphenylglycine (DNBPG)	10
Figure 2	Cellulose tris(3,5-dimethylphenylcarbamate) (Chiralcel OD)	10
Figure 3	2,2,2-trifluoro-1(9-anthryl)ethanol (TFAE)	11
Figure 4	Trans-stilbene oxide (t-stil.)	11
Figure 5	Interactions between DNBPG and a chiral analyte	30
Figure 6	Structure of cellulose	33
Figure 7a	Seven-membered glucopyranose ring of β-cyclodextran	36
Figure 7b	Individual glucopyranose unit	36
Figure 8	Categories of chirality	63
Figure 9	Three point interaction between CSP and two enantiomers	65
Figure 10	Charge transfer interactions	68
Figure 11	Three examples of chiral interactions	69
Figure 12	Basic adsorption-desorption equilibria	79
Figure 13	Effects of temperature on selectivity	80
Figure 14	Diasteriomeric complex between (R)-DNBPG and (R)-TFAE	91
Figure 15	Diasteriomeric complex between (R)-DNBPG and (S)-TFAE	92
Figure 16	Potential energy curves for physisorption and chemisorption	98
Figure 17	Diagram of the PM-IRRAS experiment	104
Figure 18	Optical setup for polarization modulation FTIR experiment	126
Figure 19	Configuration for the PM-IRRAS measurements of (R) and (S)-TFAE model CSP complexes	127

Figure 20	Initial three steps of the first synthetic strategy using monomethoxysilane	129
Figure 21	Alternative synthetic scheme with 4-ATP	130
Figure 22	Combined vapor phase and evacuated liquid phase synthesis	131
Figure 23	Synthetic steps to prepare disulfide-linked BOC-valine	132
Figure 24	Vapor phase vacuum manifold and reaction flask	133
Figure 25	HPLC apparatus with temperature control equipment	134
Figure 26	Mobile phase temperature-measuring apparatus	135
Figure 27	Heat exchanger used to pre-condition mobile phase temperature	136
Figure 28	Van't Hoff plot for TFAE on DNBPG	140
Figure 29	Selectivity vs.Temperature: TFAE on DNBPG	141
Figure 30	Plate Height vs. Temperature for three flow rates	142
Figure 31	Plate Height vs Flow rate: TFAE on DNBPG	143
Figure 32	Resolution vs. Temperature for seven flow rates	144
Figure 33	Representative chromatograms using DNBPG and OD columns	150
Figure 34	Van't Hoff plot for TFAE and trans-stilbene separated on Chiralcel OD, entropy and enthalpy controlled conditions	151
Figure 35	HETP vs. Flow rate for R & S-TFAE on Chiralcel OD	152
Figure 36	HETP vs. Flow rate for trans-stilbene oxide on Chiralcel OD	153
Figure 37	Selectivity vs. Temperature for three CSP-solute combinations	157
Figure 38	Resolution vs. Temperature: TFAE on OD	158
Figure 39	Resolution vs. Temperature: trans-stilbene on OD	159
Figure 40	Van't Hoff plot for trans-stilbene and TFAE on OD, 20% IPA	163
Figure 41	Van't Hoff plot for TFAE on DNBPG	164
Figure 42	Reduced Plate Height vs. Temperature, 20% IPA	168

Figure 43	Selectivity vs. Temperature, 20% IPA	169
Figure 44	Selectivity vs. Temperature, TFAE on DNBPG, 20% IPA	170
Figure 45	Resolution vs. Temperature, 20% IPA	171
Figure 46	Resolution vs. Temperature, TFAE on DNBPG, 20% IPA	172
Figure 47	Variation in capacity factors with different lots of IPA	179
Figure 48	Resolution vs. % Water in dried mobile phase	180
Figure 49	Resolution vs % IPA, TFAE on Chiralcel OD	181
Figure 50	R-Propranolol and AACA-ME solute structures	182
Figure 51	Capacity factor vs. % IPA for solutes on OD	183
Figure 52	Plate height vs. % IPA for solutes on OD	184
Figure 53	Resolution vs. % IPA for solutes on OD	185
Figure 54	Logarithm Capacity factor vs. % IPA for solutes on OD	188
Figure 55	Taft-Kamlett Alpha vs. Slope	190
Figure 56	AACA-ME on Chiralcel OD with and without acetonitrile	193
Figure 57	Separations of D-erythro and L-threo-4-fluoroglutamic acid	195
Figure 58	Separation of D-erythro-4-fluoroglutamic acid	196
Figure 59	Experimental design for model CSP experiment	199
Figure 60	IRRAS spectrum of the 11-mercaptoundecanoic acid-modified gold surface	200
Figure 61	IRRAS spectrum of gold surface modified with (BOC)-L-Valine	201

LIST OF TABLES

Table	I	Market share of popular chiral drugs	2
Table	II	CSP classes and chiral selectors	27
Table	III	Type II CSPs, trade name, selector group, compounds	34
Table	IV	Typical mobile phases for various CSP types	54
Table	V	Molecular interaction types and a representative functional group	67
Table	VI	Summary of molecular interactions in forming diasteriomeric complexes	75
Table	VII	Interactions between atoms for the (R)-DNBPG complexes with (R) and (S)-TFAE.	93
Table	VIII	Simple Quattro spreadsheet program	110
Table	IX	Solute and CSP physical properties	146
Table	X(a)	Summary of measured parameters at 1.0 ml/min flow rate for the DNBPG column with TFAE as solute	160
Table	X(b)	Summary of measured parameters at 1.0 ml/min flow rate for the OD column	161
Table	XI	Thermodynamic quantities for chromatographic separations	174
Table	XII	Summary of the experimentally determined slope values for ln k' vs. %IPA	189

CHAPTER 1

INTRODUCTION

1.1 Importance of Chirality

The separation of racemic mixtures is important in several branches of chemistry including organic and inorganic synthesis, biochemistry and medicinal chemistry. Biologically active molecules and metabolites are common. Since most biological systems are chiral [1,2,3] the bioactivity, potency, toxicity and pharmacokinetics of each enantiomer in the racemic mixture may be different, possibly resulting in the need to determine the above characteristics for each enantiomer separately. In June of 1992 the Food and Drug Administration (FDA) issued guidelines which continued to allow the development of chiral drugs, but "rigorous"[4] justification is required for racemates. Accordingly, more effort is being made by pharmaceutical houses to develop enantiomers by means of either asymmetric syntheses or post-reaction preparative scale chiral separations. For both approaches, improved analytical methods are needed, especially for trace amounts of chiral metabolites in complex biological matrices.

The economic importance of the chiral drug market has been estimated at $18 billion[5] for 15 popular pharmaceuticals. Another 76 racemic drugs have potential for production as enantiomers, which could have regulatory and marketing benefits. As noted above, extra testing may be required for racemic mixtures, increasing R & D costs, and there is a perception that enantiomers could be marketed as higher value products because of their higher "purity". Table I gives some estimates of the market share for these 15 popular drugs. An estimated 25% of all popular drugs are racemic mixtures.[6] If one of the enantiomers is not bioactive, then the

Table I. Market share of 15 popular chiral drugs. [a]

Drug	1990 Sales, Millions of Dollars
Chiral antibiotics	$6,360
Captopril	1,501
Enalapril	1,482
Lovastatin	751
Diltiazem	746
Cefadroxil	690
Naproxen	686
Lisinopril	430
Timolol	297
Deprenyl	141
Methyldopa	140
Dexfenfluramine	52
Ethambutol	45
Transdermal nicotine	5
Sertraline	3
Other	4,630
TOTAL	**$18,000**

[a] Adapted from reference 4.

drug's efficacy can be improved by removing the inactive isomer. In the worst case, one of the enantiomers may prove biologically harmful, necessitating full scale pharmacological and toxicological studies on both enantiomers. The drug Thalidomide (a racemic mixture of R-(+) and S-(-) -isomers of *n*-phthalylglutamic acid), a sedative, was marketed in the early 1960's in Europe with the knowledge that only the R-(+)-isomer was bioactive. It was eventually determined, after many births of malformed infants, that indeed the S-(-)-isomer was teratogenic[7].

Current methods of enantiomeric analysis include such non-chromatographic approaches as polarimetry, nuclear magnetic resonance with chiral shift reagents, circular dichroism, X-ray crystallography, isotope dilution techniques, differential scanning calorimetry, classic stereospecific organic reactions, and enzymatic assays[8]. The disadvantages of all these techniques are their relative slowness and the need for pure samples. A typical analytical problem involves the need to separate as well as quantitate both the amount of a given compound, and sometimes the exact optical rotation. Both gas chromatography (GC), and high performance liquid chromatography (HPLC) provide fast and accurate methods for separating mixtures and allow on-line detection and quantitation of both mass (and optical rotation for HPLC) if appropriate detection devices are used.

Chiral HPLC methods are either direct, involving some sort of enantiomer functional group attached to the stationary phase, or indirect, relying upon a chiral mobile phase additive and an achiral stationary phase [9]. Whichever technique is used, HPLC is more versatile than GC due to its ability to separate the vast number of low volatility compounds in the pharmaceutical, environmental, food science and synthetic organic fields, to mention just a few areas. Direct chromatographic techniques, using a chiral stationary phase (CSP), are widely available commercially utilizing many CSPs, and are interesting mechanistically. The direct approach, using CSPs, will be the subject of this dissertation.

Although convenient to use for a variety of separations, choosing a CSP and achieving a successful separation quickly is still not a trivial task. At least five major types of CSPs are currently commercially available, all relying on different mechanisms to achieve stereoselectivity[10,11,12]. There is not a universal, or even near-universal CSP in existence at this time, and the variety of separation mechanisms challenges the chromatographer when called upon to make a choice for a particular separation. If the wrong choice is made, and no amount of method optimization can achieve enantioselectivity, an expensive and time-consuming mistake has been made. Educated guesses can be made based on solute and CSP structure and application guides, but frequently several columns will have to be tried.

The key to successful selection and method optimization of a chiral stationary phase lies in an understanding of the applicable stereoselective retention mechanism. Two other major factors in addition to the chosen CSP, the mobile phase and solute structure, interact with the CSP to achieve enantiomeric separation[13]. It is important to keep in mind all three components of the overall adsorption-desorption[14] mechanism when developing a chiral separation method. In much of the early literature, novel CSPs were synthesized, with usually a specific application in mind, but little attention was paid to understanding the stereoselective mechanism for that CSP. The traditional chromatographic optimization parameters such as mobile phase, flow rate and temperature have also not received as much research effort as a chromatographer would prefer, again because much of the early work has been driven by applications needs and/or creative synthetic chemists who design new CSPs first, then find applications.

Problems currently include both the lack of column selection strategies, and the mediocre understanding and utilization of chromatographic optimization strategies. There is also a need for improvements in detection methods, both in sensitivity and selectivity. Neither the universal CSP, nor the universal chiral detector now exists. To fulfill the ever more stringent FDA requirements for low level quantitation of optical metabolites, more research

must be done to detect and identify nano- and picogram levels. The current UV/visible detector provides no chiral information, and the most common detector that does, polarimeters designed for on-column HPLC work, lack the required sensitivity. Although this dissertation concentrates on the chromatographic optimization and retention mechanism questions, the need for continued development of detectors should be noted.

The reader is directed to several comprehensive reviews of chromatographic chiral separations, the most recent and perhaps best being Taylor and Maher's 1992 paper,[15] a shorter but succinct 1987 survey from Armstrong[16], a competent effort by Däppen, Arm and Meyer from 1986[17], which adopts a different CSP classification from that of Wainer and others. Finally, important for more historical than current reasons, reviews by Davankov, et al from 1983[18], dealing with mainly ligand exchange LC methods, and Lochmüller and Souter's 1975 review[19], which includes both LC and GC methods, are noteworthy. Finally, a review by the originator of the first commercially successful CSPs, s Pirkle, was published in 1989[20] and is notable for the many geometrically clear illustrations of the specific molecular interactions involved in each of the main classes of CSPs.

1.2 Research Objectives

The objectives of this dissertation are to first explore potential benefits of the common chromatographic optimization techniques of temperature, flow rate and mobile choices as applied to enantiomeric separations using chiral stationary phases in HPLC. Resolution depends on the optimization changes on the three parts of the chromatographic master resolution equation, an empirical relationship between capacity factor, enantiomeric selectivity and column efficacy. Using the data from optimization studies, the proposed retention mechanisms for two CSPs studied in depth will be evaluated. It will become clear that the

stationary phase-solute-mobile phase triad interacts in a complicated manner, sometimes difficult to predict from the mechanisms proposed. Optimum resolution depends on the interaction of temperature and flow rate with the CSP-solute-mobile phase triad, and optimum values are dependent on the specific retention mechanism. Mechanistic inferences can be drawn and compared with the proposed mechanism, but this approach has the limitation that chromatographic data is a time dependent thermodynamic and kinetic average of the diasteriomeric complex equilibria as the solute passes through the column.

The third goal of this research is to extend mechanistic exploration to the molecular level, utilizing a model CSP and stereoisomers of a common test probe to approximate interactions on an actual HPLC column, but in an environment that can be studied with Fourier Transform Infrared Spectroscopy and the Reflectance Absorbance technique (FTIR-RA). This experiment extends work, previously done in solution phase[21] (*ex situ*), and `is a logical, useful and important addition, serving as a method for the mechanistic study of HPLC stationary phases on a molecular, *in situ* level. All chromatographically derived data, such as the thermodynamically based capacity factor and hence selectivity, represent the adsorption-desorption equilibria average of many molecules as they travel through the column. The intermolecular forces which control these equilibria vary, making it difficult to study the contribution from each type of interaction, which vary depending on the particular class of CSP involved. By immobilizing a model CSP on a highly reflective gold surface, then bringing in contact solutions of both enantiomers, the specific intermolecular forces which hold together each of the diasteriomeric complexes are probed by comparing polarization-modulation FTIR (PM-FTIR) spectra of each enantiomer. The PM technique effectively cancels out contributions from molecules in the bulk (the solvent and other interfering species), allowing a higher sensitivity for the surface-bound model CSP-enantiomer complex.[22,23] The most important interaction which can be illuminated by the FTIR approach is hydrogen bonding differences between the complexes.

1.3 Initial Optimization Studies

The research leading to this dissertation has traveled a path from the simple to the complex. The initial experimental goal was to develop chromatographic optimization strategies for two contrasting types of chiral stationary phases and two contrasting racemic test probes. After reviewing the literature available in the fall of 1990, it was noted that basic studies dealing with chromatographic parameters such as temperature, flow rate and mobile phase composition were seldom researched. This lack of data led to a series of experiments to determine how the three components of the master resolution equation are affected by changes in the above parameters. Once these basic relationships have been understood, then logical optimization strategies can be designed.

The empirical resolution equation:

$$\mathbf{Rs = (k'/1+k')\ (\alpha\text{-}1/\alpha)\ (\sqrt{N}/4)} \qquad \{1\}$$

in which k' is the thermodynamically controlled capacity factor, α is the selectivity (ratio of the capacity factor of the second eluting peak relative to the first), and N is the kinetically controlled column efficiency factor representing the number of transitions made by a solute molecule between mobile and stationary phase.

It is obvious from this equation that temperature will affect all three of these factors, thereby changing the resolution. For an enantiomeric separation, selectivity is more properly enantioselectivity, and is of primary importance. Decreasing temperature will have positive effects on the thermodynamically controlled terms (positive in the sense of improved

resolution), and a negative effect on column efficiency due to the increased viscosity of the mobile phase, which slows down the rate of adsorption-desorption of the solute. Therefore it is important to evaluate the total impact of lowered temperature on resolution, since at some temperature the gain in thermodynamic factors will be negated by the decrease in the kinetic factor, efficiency.

When these studies were begun, comparatively few researchers had looked at temperature effects. Mazzo [24](1986), Taylor[25] (1988), Weaner[26] (1986), Caude[27] (1986), and Macudiere[28](1986) have done some work in this area, but these studies are limited in terms of CSP types, mobile phase, and temperature ranges explored, as well as the extent of data evaluation. Frequently only selectivity was calculated, ignoring the contributions from efficiency changes. The consensus among these researchers was that lowering temperature results in increased selectivity. Even less had been published on the effects of mobile phase and flow rate effects for specific CSPs.

Mechanistic studies have also been rare in the 1980's literature. The key to CSP selection and method optimization is a complete understanding of the enantioselective retention mechanism for the stationary phase in question. Because mechanisms differ depending on the chiral selector chemistry in each of the six classes of CSPs, this problem is more complex than that of achiral HPLC. Research must be done on each of the different types of CSP. Traditionally, studies have centered on either the organic chemistry necessary to create a new chiral selector, or have been application driven. Retention mechanism and theoretical chromatographic evaluations have drawn less interest from researchers

Overall, there is a need for better integration of the mechanistic work with the chromatographic optimization studies, for they are intimately connected. Pirkle, a synthetic organic chemist at the University of Illinois has been a leader in developing brush-type[29] chiral stationary phases, featuring a simple chain with one or two chiral centers attached to a silica backbone and oriented outwards from the silica backbone. His research comes closest to

successfully combining both mechanistic and chromatographic considerations, beginning with a logical, "rational" design of functional groups selected for specific interactions with certain classes of solutes[30, 31]. In later work, Pirkle and Welch included the other member of the mechanistic triad, mobile phase in an effort to arrive at a comprehensive analysis of the adsorption-desorption equilibria.[32]

The central problem of current chiral HPLC then is mechanism elucidation and its import for method optimization. Much of the research to date, as in other fields of science, is reminiscent of the blind men and the elephant. Each study is partly correct, but few if any can shed light on the total problem.

To gain insight into the proposed mechanisms for the two CSPs used in the initial optimization, inferences are drawn from plots of the three components of the master resolution equation versus temperature and flow rate. This is one step removed from a simple application of the results to method development problems. These mechanistic inferences must be tempered with the understanding that they arise from molecular behavior averaged over time, and that individual molecules might vary widely from the average behavior.

A comparison between results from the well-characterized single mechanism, Pirkle brush-type dinitrobenzoylphenylglycine (DNBPG, Figure 1) and a tris cellulose(3,5-dimethylphenylcarbamate) (Chiralcel OD, Figure 2), postulated to have multiple mechanisms possible, was undertaken using data from these optimization studies. Contrasting solutes were also used, having markedly differing degrees of hydrogen donating ability. The 2,2,2-trifluoro-1(9-anthryl)ethanol (TFAE, Figure 3) can easily hydrogen bound to a CSP, whereas trans-stilbene oxide (t-stil., Figure 4) has no protons to donate. Because of this lack of acidic

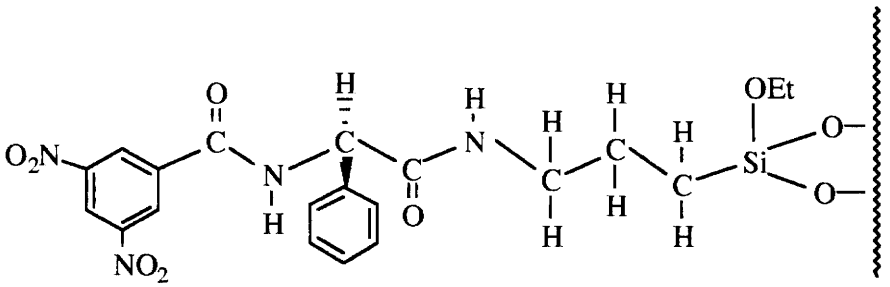

Figure 1. (R)-3,5-dinitrobenzoylphenylglycine (DNBPG)

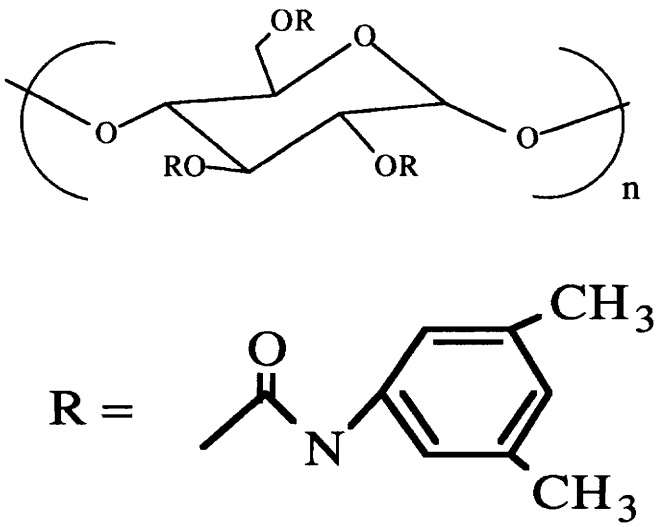

Figure 2 Cellulose tris(3,5-dimethylphenylcarbamate) (Chiralcel OD)

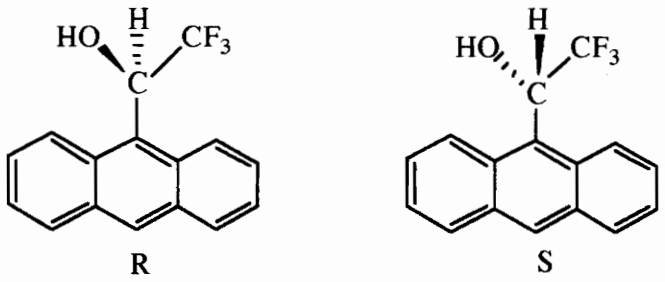

Figure 3. 2,2,2-trifluoro-1(9-anthryl)ethanol (TFAE)

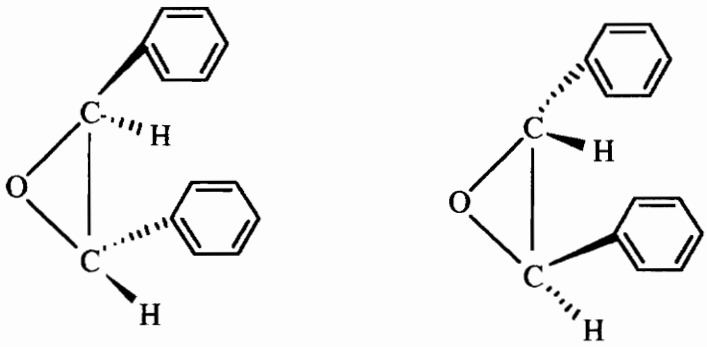

Figure 4. Trans-stilbene oxide (t-stil.)

In all temperature studies, the accuracy of calculated chromatographic parameters such as capacity factor and efficiency depend on consistent, even temperature control of the chromatographic apparatus. Increasingly more sophisticated temperature control measures were undertaken as the research progressed. Beginning with a simple ice water bath for just the HPLC column, the apparatus was improved through the addition of a circulating, cooling bath and a column jacket. In the latter experiments, a heat exchanger was added to pre-cool the mobile phase before the flow reached the column. All tubing downstream of the heat exchanger entrance, including the injector valve, was insulted with foam rubber and aluminum foil.

The range of temperatures initially explored was 25 to 3.3°C, the latter non-integer being the lowest temperature attained by the ice bath. For consistency, the first sets of data generated using the circulating bath were also run at 3.3°C. Later studies used temperatures spaced 5°C apart.

It should be noted and remembered by the reader that all initial optimization studies were carried out with a constant mobile phase composition of 30% isopropanol (IPA) in n-hexane. Although not appreciated at the time, the mobile phase composition plays an important role in determining whether improvement in total resolution is achieved at lowered temperatures. It will later become apparent that for certain CSP-solute combinations at less than 30% IPA/hexane, resolution actually decreases as the temperature drops.

1.4 Sub-Zero Temperature Studies

Since all three column-solute combinations seemed to benefit to some degree from the lowering of temperature, and because the master resolution equation predicted that at some lower temperature the loss in efficiency would counteract the gain(s) in capacity factor and selectivity, the temperature limit was lowered to -25°C, and for one series of runs, -30°C. To reduce the loss in efficiency, and to reduce column back pressure caused by the high viscosity of a 30% IPA/hexane mobile phase, a 20% IPA/hexane mobile phase was substituted. No drastic changes in the resolution versus temperature behavior were expected.

The master resolution equation parameters versus temperature were again plotted, but surprisingly radically different trends in resolution were noted for the cellulose-based CSP. No longer could a general conclusion be drawn regarding the benefits of lowered temperature; this optimization recommendation must be tempered with the caveat that resolution improvements can be seen for some CSP-solute-mobile phase combinations, but that all three of the factors interact. Again, the total resolution is a a product of two thermodynamic and one kinetic term, and there is always a trade-off when the temperature is lowered. If the kinetic term becomes very unfavorable due to a particular CSP-solute-mobile combination (such as the cellulose with TFAE and 20% IPA/hexane), then lowering temperature degrades the separation.

1.4 Mobile Phase Studies

Early in this research it became obvious that more research was required in evaluating mobile phase effects. Until recently, this area has been somewhat neglected by chiral investigators, with the exceptions of Zief, Crane and Horvath[33,34], who treated this area in moderate depth in 1984. Pirkle and Welch[35] have more recently looked at a number of mobile phases and temperatures in order to relate solvating ability of the mobile phase to the thermodynamic parameters of enthalpy and entropy. However, most researchers are content to employ either a 10% IPA/hexane for normal phase CSPs, and a methanol/water or acetonitrile/water solution for reversed-phase CSPs. Little time has been spent on mobile phase optimization studies for either new or old CSP chemistry.

Along with this criticism, it must be noted that the primary requirement for a CSP is enantioselectivity, and that no amount of chromatographic fine tuning can result in a separation if there is only one peak at the "standard" conditions of mobile phase (10% IPA for normal phase CSPs), flow rate (0.5 ml/min for 4.6 mm ID columns), and temperature (25°C). If the task is only to develop a particular chiral selector chemistry to achieve separation of a functional group family, such as the β-blocker family of drugs[36], and the separation is successful at standard conditions, then there is no strong reason to do involved optimization studies. However, if later new compounds of this class are not easily resolved, or greater resolution is needed for preparative-scale separations, it is valuable to know how to control enantioselectivity for a given CSP-solute class.

The first mobile phase study done in our research was necessitated by changes in our capacity factor results when a new lot of isopropanol was opened. We had an uncontrolled variable, and to achieve reproducible k'-temperature plots it was essential to find the cause of this problem. Small amounts of water were added, and it became obvious that water content

differences between lots accounted for the capacity factor changes. Since water is another polar modifier, as is IPA, it made sense from a mechanistic viewpoint.

It then became important to quantitatively evaluate the effect of various IPA concentrations upon the separation. Since IPA has such a high viscosity compared to hexane (2.4 versus 0.313 cp at 20°C[37]), increased IPA content will have a significant influence upon overall mobile phase viscosity, and therefore upon efficiency and total resolution of the enantiomers. Few thorough solvent mapping studies, such as suggested by Synder and Kirkland for achiral HPLC[38], have been done for chiral HPLC.

The initial study was done with the Pirkle-type DNBPG column and the TFAE solute. After the surprising results for the sub-zero cellulose-TFAE-**20%** IPA experiment were confirmed (decreased resolution at low temperatures, versus the increase seen originally for cellulose-TFAE in **30%** IPA), it became paramount to repeat this study using the cellulose column and both test solutes, TFAE and trans-stilbene oxide. Apparently the overall balance of resolution factors was being affected differently by the temperature-mobile phase combination for the two contrasting CSPs. Again, the differences in mechanisms of these columns made generalizations difficult.

Overall, IPA content was plotted versus capacity factor, selectivity, efficiency and resolution for both CSPs. The results show different degrees of improvement in resolution as the polar alcohol modifier is decreased in strength. These differences point out the importance of thoroughly understanding solvent selectivity for a particular CSP-solute combination, and underscore the need for more basic studies for new chiral selector and column chemistries.

1.6 Retention Mechanism Studies

Quantitative data which can unambiguously prove a proposed retention mechanism is difficult to obtain. The major obstacle is the nature of the chromatographic process itself and the type of data which results from a separation. The capacity factor, a measure of the interaction between solute, stationary phase and mobile phase, is a thermodynamically controlled parameter and as such is a time average of the behavior of millions of solute molecules as they travel the length of the chromatographic column.[39] It is difficult to gain specific information about molecular interactions in the chromatographic system by means of data obtained from chromatograms alone. Yet it is this molecular level data which is crucial for strong proof for a given retention mechanism.

Therefore, alternative techniques must be employed. For molecular interaction information, nuclear magnetic resonance (NMR)[40] and Fourier transform infrared spectroscopy[41] are two of the methods most often tried. Both approaches furnish data which give insight into which functional groups and even atoms are participating in the formation of diasteriomeric complexes. However, published studies have been made with the stationary phase and solute molecules interacting in a solution, or *ex situ* from the chromatographic column. These molecular level, but *ex situ* studies have complemented the chromatographic bulk level (time-averaged) *in situ* work. Both approaches then have a distinct disadvantage for mechanism elucidation work.

Quantitative structure retention relationship (QSRR)[42], and quantitative structure enantiomeric retention relationship (QSERR)[43] studies are an effort to predict retention behavior based on the solute and mobile phase structures. Capacity factor data is generated

from a series of homologous compounds (in most cases), and this data is related to a linear model which contains terms for mobile phase composition, stationary phase structure, and descriptors for various characteristics of the solute structure. Regression statistics are then used to calculate coefficients for each term, minimizing the overall error term. Many such studies have been done for normal and reversed phase systems.[44]. A few researchers are now extending this strategy into the chiral separations area. A 1992 report from I. W. Wainer's group at McGill University, working with Kaliszan,[45] a pioneer in this field, attempts to predict retention for a human serum albumin chiral column for some benzodiazepines, using a structural factor but no terms for mobile phase composition. A 1991 paper from Norinder and Hermansson, using principal component analysis, is the first QSERR study.[46] Armstrong's group combined empirically determined thermodynamic quantities to relate capacity factor to specific structural features of groups attached to a chiral center.[47] The limitation is that a large data base must be created for a specific CSP.

These statistical techniques shed light on the proposed mechanisms indirectly, since the degree of correlation between the predicted versus actual capacity factors and/or selectivities depend on proper selection of the structural descriptor variables, which are chosen based on the proposed molecular interactions between the CSP under test and the solute structure. Physical organic parameters such as polarizability, various polarity parameters, Taft-Kamlett hydrogen donating and accepting indexes, and various molecular shape and volume/size constants are just a few of the structural features used for reversed-phase predictions.

Our major experiment toward developing a method for elucidation of retention mechanisms employs reflectance-absorbance FTIR methods to probe the molecular interactions between a model chiral stationary phase (an L-valine), attached to a highly reflective gold surface by means of self-assembled monolayer technology, and an enantiomer (TFAE) in solution. Differences in band frequency and intensity between the two enantiomers support the order of elution from a DNBPG column, and support the theoretical conclusions as

to which diasteriomeric complex is stronger (the later-eluting peak). IR results will also be compared to those obtained by de Haseth's 1991 paper.[48]

1.7 Summary

There presently exists an $18 billion market in racemic drugs which are potential candidates for production as enantiomers. An increasing need then exists for improved analytical methods for chiral drug analysis, both in method development and quantitation. The direct approach to chiral separations, using a chiral stationary phase chromatography column, is currently preferred, but has disadvantages in terms of cost and column selection complexity.

A need exists for an improved understanding of optimization methods. Therefore the initial goal of this research was to study in depth the interrelated chromatographic parameters of temperature, flow rate, mobile and stationary phase changes upon the resolution of two contrasting racemic test probes. Since efficient optimization is not possible for any mode of chromatography without a good understanding of the retention mechanism(s) responsible for the separation, the second goal of retention mechanism exploration using the chromatographic data generated by the optimization studies was pursued.

Finally, because of the inherent limitations in the chromatographic data, which reflect time-averaged behavior of many molecules, a method of mechanism exploration by means of a model chiral stationary phase attached to a gold surface was developed.

CHAPTER II

HISTORICAL

2.1 Early Attempts at Chiral Resolution

Chapter I's Introduction noted some of the reasons for current interest in chiral molecules by the pharmaceutical industry. Apart from the clinical importance of asymmetric drugs, organic chemists have used optically active compounds for determining reaction mechanisms such as mono- and bimolecular substitution and elimination types, as well as reaction pathways in many other situations. In these classic cases, the analytical tool has been polarimetry.[49] The importance of optical activity in physiological reactions cannot be over stressed; proteins, and particularly enzymatic protein interactions with their receptors are always chiral in nature, as are hormones.

Louis Pasteur is proclaimed the first person to achieve an enantiomeric separation when in 1848 he discovered a spontaneous resolution of ammonium sodium tartrate.[50,51] Hemideral facets enabled Pasteur to optically separate the dextro and levo enantiomers after crystallization. His later experiments on the separate enantiomers proved that in a fermentation reaction, only the dextro isomer was consumed, leaving behind the levo enantiomer.[52] He further advanced the field by combining the asymmetric crystals with both chiral and achiral compounds, and observing that the physical properties of the resulting diasteriomeric complexes were no longer equivalent, as is the case for enantiomeric pairs.[53] This methodology of diastereomer formation is the basis of modern chromatographic chiral separations.

As interesting and important as Pasteur's spontaneous discovery was, it is very rare to be able to form enantiomeric crystals, with an optically recognizable morphology, from a racemic mixture. But for more than 100 years, the only methods available for racemic mixture purification were spontaneous resolution, diasteriomeric separation and enzymatic reactions.

In 1874, both Van't Hoff[54] and Le Bel[55] separately theorized that the molecular basis of the dissymmetry that Pasteur had noticed was an asymmetric carbon atom, with Van't Hoff favoring the correct tetrahedral shape, and Le Bel a square pyramid.[56]

In chronological order, the next noteworthy development occurred in 1939 when Henderson and Rule[57] separated d-l-p-phenylenediiminocamphor on l-lactose.The polysaccharide starch was used by Prelog[58] to resolve Troeger's base in 1944. Both Kotake[59] et al in 1951, and Dalgliesh[60] in 1952 employed paper chromatography for the separation of amino acids. However, Dalgliesh correctly postulated that the enantioselectivity was due to the adsorption by chiral cellulose molecules, and most importantly historically he proposed the now well-known "Three Point Rule". This simple axiom, later restated by Pirkle[61] requires that three points of interaction must be present for stereochemical selection, and that at least one must be dependent on the specific stereochemistry of each enantiomer.

In 1960, Klemm and Reed[62] were the first to utilize a silica support for chiral chromatography. Chiral nitroaromatics were adsorbed on to the silica, and partial separations of naphthylether and phenanthrene racemic mixtures were accomplished.

According to Feibush and Grinberg[63], the first direct enantiomeric separation by gas chromatography was done in 1966[64], surprised one of the pioneers in the G.C. field, A. J. P. Martin, who had not thought that a sufficiently strong interaction could be established between the CSP and enantiomeric solute. Similar sentiments were expressed by Feibush's graduate committee concerning his PhD. research proposal, who also notes that most of the enantiomeric separations development through the 1950s and 1960s was in the field of GC.

Taylor and Maher[65] list some of the major European studies in chiral liquid chromatography through the 1960s involving such stationary phases as starch, cellulose acetate, microcrystalline cellulose, cross-linked dextran (Sephadex), surface-coated alumina and silica gel, and synthetic polymers with asymmetric units.

2.2 Non-Chromatographic Methods

Allenmark[66] discusses a series of techniques which can be used independently of chromatography to determine optical purity, but these methods should be familiar to a chiral chromatographer. More development of information-rich detectors for chiral separations is needed and some of these non-chromatographic techniques are proving useful at present or might in the future. These methods all require enantiomerically pure samples.

The oldest and most familiar technique is polarimetry, and because it has been used as the operating principle for commercially available HPLC detectors[67] , discussion in moderate depth is warranted.

The operating principle depends on the differential velocity of the left and right circularly polarized vector components after they have interacted with a chiral molecule. This rotation of the plane of polarized light is termed α, or optical rotation, and is measured in degrees, according to :[68]

$$[\alpha]_{\lambda}^{T} = 100\alpha/lc \qquad \{2\}$$

where a is the measure optical rotation, T is the temperature in °C, l the cell path length in decimeters, λ the enantiomer in question (D or L), and c the concentration of the compound in grams per 100 ml. Only by using a detector such as a polarimeter can one determine the specific optical rotation of a given peak; in the usual case of a chiral column and a UV

detector, no assignment of optical configuration of specific optical rotation can be made unless known standards are available and the sample retention times match the standards. This shortcoming of UV detectors is particularly noticeable in method develop for newly synthesized chiral compounds,with no standard available, and with the sample contaminated by reaction byproducts and/or catalysts. In the worst case, the analyst cannot even be sure of having attained an enantiomeric separation due to the number of peaks.

Another approach utilizes nuclear magnetic resonance NMR) combined with optically active shift reagents such as 2,2,2-trifluoro-1-phenyl and anthrylethanol, as developed by Pirkle. Here the chemical shift reagent combines with the enantiomers and results in a chemical shift difference between them, allowing calculations of enantiomeric purity based on peak separation to be made.

Isotope dilution is a technique which relies on mixing the sample with a radio-labeled sample of the same compound of known optical purity. Both the specific rotation of the mixture, and the specific rotation of the pure compound must be known. The isotope content and optical rotation of the mixture is then determined, and the optical purity of the original sample calculated using a series of algebraic relationships. Overall, a time-consuming and complicated process.

Other less often used methods include differential scanning calorimetry and classic enzymatic techniques involving oxidizing or decarboxylating enzymes.

X-Ray crystallography, along with polarimetry, is capable of determining absolute configurations , but is very costly and requires a great deal of training and experience on the part of the operator. It cannot be used on-line as a chromatographic detector.

Finally, some promising new techniques which make use of such spectroscopic methods as optical rotatory dispersion (ORD)[69] and circular dichroism (CD).[70,71] These approaches are suitable for on-line HPLC use, and can provide very information-rich data which includes 3-dimensional plots of time, wavelength and differential absorbance.[72]

2.3 Indirect Chromatographic Methods

There is some disagreement in the literature about the use of the terms "direct" and "indirect" to differentiate the various approaches to enantiomeric resolution. Allenmark[73] and Lochümuller[74] both agree that direct methods include separations using chiral stationary phases, but Allenmark equivocates by including the chiral mobile phase additive approach in the "direct" classification. Lochmüller does not. Both authors agree that derivatization methods, requiring separate sample preparation steps, are indirect. Taylor[75] and Armstrong[76] both include the chiral mobile phase additive method under "direct". Lindner[77] clarifies the situation by stating that direct methods include all situations in which a *labile* diasteriomer is formed, depending on transient complexes[78] between the two enantiomers formed by hydrogen bonding, dipole-dipole, p-p bond, and hydrophobic interactions. Indirect methods are those which use *covalent* bonds to form the diasteriomer, requiring some chemical reaction to release the original sample.enantiomer.

Advantages of the indirect approach include (i) lower column costs (less expensive, achiral silica and reversed-phase packings can be used, important if analysis conditions are harsh or samples cannot be cleaned); (ii) many types of derivatization chemistry are available, and the cost of each reagent is much less than for a chiral column; (iii) the wide range of derivatives allows different selectivities than may be available with current CPSs, although this advantage is diminishing in importance as the commercially available CSP selection increases.[79] If a sufficiently experienced chemist is available to choose the proper reagent and prepare the sample, then laboratories which are required to analyze small numbers of many chiral samples could save money using the indirect approach instead of spending much more for a number of different CSPs.

Problems with indirect resolution techniques include expense of some reagents if the sample load is high, the need to synthesize in-house any non-commercially available reagents, the undesirability of covalently bonded diasteriomeric pairs present in samples when doing preparative work, and the opacity of many derivatives at the low UV wavelengths needed for weakly absorbing chromophores or when working at low concentrations. Perhaps the greatest disadvantage for methods which will be used for a validated analysis is the additional time needed to verify the the derivatization chemistry during validation and the additional sample preparation time later.

Only a brief summary of non-chiral stationary phase methods will be offered here, since the current trend is to CSPs and this research utilized only chiral columns.

An excellent overview of the the indirect separation methods is given by Lindner in Chapter 4 of Zief, [80] who discusses covalent derivatizing chemistry for both GC and LC applications, with special emphasis in the bioanalytical area. Over 30 chiral substituents are listed, along with the functional group needed for their use. Lindner notes that as early as 1960 Weygand and Hoppe-Seylers used N-fluoroacetyl-methylester derivatives to separate L-Ala-D,L-Phe mixtures.

Hare[81] reviews chiral mobile phase additives, which form labile diasteriomeric complexes with chiral analytes, and their application to the separation of amino acids. Two possibilities of diasteriomer formation arise when a chiral mobile phase component is present: the diasteriomer may remain in the mobile, or the chiral additive may interact with the achiral stationary phase, producing a temporary chiral surface, which then can form labile diasteriomers with the sample molecules. If derivatization is required to increase detectability by adding chromophores or fluorophores to the sample, then combining a chiral covalent derivatizing group or the copper-proline complex (ligand exchange) with a reagent such as *o*-phthaldialdehyde (OPA) is convenient. If the underivatized level of detection is sufficiently high, then a labile mobile phase additive can be used.

Another in-depth review of specifically ligand exchange-type chiral separations is given by Davankov[82] . Both chiral complexing stationary phases and chiral copper mobile phase additives are discussed in some depth, with applications mainly for amino acids. He noted that the ligand exchange kinetics for stationary phase complexes may be a problem for "modern high speed chromatography."

There has been much recent interest in the use of cyclodextran mobile phase additives, both for conventional HPLC, micro-LC and capillary eletrophoresis applications. Briggs et al[83] used β-cyclodextran added to a buffered acetonitrile mobile phase to resolve dansylated amino acids on a C_8 reversed-phase column. Debowski[83] separated mandelic acid derivatives with the same additive on a C18 column, and Iishi[84] used the same additive for dansylated amino acids, but with a micro-HPLC column. Pettersson has used chiral ion pairs of proline[85] and quinine[86], among others, to resolve various acid and aminoalcohols.

The techniques of capillary electrophoresis (CE) and the complementary technique of micellar electrokinetic chromatography (MEKC) do not allow the use of conventional chiral stationary phases, and the use of cyclodextran and other chiral mobile phase additives is required. Terabe[87] has separated very hydrophobic polyaromatic hydrocarbons, as well as chiral compounds, by adding cyclodextrans to sodium dodecylsulfate micelles. Guttman[88] et al combined β-cyclodextran with polyacrylamide gel-filled capillaries to resolve dansylated amino acids, and Kuhn[89] employed an 18-6 crown ether as a pseudostationary phase to separate 20 optically active amines. Birnbaum and Nilsson[90] employed a bovine serum albumin (BSA) protein crosslinked to a glutaraldehyde gel-filled capillary and separated tryptophan isomers, concluding that the CE approach increased the overall efficiency of the protein affinity chiral separation compared to similar packings in conventional pressure-driven HPLC.

2.4 Direct Chromatographic Methods (CSPs)

The range of commercially available CSPs includes five types, according to Wainer.[91] (Note that other authors have used different Roman numerals to designate the same general types of CSPs, such as Dappen[92] and Taylor.[93]) These include the Type I or Pirkle phases, which depend on attractive and repulsive interactions, especially π electron donor/acceptor mechanisms .[94] The Type II phases, utilizing microcrystalline cellulose, include both functional group interactions and a stereospecific inclusion complex to separate enantiomers.[95] The Type III CSPs, based on cyclodextrin, cellulose, poly(methacrylate) and recently crown ether complexes, develop the diasteriomer after part or all of the solute inserts into a chiral cavity forming the inclusion complex.[96,97,98] The Type IV CSPs depend on a chiral ligand exchange process, with a selector ligand either bonded to the stationary phase or in the mobile phase with copper(II) sulfate .[99] Proteins, such as bovine serum albumin and α-acid glycoprotein, can be attached to a stationary phase, thus forming the Type V CSPs.[100,101] Hydrogen bonding and hydrophobic interactions are thought to be the major retention mechanisms in these Type V phases.

This classification system is based on the proposed mechanism responsible for the CSP-solute diasteriomeric complex formation. Table II[102] shows the chiral selector agent responsible for enantiomeric discrimination for each of these five classes, plus some of the suppliers for each phase. There is a great variety of Type I CSPs, including both ionic and covalently-bonded varieties, with one or more chiral centers using at least one amino acid. The Type II varieties, marketed by Daicel as the Chiralcel series, feature coated rather than covalently bonded cellulose on a silica support. The chiral selector, in addition to the chiral

glucose rings, are attached through an ether linkage to three of the ring carbons, hence the "tris"

Table II. CSP classes and the chiral selector for each.

CSP Type	Chiral Selector	Vendor
I	(R and S)-N-(3,5-dinitrobenzoyl)phenylglycine (coval..and ionic)	B, R
	(S)-N-(3,5-dinitrobenzoyl)leucine (covalent and ionic)	B, R
	(R and S)-N-(β-naphthoyl)alanine (covalent and ionic)	R
	(S)-1-(α-naphthyl)ethylaminoterephthalin acid (covalent)	SM, R
	(S)-2-(4-chlorophenyl)isovaleroyl-(R)-phenylglycine (ionic)	SM, R
	(1R, 3R)-trans-chrysanthemoyl-(R)-phenylglycine (ionic)	SM, R
	N-tert,-butylaminocarbonyl-(S)-valine (covalent)	SM, R
	N-3,5-dinitrophenylaminocarbonyl-(S)-valine (covalent)	SM, R
	(R & S)-N-1-(α-naphthyl)ethylaminocarbonyl-(S)-valine	SM, R
	(R & S)-N-1-(a-naphthyl)ethylaminocarbonyl-(R)-phenylglycine	SM, R
	(R)-a-methylbenzylurea (covalent)	SU
II	Cellulose Triacetate	B, D
	Cellulose Tribenzoate	B, D
	Cellulose trisphenylcarbamate	B, D
	Cellulose Tricinnamate	B, D
	Cellulose Tris(3,5-dimethylphenylcarbamate)	B, D

CSP Type	Chiral Selector	Vendor
III	Microcrystalline Cellulose Triacetate	B, D, M
	β-Cyclodextran	A, SR
	α-Cyclodextran	
	poly(triphenyl methyl methacrylate)	B, D, M
	Polyacrylamide	M
	Polymethacrylamide	M
IV	Proline	B, D
	Amino Acid	B, D
	Hydroxyproline	MN, SR
	Valine	SR
V	Bovine Serum Albumin (BSA)	AN
	α_1-acid glycoprotein (AGP)	L

After Reference 100, I. W. Wainer.

Key to suppliers:

A = Advanced Separations Technologies, Inc., Whippany, NJ 07981
AN = Anspec Co. Inc., Ann Arbor, MI 48107
B = J. T. Baker, Phillipsburg, NJ 08865
D = Daicel Chemical Industries, LTD., New York, NY 10166
L = Pharmacia-LKB, Uppsala, Sweden
M = E. Merck, Darmstadt, Germany
MN = Machery, Nagel and Co., Duren, Germany
R = Regis Chemical Co., Morton Grove, IL 60053
SM = Sumitomo Chemical, Osaka, Japan
SR = Serva, Heidelberg, Germany
SU = Supelco, Inc., Bellefonte, PA 16823

The Type III cyclodextrans are easily functionalized around the ring mouth, as Armstrong as so thoroughly demonstrated in his research.[103] All the Type IV amino acid phases involve the copper ligand exchange chemistry. Type V protein columns are generating much interest at present, especially in the pharmaceutical applications area.[104,105,106] However, the stationary phase is fragile, their cost is high, and optimization is not well understood at present due to the multiple mechanisms which can occur due to the great variety of chiral amino acids interacting with the solute.

Type I CSPs: "Pirkle Phases"

Pirkle's group at the University of Illinois is generally credited with developing useful chiral stationary phase, silica-based columns using the "brush" (Dappen's term) or multiple interaction approach.[107] An amino acid is covalently attached, usually through amide linkages, to a π-acidic (electron-withdrawing) or π-basic (electron-donating) aromatic ring, and the entire assembly is then ionically or covalently attached to a silica gel support. Interactions such as (1)p-p electron charge transfer complexes between the p-donor and acceptor aromatic rings; (2) hydrogen bonding involving secondary amines and carbonyl groups on the CSP with hydrogen, hydroxyl and amino groups on the solute; (3) dipolar interactions in a geometric configuration which can orient itself in a "stack"; (4) steric interaction between bulky groups attached to the CSP brush groups near the chiral center of the solute which cause an enantiomerically specific orientation of the diasteriomeric complex.

Figure 5 shows the generally accepted interactions between the (R)-N-(3,5-dinitrobenzoyl)phenylglycine (one of the CSP s used for the optimization studies in this research) and trifluoroanthrylethanol (TFAE), a common chiral test probe.

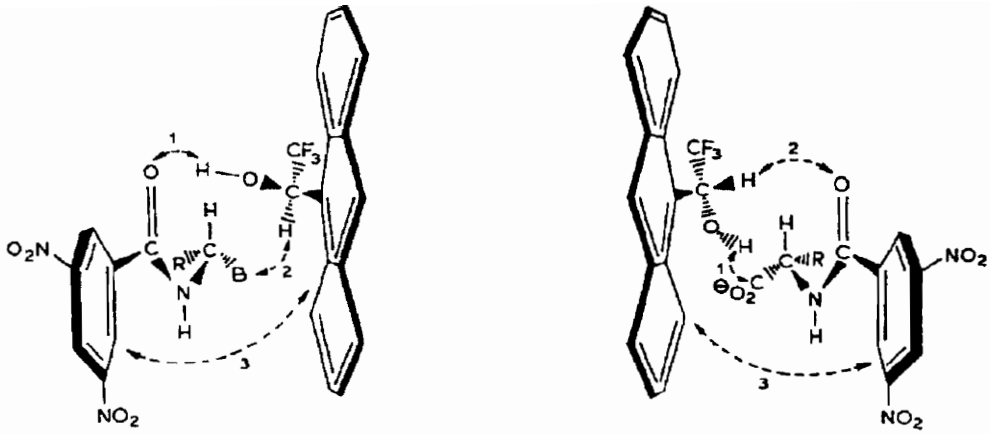

Figure 5. Interactions between the (R)-(3,5-dinitrobenzoyl)phenylglycine CSP and (R)-TFAE (*a.*) versus interactions with (S)-TFAE (*b.*). (After Pirkle, reference 20)

It should be noted that European[108] and Japanese[109] researchers have also contributed to the development of the brush-type CSPs, but Pirkle has successfully developed commercial versions of the column that bear's his name, and has done extensive mechanistic studies, both utilizing computer modeling of diasteriomeric complex interaction[110]. and numerous homologous series studies to elucidate the of structural changes on the solute to the overall complex stability.[111]

Type I columns can resolve such compounds as alkyl and aryl carbinols, aryl-substituted hydantoins, lactams, succinamides, phthalides, sulfoxides, sulfides, amides and imides. Problems arise with molecules having very active hydrogen bonding sites such as primary amines and carboxylic acid groups, which tend to interact too strongly with the CSP, making elution very difficult. On the other extreme are compounds which lack enough groups to hydrogen bond or participate in charge transfer interactions with the CSP. In some cases these groups may be present, but are more than one carbon away from the chiral center, making the interaction useless for chiral selection.

Derivatization involves conversion of amines to amides or carbamates, and carboxylic acids to amides or esters. An important factor is whether the CSP is a π-acid or base; if the former, then the p-base derivative is chosen, usually a naphthyl. If the CSP is a π-base, then a 3,5-nitrobenzoyl-(usually chloride) compound is used.[112]

Mobile phases for the Type I columns are almost always non-aqueous "normal phase" varieties, with hexane modified by an alcohol, usually 2-propanol. Frequently, 0.1 to 2.0% of acetonitrile is also added to decrease band broadening and retention. The exact mechanism is not known, but may be due to a suppression of active silanol sites, in a manner similar to that occurring for silica gel columns.[113]

Type II CSPs: Cellulose Based "Chiralcel"

Ichida and Okamoto developed in Japan the first commercially successful series of CSPs using cellulose triacetate initially coated[114] and later bonded[115] to a silica gel support. Cellulose is composed of β(1,4)-linked D-(+)-glucose units which form a three-dimensional structure by means of hydrogen-bonding of each 40-glucan unit flat plate; the plates then stack vertically and are staggered 1/2 a glucose unit[116] (see Figure 6). Taylor, in his review, notes that these asymmetric glucan units form helical structures. Figure 2 shows a Chiralcel OD (derivatized cellulose) structure, a CSP used in this research.

Other groups have studied the cellulose materials extensively, and Wainer has concluded that the stereoselectivity depends on a combination of molecular interactions, predominantly hydrogen bonding, stabilization of the diasteriomeric complex by insertion of a portion of the solute into the chiral cavity, and finally enantiomeric discrimination between the two diasteriomers through differences in their steric fit in the cavity.[117] Several authors have termed these CSPs the most universal due to their multiple mechanism capabilities. Wainer notes that, in contrast to the Type I (Pirkle) phases, Type II materials have their derivatized chiral groups in "cavities", below the cellulose surface, while the Type I brushes have the asymmetric groups protruding outward from the silica surface[118] allowing the chiral cavity to participate in the complex formation.

All compounds resolvable on the Type I phases, as well as many others including some with an axis of dissymmetry (such as trans-stilbene oxide, Figure 4) can be separated on many of the sub-types of cellulose. For a complete list of these CSPs, see Table III. Note that the "R" group, or chiral selector, represents the functionalized hydroxyl group at three positions on the glucose ring. This chemistry involves either an ester (CA-1, OA, OB, OJ, OK), a carbamate (OC, OD, OF, OD), or a synthetic polymer (OP, OT), which are chirally active due to their helical tertiary structure, and formerly belong in the Type III category.

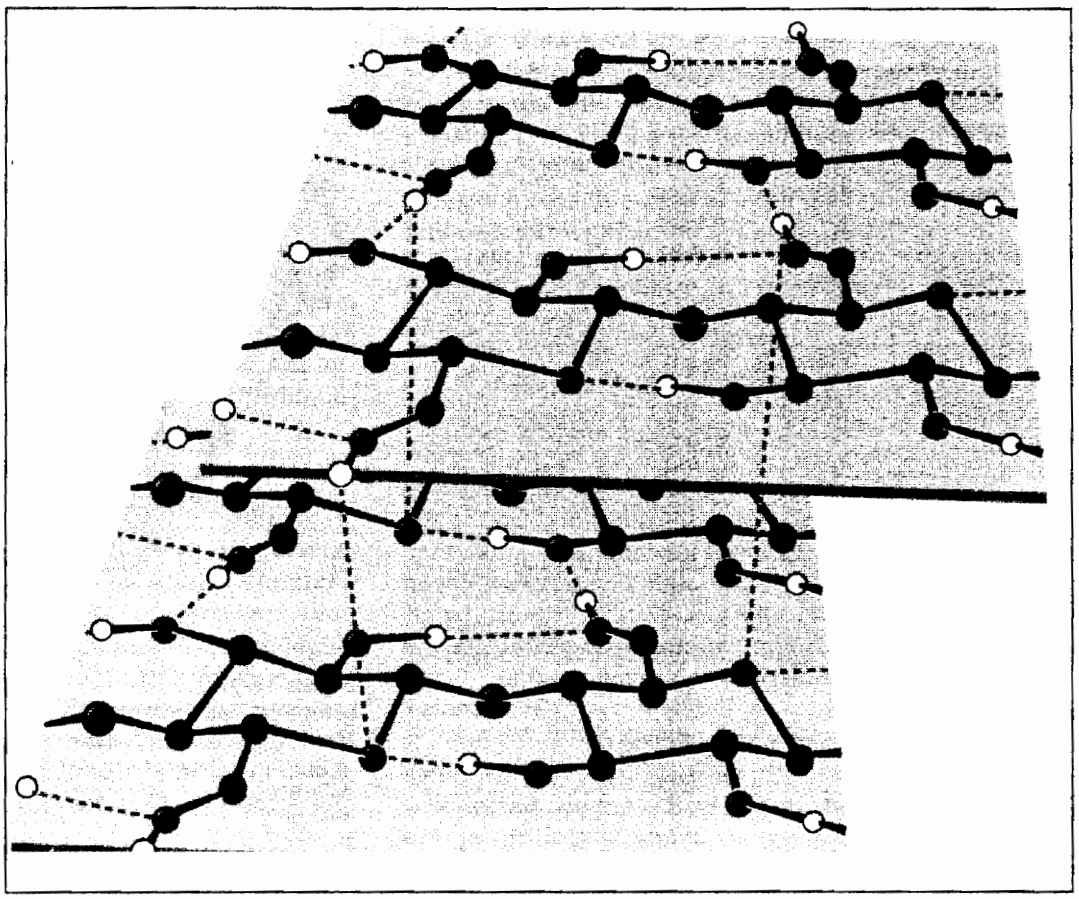

Figure 6. β(1,4-glucose) units, with hydrogen-bonded flat sheets of ~40-glucan units each. (From ref. 116)

Table III. Type II CSPs, Trade Name, Selector Group, Compounds Separated

Name	Selector Type (R group)	Compounds Separated
Chiralcel OA	Cellulose, -(CO)-CH_3	Aromatic groups, carbonyls
Chiralcel OB	" , (CO)-Ph	nitros, sulfinyl,
Chiralcel OC	" , (CO)-NH-Ph	cyano, hydroxyl, etc.
Chiralcel OD	" , (CO)-NH-(3,5-CH_2)Ph	
Chiralcel OF	", (CO)-(NH)-Ph-Cl	
Chiralcel OG	", (CO)-(NH)-Ph-CH_3	
Chiralcel CA-I	", (CO)-CH_3 (microcrystalline)	
Chiralpak OT, OP	Polymethacrylate	Aromatic, polyaromatics
Chiralcel OJ	", (CO)-Ph-CH_3	
Chiralcel OK	", (CO)-CH=CH-Ph	

(After ref. 130,s and Daicel brochure, "Crownpak Chiralpak Chiralcel"[119]

All of these cellulose phases depend only on adsorption to anchor the CSP to a silica gel support, and the stationary phase can be stripped away immediately if the wrong mobile phase is used. Strict guidelines must be followed for maximum column lifetime, avoiding any chlorinated solvents, tetrahydrofuran, benzene, or toluene.[120] As with the Type I phases, the usual mobile phase is hexane with a polar modifier, usually 2-propanol. A maximum of 10% water may be used, and all alcohols are acceptable, but J. T. Baker recommends daily flushing with 100% hexane for best results.[121] In general, it has been our experience that the cellulose phases (OB and OD) are more pressure sensitive (750 psi maximum for extended periods) and less durable than the bonded Pirkle types, but this limitation is compensated for by their versatility in resolving underivatized analytes.

Compounds containing an active hydrogen (or α-hydrogen[122]), such as amines and carboxylic acids have to be derivatized, just as with Type I phases, but the added chiral cavity, making possible inclusion complex interactions, give the cellulose columns good selectivity for a wide range of compounds.

Type III CSPs: Chiral Cavities

The heavy reliance on inclusion complex interactions for stereoselectivity is the defining characteristic for Type III phases, according to Wainer and others. This class includes the previously mentioned microcrystalline cellulose triacetate and biopolymers such as the cyclodextrans, as well as the new crown ether phase. In addition, synthetic methacrylate polymers[123] also rely on an inclusion complex and are considered Type III phases.

The most often used CSPs in this category are the cyclodextrans, featuring either six (α), seven (β) or eight (γ) D-a-glucose units which form a cone-shaped tertiary structure (see Figure 7).

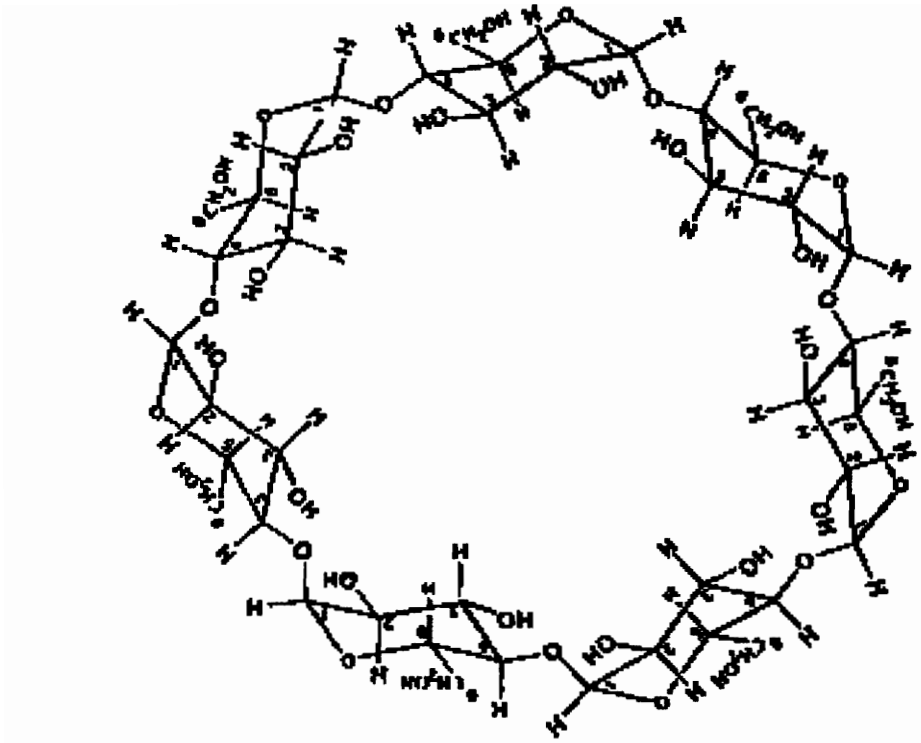

a.

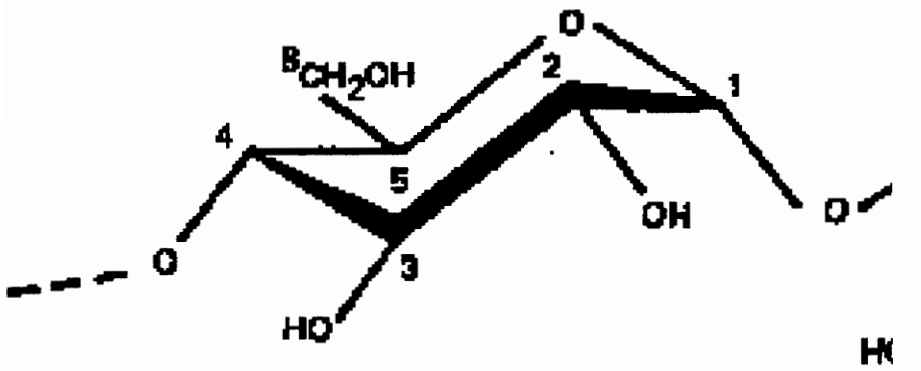

b.

Figure 7. a. Seven-membered glucopyranose ring of b-cyclodextran, shown in axial view. b. Individual glucopyranose unit, linked to neighboring groups through the 1, 4 positions.

Cram's group first used the chiral cavity approach in 1975 to resolve ester salts, and this experiment utilized a crown ether bound to silica and not a cyclodextran.[124] However, it has been only recently that a commercial 18-6 crown ether has been available from Daicel (Crownpak CR).

Armstrong's efforts[125, 126] have helped make cyclodextrans (CDs) perhaps the best known and most often used material for chiral resolution, both as stationary phases in LC and GC, and as mobile phase additives in LC, GC and more recently CE.

The overall CD structure is a toroid shape, with diameters ranging from 5.7 Å for the α–CDs to 9.5 Å for the g-type, with the interior being hydrophobic and the exterior hydrophilic.[127] Armstrong has become noted for his many specialized studies of the enantioselective changes which can be brought about with careful derivatization of the hydroxyl groups around the mouth of the CD cylinder. [128] Thin layer chromatography has also benefited from the use of CD supports, as illustrated in the separation of amino acids.[129]

The inclusion mechanism depends on a difference in inclusion energy between the two enantiomers, with the usual scenario involving insertion of an aromatic ring into the toroid with a relatively snug fit, and the more hydrophilic groups of the analyte staying outside to hydrogen bond with hydroxyl groups at the mouth of the toroid.

Aqueous mobile phases are completely compatible with the hydrophilic oligosaccharide CDs. Methanol, ethanol, acetonitrile, dimethylformamide and dimethylsulfoxide[130] are used with buffered water for cyclodextrins, and alcohols or alcohol-hexane mobile phases are common for the poly(triphenylmethylmethacrylate) polymers (Chiralcel OP, OT), which are damaged by aromatic hydrocarbons, chlorinated hydrocarbons and tetrahydrofuran. However, Wainer does note that Merck's polyacrylamide can be used with toluene-dioxane mixes, in contrast to the Chiralcel phase.[131] Blaschke also mentions the use of a toluene-dioxane mobile phase in his 1986 paper on chiral drug separation using polyamides.[132] This is of note in view of the need for aromatic solvents when solvating and

separating atropic polyaromatic hydrocarbons, which have a chiral helix configuration. The polymers are a good choice for separating molecules without any polar sites available for hydrogen-bonding interaction, a requirement for most CSPs.

Type IV CSPs: Chiral Ligand Exchange Columns

Davankov[133] was the developer of ligand exchange technology, first reporting the use of S-proline residues attached to styrene-divinyl benzene resins in 1971. His 1983 review notes that the chiral amino acid may be either covalently bonded to the stationary phase or used as a mobile phase additive, along with the transition metal ion, usually Cu^{2+}. The analyte must be capable of binding at two sites with the transition metal, and the use of ligand exchange columns is usually confined to underivatized amino acid separations.

Feinbush, Cohen and Karger improved upon the original Type IV chemistry in 1983[134] by incorporating C_4 and C_{10} spacer chains between the groups interacting with the metal atom and the silica support. This modification improved both efficiency and selectivity. In 1981, Karger et al developed nickel-based chelators complexed with long chain amides.[135]

Currently, the availability of crown ether CSPs for underivatized amino acids make the use of ligand exchange technology less attractive, especially in view of the possibility of perchloric acid mobile phase gradient use with crown ethers to speed the elution of the more hydrophobic peptides.[136]

Type V CSPs: Proteins as Chiral Selectors

Taylor's review notes that Stewart and Doherty were the first, in 1973, to report success in separating an amino acid racemate with a bovine serum albumin (BSA) bound to an agarose support. Later Allenmark made advances with various BSA columns using silica and a true HPLC approach. Of his many papers, two which help explain some of the retention behavior of these BSA columns appeared in 1992[137] and 1984.[138] He concludes that both

hydrophobic and electrostatic forces mediate enantioselectivity, and that changes in mobile phase buffer strength, pH and organic modifier influence both capacity factor and selectivity. This flexibility in mobile phase optimization strategies is in contrast to the rather narrow range of options for other CSPs. BSA has been used for a number of neutral and anionic, but not cationic drugs and biologicals, according to Taylor. Wainer,[139] includes cationic species as well.

Other proteins used for chiral chromatography include ovamucoids,[140] and α_1-acid glycoproteins.[141] All these phases share the characteristics of being expensive and less durable than the Type I Pirkle phases, but their multiplicity of chiral amino acids can provide a high degree of selectivity, especially for pharmaceuticals.

2.5 Previous Optimization Research: Temperature, Flow Rate, Mobile Phase Effects

Introduction

Previous to 1990, the majority of chiral HPLC research was concerned with the development and application of new stationary phase chemistry, with only cursory effort directed toward secondary optimization parameters such as column temperature, flow rate and mobile phase effects on resolution of enantiomers. This is in contrast to the more mature liquid chromatographic modes of liquid-solid (adsorption), reversed-phase, ion-exchange, size-exclusion and ion-pair chromatography, where major stationary phase development has leveled off. As an indication of this maturity, the classic Snyder and Kirkland text, *Introduction to Modern Liquid Chromatography* [142]was last updated in 1979, and for the most part continues to be the most authoritative basic reference for the five column modes noted above.

Chiral HPLC development has in many cases been carried forward by scientists with backgrounds in organic and biological chemistry, and to a lesser extent by analytical chemists and chromatographers. Many of the early publications on CSPs concentrated on the specific procedures used to synthesize and attach the chiral functional groups to the chromatographic support , followed by only limited chromatographic characterization of the results.,Selectivity (α) and capacity factor were sometimes the only parts of the master resolution equation[143] that were measured for a given CSP-mobile phase-solute combination, ignoring the efficiency term and total resolution of the racemic mixture.

Mobile phase choices tend to be somewhat constrained by the binding chemistry and enantioselective mechanism of the CSP in question, with the major division being between those stationary phases which operate only under "normal-phase" conditions (a non-polar organic solvent with a polar modifier), and those which are tolerant only of "reversed-phase" solvent conditions (predominantly aqueous mixtures with less-polar organic solvent modifiers). Some CSPs, such as the Type I "Pirkle" and some of the Type III synthetic polymers, may be chemically stable in either extreme, but their selectivity may be nullified by a particular solvent combination, such as the use of a Type I under reversed-phase conditions. In this situation, the over-abundance of the polar modifier allows so little CSP-solute association that no enantiomeric separation is possible, analogous to using a reversed-phase column with near 100% organic solvent.

For these reasons, then, little research has been done to optimize conditions for chiral separations. The same has until recently been the case for temperature effects. One can substantially improve resolution by lowering temperature for many separations, although decreases in efficiency are always seen due to the less favorable kinetics. Flow rate changes effect chiral separations in the same manner as in achiral chromatography, but by combining low temperatures with increased flow rates, good resolution can be maintained with a decrease in the total analysis time, as demonstrated by some of the results of this research.

It should be remembered that for any of these secondary optimization strategies (with CSP selection being the primary decision) if no separation is seen at "standard" conditions of temperature (25°C), flow (0.5 to 1.0 ml/min.) and mobile phase (90% hexane-10% 2-propanol for normal-phase CSPs, and the recommended mobile phase for other CSP types), then little time should be wasted on secondary optimization steps. Another CSP or other technique should be tried. However, for marginal resolution and for cases in which peak shape or efficiency (rate of band broadening) is poor, fine tuning of temperature, flow and mobile phase may be worth the time.

Temperature Optimization Studies

The methodology used for many reversed-phase HPLC temperature studies can be applied to chiral HPLC and is worth reviewing here.

In 1978, Melander, Campbell and Horvath[144] used the method of enthalpy-entropy compensation temperature to conclude that the same intrinsic mechanism of retention between solutes and a hydrocarbonaceous (reversed-phase) stationary phase was in operation for a variety of mobile phase, stationary phase and solute conditions. Thus by employing the enthalpy-entropy compensation method, some information about mechanisms could be obtained, but only to the extent that the existence of multiple mechanisms, which depend on specific analysis conditions, could be ruled out. The method does not provide a specific description of the mechanism that is in operation.

The procedures employed by Melander are useful for many temperature studies and so will be briefly summarized here. He found a linear correlation between the natural logarithm of capacity factors, for a series of homologous compounds measured at the same reference temperature, and the enthalpies (ΔH) of the solute-stationary phase partitioning process for these same compounds. The experiment involves first constructing a van't Hoff plot (capacity factor versus reciprocal of temperature) to obtain the slope for each compound, from which

enthalpy can be calculated (see Chapter III of this work). If the natural log of capacity factor, at a temperature near the mean of the experimental range, is then plotted against enthalpy, a straight line results, indicating the same retention mechanism is operating for these compounds.

Mathematically, the relationship is:

$$\Delta H^\circ = \beta \Delta S^\circ + \Delta G^\circ_\beta \qquad \{3\}$$

where ΔG°_β is the Gibbs free energy at the compensation temperature β and ΔH° and ΔS° are the standard enthalpy and entropy. The concept says that the free energy change is independent of temperature, since changes in enthalpy are counteracted by entropy changes.

Experimentally, a family of chemically similar compounds is required, and mobile phase must be held constant. Melander concluded that the linearity of the temperature compensation plot supported the concept of a single, partitioning-type retention mechanism. Compensation temperatures for the same compounds separated under "normal-phase" conditions (polar stationary phase and non-polar mobile phase) were significantly lower, pointing to a different mechanism (adsorption versus partition).

The use of particularly van't Hoff plots is a worthwhile method for any mode of chromatography, yielding estimates of enthalpy, entropy and selectivity, which can be qualitatively gauged by the distance separating the lines . In 1979, Melander combined temperature compensation results with mobile phase data and related retention to both mobile phase composition and temperature.[145] Also in 1979, Gant, Dolan and Synder developed an algorithm to predict capacity factors based on input of a temperature, mobile phase composition and retention time for a few compounds.[146] Vigh and Varga-Puchony also developed a predictor of capacity factor, as a function of temperature and carbon number, and also concluded that identical retention mechanisms are present for three different groups of compounds on two different reversed-phase columns.[147], based on temperature compensation plots.

Hancock, et al[148] in 1986 utilized temperature data in connection with his many studies on protein and peptide separations by reversed-phase HPLC. He noted that, in contrast to many biochemical systems in which an **increase** in temperature results in increased interaction, in HPLC of peptides an increase in temperature results in a decrease of capacity factor, as noted previously in liquid chromatography.[149] He also noted that for insulin and a lipid-binding peptide (LAP), separated on reversed-phase columns, the insulin showed an entropy-driven separation, in contrast to the LAP which exhibited enthalpy-controlled separation.

These conclusions were reached by means of van't Hoff plots, and are pertinent to optimization studies since the enthalpy term is temperature-controlled, whereas the entropy term is not, as shown by Melander in 1978[150]:

$$\ln k' = -\Delta H°/RT + \Delta S°/R + \ln \varphi \qquad \{4\}$$

where φ is the phase ratio, R the gas constant, and T the temperature in degrees Kelvin. This relationship will be derived in Chapter III.

Two recent (1992) papers by Cole and Dorsey examine the temperature dependence of retention as it relates to stationary phase,[151] and mobile phase[152] considerations. By using van't Hoff plots and examining trends in enthalpy and entropy, they found that entropy contributions increased in proportion to enthalpic ones when the bonding density of the reversed-phase surface was increased, and concluded that this evidence lends support to the theory of partitioning, rather than adsorption, being the "relevant model of retention." In addition, they noted different van't Hoff plot shapes for methanol/water versus acetonitrile/water mobile phases, giving weight to the argument that the hydrophobic effect is not a "satisfactory" explanation for reversed-phase retention.

Although the above research is for reversed-phase, achiral systems, it is mentioned because of the use of temperature and van't Hoff plots as a means for retention mechanism studies. Similar experiments have been used in this research to investigate proposed chiral retention mechanism theories.

The exploration of temperature effects on chiral stationary phase separations has become more common in the literature, but comparatively few citations were noted before 1990.

One of the first references to optimization of a chiral HPLC method by changing column temperature is by Feitsma and De Zeeuw, et al[153] in 1985 detailing the improvement in resolution of some aromatic carboxylic acids at elevated temperatures. They were using an early β-cyclodextran CSP and experienced severe tailing of the second eluting peak at 25°C. This severe peak shape deformation and excessive band broadening degraded overall enantiomeric resolution. Column temperatures as high as 55°C were employed, resulting in decreases in capacity factor and selectivity, but an overall increase (from 1.6 to about 1.65) in resolution. Although not so stated or plotted in the publication, this improvement in resolution is an example of an efficiency gain (a kinetic parameter) at elevated temperatures being great enough to outweigh the decreases in the thermodynamic parameters (capacity factor and selectivity). Another possible factor could be the more rapid desorption at higher temperatures from residual silanol groups.

In 1986 Mazzo[154] et al developed a reproducible chiral separation for an aromatic carboxylic acid, MK-286, an antihypertensive drug. This method features a 0°C temperature, which gave the required baseline resolution (R = 1.25), improving upon the 0.75 result obtained at 25°C. An increase in capacity factor was mentioned, but selectivity changes were not documented. This separation used a Pirkle-type covalent dinitrobenzoyl-L-phenylglcine column from Regis, with a methanol/aqueous buffer mobile phase.

Two reports of sub-ambient temperatures used in reversed-phase separations are worth a brief mention. In 1986 Papas of the Food and Drug Administration (FDA) achieved resolution of several unnamed compounds by placing the C18 column and heater inside a small refrigerator. The column was cooled below the desired temperature, but the column

heater was able to warm the column to the 5°C target. Resolution was improved from less than 0.5 to 1.2 and 1.4 for two pairs of peaks, the identity of which was not revealed.

In 1989, Sander and Wise[155] of the National Institute of Standards and Technology (NIST), studied what they termed the shape selectivity of two polymerically-bonded reversed-phase C18 columns, and a monomeric C18 type toward resolution of several polyaromatic hydrocarbons (PAHs). Maximum selectivity was obtained at sub-ambient temperatures, below 12°C for some PAHs. They attributed this selectivity increase to a liquid-crystal-like state of the stationary phase, with the C18 brush becoming more rigid at temperatures below 10°C, although the greatest selectivity improvement was seen at -20°C or lower. This paper is interesting in the light of a recent report [156] which has discussed the importance of rigidity for maximizing enantioselectivity in the brush-type CSPs.

Pescher, Caude, Rosset and Tambute[157] studied both temperature and mobile phase composition in a 1986 publication which used a Pirkle-type dinitrobenzoylalanine CSP to separate chiral tertiary phosphine oxides. This thorough research was concerned with aspects of mobile phase composition (which is discussed below), but temperature was varied between 50 and -15°C using a hexane/chloroform/ethanol mobile phase (25/66.9/8.1 ratio). Results for capacity factor, selectivity and efficiency (as reduced plate height) were plotted versus the reciprocal of temperature. The authors noted that few experiments using a CSP had reported results for temperatures below 0°C. Overall, an increase in resolution from 1.5 at 50°C to 2.7 at -15°C was noted, with the gain in selectivity (and concomitantly capacity factor) compensating for the loss in efficiency. They also add that low temperatures will be useful for separating extremely temperature labile species.

For the Pirkle CSP and tertiary phosphine oxides of Pescher et al temperature had a predictable and consistent affect on the resolution parameters. However, in 1988 Weaner and Hoerr[158] reported in the *Journal of Chromatography* about a method they had developed, using a dinitrobenzoylphenylglycine CSP and hexane/2-propanol mobile phase, for the

separation of several fatty acid ester and amide epoxide compounds. Efforts to optimize the separation involved changes to both the stationary phase (covalent and ionic types) and mobile phase, as well as temperature and flow rate. This time, the maximum resolution occurred at different temperatures for the ester and amide enantiomers, with the overall profile of resolution versus temperature plots being an inverted parabola. Maximum resolution (and selectivity) for the ester was 1.6 between 0 and 5°C, and for the amide it was 1.7 at the much higher temperature of 38°C. Selectivity for the ester decreased rapidly above 0°C, but for the amide it reached a peak at 10°C and stayed constant through 40°C. The authors attribute these results to the weak solute-CSP interaction for the ester, in contrast to the strong amide-CSP situation. It is stated that ester selectivity is improved at low temperatures, but that the more strongly retained amide "separates better" at high temperatures, and that cooling is detrimental. Although no data for efficiency is shown, it is probable that the loss of efficiency for the amide at low temperatures overcomes the reported gain in capacity factor, resulting in a net loss of resolution for the more strongly retained species. The authors also report, probably erroneously, that cooling the column for the weakly interacting ester "reduces band broadening" as well as improving selectivity. An improvement in column efficiency (N) at lower temperatures would seem to be kinetically impossible.

The Weaner and Hoerr paper is interesting for several reasons, most notably because the differences in the effect of lowered temperature upon resolution are: (1) dependent upon solute structure (i.e. degree of solute-CSP interaction); and (2) are NOT linear with temperature, but instead exhibit a maxima which seems to be related to the degree of solute-CSP interaction.

Few other examples of a temperature-dependent resolution maxima have been reported. One instance is in *Chirality*, [159] where Witte showed an apparent maximum in resolution between 5 and 10°C for a particular aminotetralin (ATN) racemate separated on tris-3,5-dimethylphenylcarbamate (a Chiralcel OD cellulose Type II CSP). Although only six points

were plotted in the graph, it appeared that resolution was decreasing again below 5°C. Generally, Witte et al noted that all the ATN molecules which showed an increase in resolution at lower temperatures had several functional groups with π-electrons which could interact in p-p charge transfer relations with the CSP. The ATN structure with only one hydroxyl group and no p-electrons at the six substitution locations showed a DECREASE in resolution as the temperature decreased. The authors attributed this to the weakness of p-p interactions, compared to hydrogen bonding interactions, and the subsequent decrease in the strength of p-p interactions as the temperature is increased. An enantiomer which depends solely on hydrogen bonding to interact with the CSP would be much less affected by temperature, and in fact may exhibit increased resolution as the temperature is increased due to better efficiency.

Another point to remember from the Weaner and Hoerr study is the class of solute involved: an epoxide. Our research also shows a temperature maxima for the epoxide test solute (trans-stilbene oxide) when separated on Chiralcel OD.

Generally, then, we see emerging from the research empirical support for the importance of the CSP-solute-mobile phase triad and the complex interactions between temperature and this triad which make generalizations difficult.

Akanya and Taylor in 1988[160] presented a clear, concise quantitative discussion of thermodynamics underlying the separation of several amino acid esters and TFAE on an N-formylphenylalanine Pirkle-type stationary phase. The difference in Gibbs free energy between the two enantiomers (DDG), enthalpy (DDH) and entropy (DDS) are calculated from van't Hoff plots, with accompanying explanations in a very organized manner. Overall, the authors conclude that DDG values do not vary in any particular pattern, and that fairly large experimental error was encountered. Moreover, the signs of the enthalpic and entropic quantities depended upon the nature of the solute mixture. This again underlines the importance of solute structure.

Maxima in plots of ln k' versus temperature have been reported in work by Gilpin, Ehtesham and Gregory in 1991.[161] They separated D and L-tryptophan on bovine serum albumin (BSA) bound to a silica gel support, and varied temperature and pH. Their curvature in the capacity factor versus reciprocal of temperature plots is unusual and has not been reported for any other CSP. The authors speculate that the initial increase in k' with temperature, which is "thermodynamically inconsistent with a simple retention mechanism", may be due to either gross changes in protein surface orientation or induced conformational changes of the protein, which then provide an increased number of binding sites. In either case, non-linearity of the van't Hoff plot may indicate changes in the retention mechanism.

In all the temperature studies cited so far, the capacity behavior of both enantiomers has been similar, and in most cases k' has increased as the temperature has decreased. However, in a publication from Pirkle and Burke in 1991[162] concerning the design of some special CSPs designed for β-blocker drugs, the effect of decreased temperature on the first and second eluting peaks was not the same. The first peak's k' is DECREASED, while the later eluting peak's k' is INCREASED. The net result is an increase in selectivity as the temperature is lowered, and a pleasantly DECREASED overall analysis time. It is very usual to get this sort of "free lunch" in life or chromatography, and Pirkle offers no explanation, except to note that a "number of equilibria"are possible in complex systems, and that they may respond differently to temperature.

This is yet another example of the intricacy of the CSP-solute -mobile phase triad, and the risk in making assumptions about the response of an unknown system to decreased temperature.

In 1992, Armstrong's group[163] used the classic technique of compensatory temperature plots to provide evidence of multiple retention mechanisms for cyclodextrin chiral stationary phases used in gas chromatography. Derivatized cyclodextrans ((2,6-dipentyl-

3-(trifluoroacetyl)cyclodextran) were coated on 20-meter, 0.25 mm internal diameter fused silica columns, and 24 enantiomeric pairs of test solutes were evaluated. Gibbs free energies, enthalpies and entropies were calculated, and temperature compensation plots were constructed. It was found that the test solutes split into two groups. Group compounds did not give a linear compensation plot (ln k' vs. ΔH), but did gave large enthalpy and entropy values. These Group I compounds are resolved mainly through an inclusion complex mechanism. The Group II compounds, which were linear for ln k' vs. DH, and gave lower enthalpy and entropy values, are believed to be separated by a looser, functional group association around the outside of the cyclodextran ring.

The relevance of this Armstrong study for our liquid chromatographic research lies in the possible similarity between the multiple-mechanism cyclodextran and the multiple mechanism cellulose (Chiralcel OD) CSP. We have seen different results for Van't Hoff plots for different solutes when separated on the OD phase, and will later discuss these results in terms of multiple retention mechanisms. As Armstrong notes, the enantioselective mechanism of some compounds "may be temperature dependent." If the inclusion or repulsive-attractive interaction mechanisms are competing, temperature may determine which is predominant, and therefore help explain differences in the van't Hoff plot results for different solutes and temperatures.

Mobile Phase Optimization Studies

A few more attempts have been made to explore the influence of various polar modifiers since 1986 when Pescher et al[164] noted that most researchers use hexane–2-propanol as the usual mobile phase, without "taking account of the potential solvent-CSP interactions." The same criticism, but to a lesser extent, can be directed toward studies done with reversed-phase elution conditions using CSPs.

Table IV shows the five types of chiral stationary phase and the usual mobile phase compositions for each. Note that for several types, such as the ligand exchangers (IV), and crown ethers (a variety of Type III), the choice is limited or nonexistent, and so there is little justification for in-depth optimization studies. However, depending on the solute, a much greater range of compositions is possible for the Types I, II III (cyclodextrans) and V phases. The protein Type V is perhaps the most interesting in terms of mobile phase optimization possibilities, since enantioselectivity is a function of mobile phase pH and ionic strength (due to the presence of charged amino acids in the protein) as well as the balance between aqueous and organic solvent constituents.

Generally, the mode of chromatography in a direct chiral separation is of the adsorption-desorption variety, as described by Snyder and Kirkland[165], and later Snyder ,[166] for liquid-solid separations on silica and alumina stationary phases. Although mechanistic details will be discussed in Chapter III, it needs to be noted for our discussion of mobile phase effects that in the adsorption-desorption process, a mobile phase species is competing with the enantiomeric solute for an association site on the CSP. After column equilibration, polar modifiers occupy these sites in a normal-phase situation, and organic solvent modifiers associate with cyclodextran and synthetic polymers for a reversed-phase separation. As the solute "plug" enters the column, solute molecules begin displacing solvent molecules from interaction sites on the CSP. The relative affinities of the solute versus solvent species for these CSP sites determine the capacity factor for a given solute, and the *difference* in affinities between the solute enantiomers and the mobile phase determine the enantioselectivity.

For a given solute, we can compare adsorption of various solvent molecules to the CSP by measuring relative elution times (capacity factors). A decrease in elution time of a given solute would indicate that the new solvent molecule has greater affinity for the CSP and the solute has greater difficulty in displacing it.[167]

Mobile phase studies have been few, as previously noted, and most have been done with the Type I Pirkle CSP, using hexane and various polar modifiers, usually alcohols. Zief and Crane,[168] and Zief, Crane and Horvath[169] compared a variety of solvents and the resulting capacity factors and selectivities for two solutes (TFAE and 1-(a-naphthyl) ethylamine) separated on a dinitrobenzoylphenylglycine (DNBPG) column. Solvents to be tested were chosen on the basis of the Snyder solvent selectivity triangle,[170] with hydrogen donor-acceptor, hydrogen donor and acceptor only, and large dipole moment examples representing major extremes in the triangle. Overall, Zief concluded that the hydrogen acceptor strength of the solvent was the most important criteria for determining the strength of the solvent-CSP adsorption. Taft[171] et al have quantitatively determined constants for a molecule's proton-accepting ability, pK_{HB}. The order of solvent adsorption onto the DNBPG column, with the corresponding Taft constant if applicable, was:

2-propanol > tetrahydrofuran (1.26) > ethyl acetate (1.08) > ethyl ether (0.98) > methylene chloride (large dipole moment) > chloroform (pure hydrogen donor).

For solvent mixtures of hexane and a modifier, the solvent polarity parameter P' may calculated based on the volume fraction of the individual P' values for the pure solvents.[172] Generally, the trend is towards greater CSP-mobile association, and hence lower capacity factor values, as the overall polarity of the mobile phase increases.

One other interesting, but seldom exploited result of the Zief research is that enantioselectivity increases as the steric bulk of the alcoholic modifier increases. Tertiary butanol gave a selectivity value (α) of 1.62 versus 1.56 for 2-propanol, and 1.33 for ethanol, in a 90:10 hexane-alcohol mixture when separating TFAE on the DNBPG column. Zief's explanation is that, although both R and S-TFAE are able to displace the bulkier alcohol modifier more easily from the CSP, the lower energy (more tightly bound) S-isomer induces more desolvation of the CSP than the R (first eluting, less tightly bound) isomer, and so the S-TFAE increases its retention, and thereby the selectivity increases. This may be comparable to

the change in selectivity seen by Pirkle and Burke, although in that case temperature was the variable changed to produce BOTH an increase of the second peak's k' and a decrease in the first eluting peaks k'.

The most in-depth mobile phase study to date, albeit for only the single Type I CSP, has been reported by Pescher et al[173] in 1986. Several tertiary phosphine oxides served as solutes, and alcohols, chloroform, dioxane, THF, ethyl acetate and methylene chloride were tested as polar modifiers. This study also concluded that selectivity increases as the alcohol's steric hindrance increases. All three components of the resolution equation (capacity factor, selectivity and efficiency) were measured and are shown in data tables. Pescher also concluded that for binary versus ternary mixtures of hexane-alcohol-chloroform, the selectivity per unit time is always greater for the ternary systems due to solute-CSP solubilities.

The work by Pirkle and Welch[174] coupled mobile phase variation with thermodynamic calculations to show that capacity factor and selectivity decrease as the mobile phase polarity increases, and that highly exothermic $\Delta\Delta H°$ values correlate with high enantioselectivity. More polar modifiers such as THF in hexane gave lower values of $\Delta\Delta H°$ compared to methylene chloride in hexane. The more polar, hydrogen-bonding THF solvates the chiral selector sites on the CSP, and "enthalpically costly" desolvation by solute molecules must take place for chiral selection, versus less solvation of these sites by the less polar methylene chloride. Complete data (capacity factor, enthalpy and entropy for both isomers for four solutes and sixteen different mobile phases is given, but few conclusions or explanations are included.

Finally, the use of gradient elution for separating some peptides on a crown ether column is described by Esquivel et al in a 1991 paper.[175] This paper present some interesting insight into the chiral recognition mechanism of the 18-6 crown ether CSP from Daicel (Crownpak CR+) used with a perchloric acid-water mobile phase. The mechanism is fundamentally a host-guest inclusion complex, but mediated by hydrophobic and ionic

interactions, which can be controlled by varying the perchloric acid content of the mobile phase. Highly hydrophobic solutes may be more quickly and chromatographically more efficiently eluted by employing a decreasing perchloric acid-water gradient, with the "weak" (high capacity factors) composition being 0.1 M (pH 1.0), perchloric acid. The "strong" mobile phase was 100% water. Retention of these underivatized amino acids depends on the formation of quaternary amines, which fit into the center of the "crown" of the stationary phase. If there is no acidic species in the mobile phase, then this quaternary amine cannot form and no retention is possible. Use of the gradient both decreased analysis time for a glycine-$_{D,L}$-phenylalanine dipeptide, but also increase resolution, probably due to a decrease in band broadening.

Table IV. Typical Mobile Phases for the Various CSP Types

Type	Description	Mobile Phase
I.	Pirkle (Attractive-Repulsive Interact.)	Hexane-Alcohol (usually IPA)
II.	Tris-cellulose (A.-R. plus Inclusion)	Hexane-Alcohol; no chlorinated HCs
III	Cyclodextrans	Aqueous-Alcohol Mod. (control pH)
III.	Synthetic Polymers (tritylmethacrylate)	Hexane-Alcohol or Methanol alone
III	Synthetic Polymers (methacrylate)	Benzene or Toluene/Dioxane
III.	Crown Ethers	Acidic Aqueous (usually perchloric)
IV.	Metal Ligand/Amino Acid	Aqueous Amino Acid plus Bidentate Metal (Cu^{2+})
V.	Proteins (BSA, AGP, HSA)	Buffered Aqueous-Organic Mod. (control pH, ionic strength)

Compiled from ref. 6, 8, 20 and 34.

2.6 Chiral Retention Mechanism Studies

The task of devising an experiment and gathering data to prove or disprove a given retention mechanism hypothesis for chiral or achiral separations is difficult. In this section, various approaches which have been used are reviewed, including those both chromatography-based and those which use alternative analytical methods such as nuclear magnetic resonance and infrared spectroscopy.

Studies Involving Functional Group Changes on a Common Skeleton

A number of chromatographers have studied both chiral separations and achiral modes with a planned series of test probes carefully designed to interact with the stationary phase. Also common are studies in which derivatives of a common stationary phase are produced, but because of the time and trouble involved in synthesizing and attaching the stationary phase to a support, then packing the column, this is a less used method.

Capacity factors and selectivities are evaluated and the structural changes can then be related to retention changes in a systematic manner. This approach is generally termed Quantitative Structure Retention Relationship study (QSRR)[176], or for the special case of chiral separations, Quantitative Structure Enantiomeric Retention Relationships (QSERR). Research into reversed-phase QSRR by Kaliszan[177], Jandera[178] and Jinno[179], to note three prolific scientists, has been responsible for improving the understanding of this well-characterized mechanism. Frequently, a method which relies on easily calculated physical-organic structural parameters can be computerized (Jinno[180]). Other approaches need quantum mechanical data for the particular compounds, and require sophisticated computer resources to function.[181]

For chiral separations, Armstrong and Pirkle have frequently used functional group series for both solute probes and stationary phases. In 1980, Pirkle, House and Finn[182] tested 67 derivatives of a 3,5-dinitrobenzoyl system, making amines, alcohols and thiols by functionalizing three groups attached to a chiral carbon. A fluoroanthrylalcohol (TFAE) was attached through a propylthiol linkage to silica gel as the stationary phase. The results confirmed their theory concerning $\pi-\pi$ interaction between the dinitrobenzoyl and anthracene groups (π-electron acceptor and donor groups, respectively), and hydrogen bonding between the benzoyl carbonyl group and the hydroxyl proton on the CSP.

In 1984[183], Pirkle again applyed this strategy, but to a series of 20 derivatives of a naphthyl-CSP, and then varied the alkyl chain length of the dinitrobenzoyl-derived solute. He concluded that competing mechanisms were present, and that the balance between mechanisms could be shifted by changing the functional groups attached to the CSP.

Armstrong[184], to cite just one of many efforts in this area, demonstrated the first *normal-phase* chromatography of derivatized β-cyclodextrans by derivatizing 20 different CD stationary phases. He concluded that retention was due to the same sorts of interactions thought responsible for the Pirkle-type enantioselectivity - namely π-π interactions, hydrogen bonding and dipolar dipolar. This is in contrast to the usual inclusion complex (host-guest) mechanism responsible for retention in reversed-phase cyclodextran separations.

More recently, Armstrong's group[185] employed 81 different substituents attached to a chiral carbon and evaluated the free energy contributions to the chiral recognition by two different stationary phases, R and S-(naphthylethyl)carbamoylated cyclodextrans (NEC-β-CD). Using the sum of the four substituents' contributions to total free energy, a selectivity for the molecule was then calculated, since selectivity can be related to $\Delta\Delta G°$ of the enantiomeric pair. The work is interesting as a quantitative method of estimating the degree of contribution from each of the principle interactions ($\pi-\pi$, hydrogen bonding and dipole stacking), and could be used to estimate if it was probable that a given solute would separate on the NEC-β-CD

stationary phase. Armstrong suggests this same approach could be used for other CSPs "provided a sufficient data base is obtained." This is a serious proviso, and one not likely to be possible in most working analytical laboratories. The time and effort required to generate such a large data base, and the limitation that this data could only be used for one stationary phase, is a serious problem with such a labor-intensive empirical method.

Overall, the use of a homologous or analogous series of compounds can allow inferential conclusions to be drawn about mechanisms of interaction occurring in a time-weighted fashion and that reflect differences in the Gibbs free energy of association between the enantiomers and the CSP.[186] However, chromatography cannot provide direct, molecular evidence which could tell the researcher exactly which groups are interacting. A major operational disadvantage of the homologous series method is the time and expertise required to prepare a given series, especially for CSP variation, and the time necessary to generate and analyze the data base. This approach is most often useful to academic labs headed by experienced synthetic/analytical chemists such as Pirkle and Armstrong.

Thermodynamic Studies

Other thermodynamically-based approaches have been used to make conclusions about mechanisms, as noted earlier. These studies can involve many compounds, as did Armstrong's empirical method, or a more limited number. Galli et al[187] utilized enthalpy and entropy data to study the possible mechanisms for a new diaminocyclohexane polymeric CSP they had designed, and compared results to monomeric brush-type CSPs. They concluded that their polymer CSP was more rigid, based on entropy values.

A group from the Netherlands reported in 1992[188] that they were able to justify empirically obtained selectivity and capacity factor values for styrene oxide enantiomers separated on a modified cyclodextrin column by gas chromatography. They combined enthalpy and entropy calculations with molecular modeling and molecular dynamics results to

conclude that the size of the cyclodextran cage relative to the solute impacts its orientation, and that dipole-dipole interactions between the solute and the CD mouth influence selectivity.

Finally, in the de Zeeuw work previously cited, they make mechanistic conclusions, based on thermodynamic data, about molecular interactions responsible for aminotetralin separation on a Type II cellulose CSP. The same CSP was used in our research, but in this work no mention is made of the inclusion complex mechanism, and no breakdown of the temperature changes for the individual resolution parameters of selectivity and efficiency are attempted. They do note that there is no clear correlation between the second peak's capacity factor and total resolution, but seem not to be aware of the interaction between capacity factor, selectivity and efficiency which produce enantiomeric resolution.

Enthalpy-Entropy Compensation

The basic methodology was described earlier, but a brief mention is warranted in this section. A different slope for the ln k' versus enthalpy plot indicates different retention mechanisms are operating for different classes of compounds or CSPs. The disadvantage of this method is that it requires a series of structurally similar solutes which can all be separated under the same conditions for a given CSP and mobile phase. Again, the results can only be used to infer that the same or different mechanisms are present, and the results are only applicable to compounds of a similar structure.

QSERR Techniques

To date, only two papers have been published using physical-organic structural parameters to predict retention and enantioselectivity for a CSP. The most recent effort comes from Kaliszan, Noctor and Wainer,[189] and an earlier work is noted from Norinder and Hermansson.[190] Kaliszan et al used multiple linear regression models to predict retention for both the first and second eluting enantiomers of a series of 1,4-Benzodiazepines on a human

serum albumin (protein) CSP with fixed temperature, flow rate and mobile phase conditions. Non-empirical structural parameters, including a submolecular polarity parameter, a hydrophobicity parameter, and excess electron charge, were calculated. Another structural descriptor, molecular width, was included in the model and found to be a negative predictor of retention. A sophisticated molecular modeling program, MOPAC, was used in combination with an advanced work station (IBM RISC 6000) computer. The final model equations are interesting because it is possible to assign statistical probabilities to the significance levels for each of the structural independent variables, thereby getting a quantitative estimate of the contribution to solute-CSP interaction from that particular individual interaction. This is very valuable for mechanism studies, telling the researcher exactly which part of the solute and CSP is involved and to what extent.

Disadvantages to the model include its complexity, the need for specialized hardware and software, and the expertise to use it, not common in most chromatography labs, and the lack of terms for mobile phase composition. In addition, the data is specific to benzodiazepines and the HSA column.

Other Analytical Techniques for Mechanism Study

Lochmüller, Harris and Souter published a study in 1972[191] detailing the use of proton and ^{13}C nuclear magnetic resonance, together with vapor-pressure osmometry and gas chromatographic measurements, to probe the hydrogen-bonding sites for a ureide ester-amide complex in solution. This early mechanistic study is noteworthy because of the multiple techniques and the conclusion that only two interaction points were discovered, one being hydrogen bonding between the ester carbonyl and the amido hydrogen, the other being steric hindrance.

The shortfall of Lochmüller's study and all subsequent ones remains the lack of a true stationary phase: all research using various instrumental techniques has required the diasteriomeric complex components to be free, *ex situ*, in a solution.

Other NMR studies have been attempted, but a recent one from Li and Purdy[192] combined proton NMR with circular dichroism (CD) and ultraviolet (UV) spectroscopy to examine the chiral recognition mechanism between a β-cyclodextran and dinitrophenyl derivatives of the amino acids valine, leucine and methionine in solution. The authors include a long list of previous inclusion complex studies by electron-spin resonance (ESR), NMR, UV, circular dichroism, Raman, and fluorescence spectroscopy , X-ray methods, potentiometry, positron annihilation and thermoanalytical methods. No mention is made of any but solution phase studies.

Purdy concludes that the UV, CD and NMR results prove that previous inclusion complex theories are valid, and that other interactions are required for enantioselectivity, notably those which are termed secondary, occurring between the mouth of the chiral center and the solute. They also add that their study still neglects "the intricate effect of the silica surface."

Another spectroscopic solution study, using Fourier Transform Infrared Spectroscopy (FTIR), was published by de Haseth's group at the University of Georgia[193] . A brief summary of mechanism study techniques is first given, including computer-based molecular modeling, which is discussed below. The major conclusion is that the complex between S-TFAE and BOC-l-val-propylamine is stronger than the corresponding R-TFAE-valine according to the carbonyl, N-H and O-H stretching bands and the spectral subtraction pattern. This result agrees with the observed elution order, S being second and the more strongly bound diasteriomer on various CSPs. In addition, molecular modeling (MM2) computer calculations correlated well with the FTIR results.

Molecular Mechanics/Modeling Computer Techniques

Contributions from Rogers[194] and particularly Lipkowitz et al[195,196197,198] rely on calculations of minimum energy configurations for first the individual molecules, then for various conformations of the docked pair. If the modeling is successful, then energy differences will be seen between the the R and S enantiomers docked with the same model CSP. Rogers used homologs of two BOC-valine molecules as model stationary phases, with R and S TFAE as the solutes. Calculated results agreed with chromatographic elution order. Various types of interaction energy were determined, including non-1,4 van der waals, compression, stretch-bend, dipole, 1,4-van der waals, torsion and bending for the complexes. Allinger-based MM2 calculations were used.

Lipkowitz has steadily evolved his modeling efforts, and in the 1988 publication incorporated calculations to determine the relative populations of various possible conformations of S-TFAE bound to the dinitrobenzoylphenylglycine CSP. Statistical thermodynamics, molecular mechanics, molecular orbital theory and molecular graphics are used. The software to duplicate his efforts is available, but some amount of expertise is required. Conclusions generally support Pirkle's models, with some deviation in the details.

The significant problem with the computer modeling to date is the lack of accounting for mobile phase effects. Again , only two out of the three crucial parts of the CSP-solute-mobile phase triad is being considered.

CHAPTER III

THEORY

3.1 Diasteriomeric Complex Formation

In the introductory chapter, the necessity of diasteriomeric complex formation for the chromatographic resolution of enantiomers was noted. The two complexes formed, one from each of the two enantiomeric analytes in the sample mixture, possess differing amounts of internal energy,[199] and so can be separated via chromatography. This implies, as Pirkle said in 1989,[200] a preferential interaction between one of the enantiomers and a chiral selector, which can be in the mobile phase or attached to a solid support.

Chiral molecules (from the Greek "cheir", meaning hand) are defined as objects which cannot be superimposed upon their mirror image.[201] Chiral structures can take any of three forms, as shown in Figure 8: (1)those containing a central chiral atom surrounded by two or three different species TFAE is an example); (2) molecules, usually alkenes, having a chiral axis; and (3), molecules with a chiral plane of dissymmetry (such as trans-stilbene oxide), also known as atropic molecules.

As several authors have noted, a chiral center (an atom having different species attached to it) may or may not be a chiral molecule. If the mirror image of the chiral center center cannot be superimposed upon it, then it is a chiral molecule.[202] Our discussion from now in this section will be specifically targeted to the formation of diasteriomers between enantiomers with central chirality and a chiral selector group attached to a solid support (a CSP).

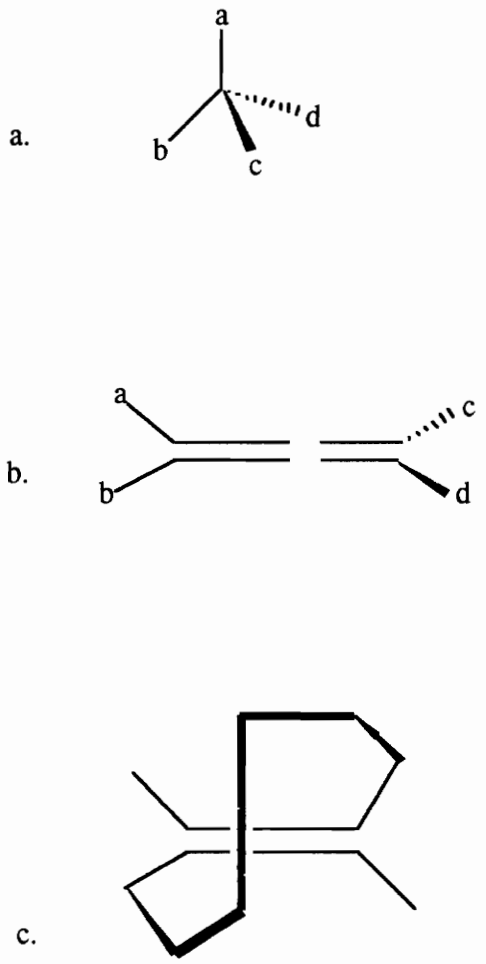

Figure 8. The three possible categories of chirality: a. central; b. axial; c. planar.

Pirkle and Pochapsky's 1989 review outlines the basic steps necessary for the diasteriomeric complex to form. Each enantiomer forms a transient diasteriomeric adsorbate with the chiral selector ,group on the CSP, in contrast to a permanent and covalent complex formed with a chiral derivatizing reagent. The adsorbates of each enantiomer must differ adequately in free energy of formation for separation to occur. Three separate interactions must be present between the enantiomer and the CSP, but these interactions may be attractive or repulsive, and they may be single-point (hydrogen-bonding, for example) or multipoint (dipole stacking and π-π charge transfers). At least one of the interactions must be unique to one of the enantiomers for enantioselectivity. Figure 9 is the classic "three-point rule" example, but represents only single-point interactions, and implies that all three interactions are associative, which may not be the case. If there are large groups present (such as phenyl rings), then one of the CSP-enantiomer interactions could be disrupted by steric hindrance.[203]

Before elaborating on the interactions responsible for complex formation, the relationship between enantioselectivity and differences in the internal (free) energy of the diasteriomeric complexes should be outlined. Pirkle,[204] Melander et al,[205] and Dorsey[206] have all related selectivity to Gibbs free energy in the following manner:

$$\alpha_{DL} = k'_D/k'_L \qquad \{5\}$$

where k'_D is the second eluting enantiomer, k'_L the first and aDL the enantioselectivity.The capacity factors are equilibrium constants, or in chromatographic terms solute partition coefficients (K) , which can be related to selectivity and energy:

$$\alpha_{DL} = K_D/K_L = \exp(-\Delta G^m_D/RT)/\exp(-\Delta G^m_L/RT) \qquad \{6\}$$

where ΔG^m_i is the molecular free energy of adsorption of the ith enantiomer. Rearranging relates selectivity to the free energy difference between the two diasteriomeric complexes:

$$\Delta(\Delta G)^m = -RT \ln \alpha_{DL} \qquad \{7\}$$

Note that selectivity is temperature dependent (enthalpy controlled), and that entropy plays a relatively small part in separations near ambient temperature, according to Pirkle.

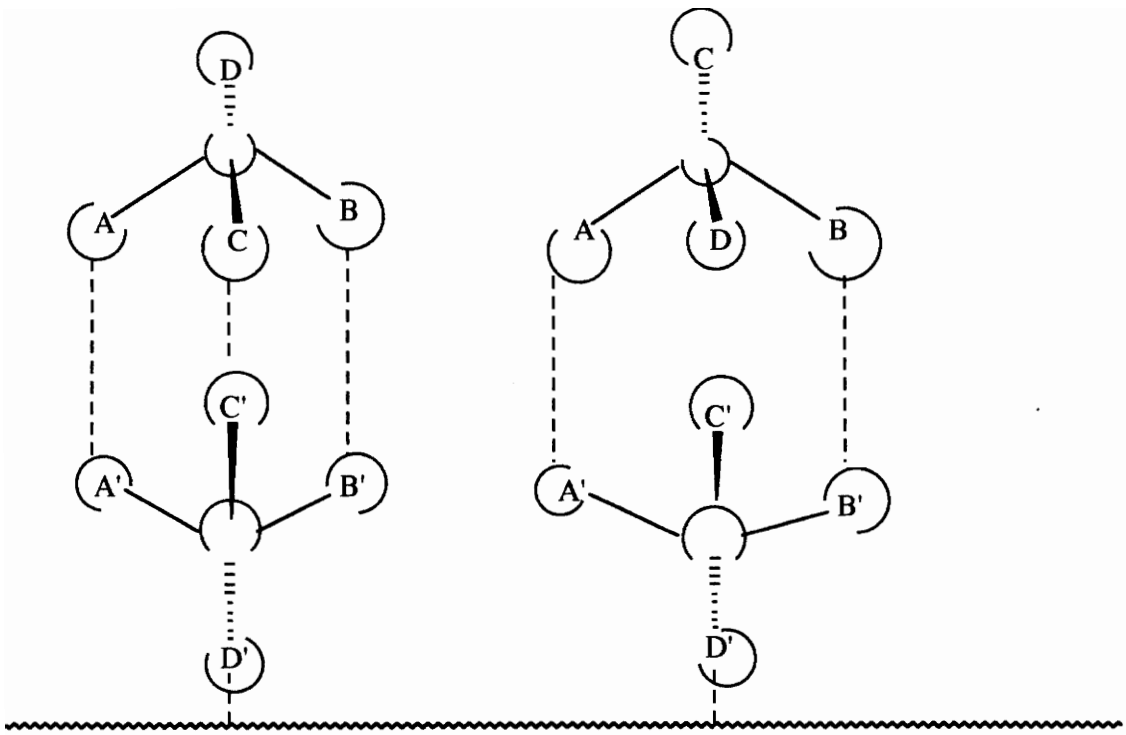

Figure 9. Three-point interaction between the CSP and two enantiomers. The stronger complex is on the left, and the weaker on the right.

Expanding the above equation, taking into consideration the basic Gibbs-Helmholtz relationship,[207] rearranging and dividing by -RT gives:[208]

$$\Delta\Delta G^\circ = \Delta\Delta H^\circ - T\Delta\Delta S^\circ \qquad \{8\}$$

$$\ln \alpha_{DL} = -\Delta\Delta H^\circ/RT + \Delta\Delta S^\circ/R \qquad \{9\}$$

If only the capacity factor is considered, then:

$$\ln k' = -\Delta H^\circ/RT + \Delta S^\circ/R + \ln \varphi \qquad \{10\}$$

where φ is the phase ratio and equal to:

$$\varphi = Vs/Vm \qquad \{11\}$$

the volume of the stationary phase divided by the volume of the mobile phase.

As Pirkle and others have noted, the CSP should be designed to maximize enantioselectivty ($\Delta\Delta G^\circ$), and minimize ΔG° for each enantiomer to provide the greatest possible selectivity with the shortest possible overall retention (ΔG°) to minimize band broadening. As a corollary, difference in enthalpy between the enantiomers should be maximized, and the individual enthalpies minimized.

Table V. Molecular interaction types and a representative functional group.

INTERACTION	FUNCTIONAL GROUP
A. π-electron donor-acceptor	Dinitrobenzoyl, Phenyl
B. Hydrogen Bonding	1°, 2° Amine, Carbonyl, Hydroxyl
C. Steric	Bulky Substituents (rings, etc.)
D. Dipole Stacking	π-ring systems, H-Bond pairs

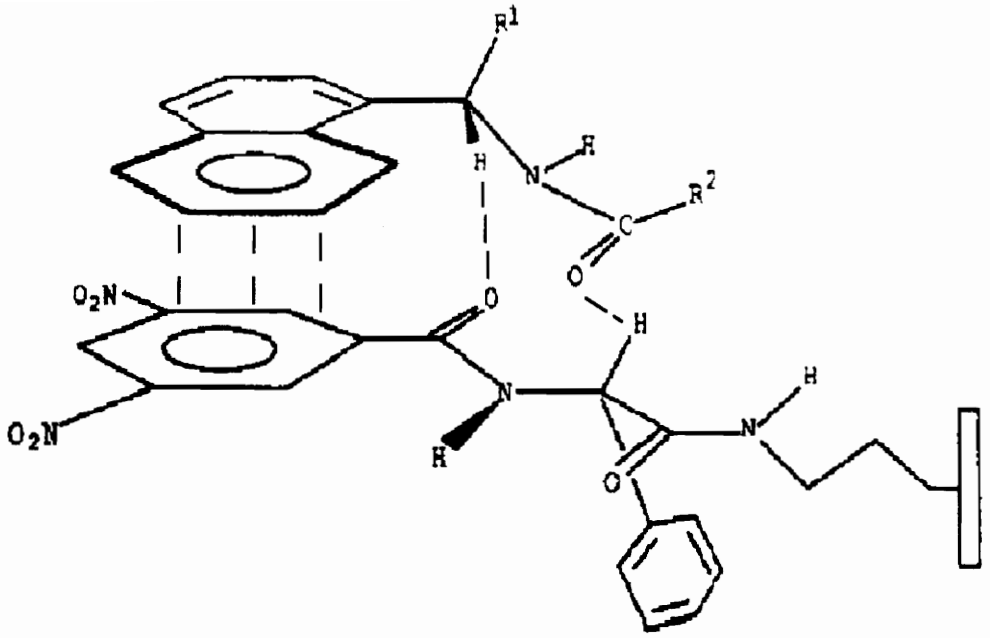

Donor-Acceptor

Figure 10. The above figure illustrates a combination of charge transfer interactions, between the aromatic groups, and hydrogen-bonding between hydrogens and carbonyls.

After D. R. Taylor, K. Maher. *J. Chrom Sci.* **30** (1992) 67.

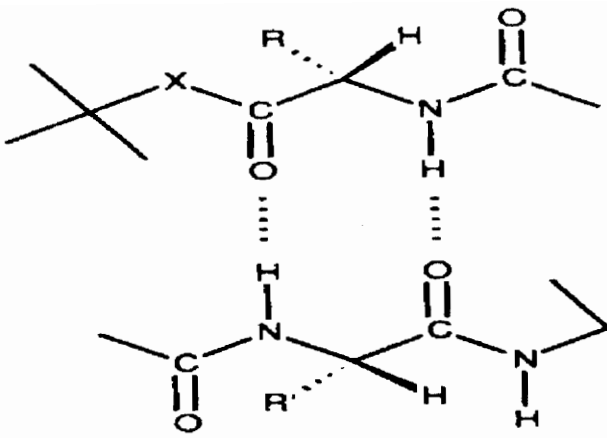

Hydrogen-bonding model

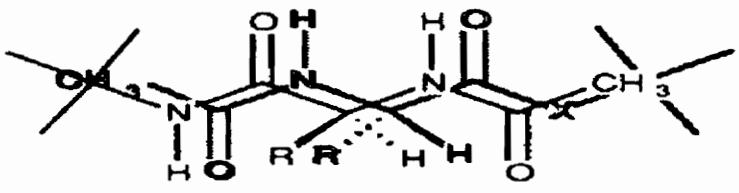

Dipole-stacking model

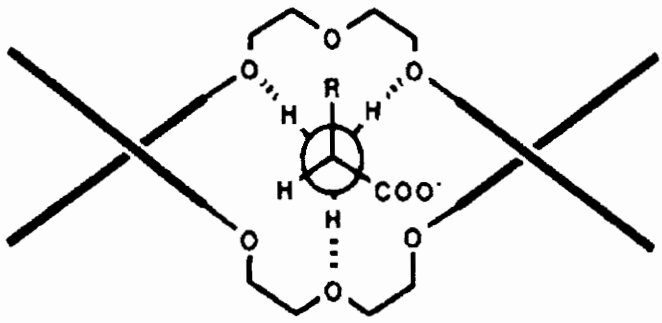

Inclusion Complex (Crown ether CSP)

Figure 11. Three examples of interactions involving hydrogen bonding, dipole-dipole formation and inclusion complex formation (with hydrogen bonding also).

Figures 10 and 11 summarize the major interactions which are responsible for complex formation for several types of CSPs, and gives structural examples for several stationary phases. Many authors have described these essential physical-organic functional group interactions, but Kaliszan[209] has a particularly good description , with some explanation of the underlying mathematics. His discussion is directed towards QSRR for achiral chromatography, but the same types of interactions are responsible for enantioselectivity for a CSP. These van der Waals interactions are:

1. Ion-Dipole
2. Dipole-Dipole (Keesom)
3. Dipole-Induced Dipole (Debye)
4. Instantaneous Dipole-Induced Dipole (London effects)
5. Hydrogen Bonding
6. Electron Pair Donor-Acceptor (Charge Transfer)

The first four types progress from those with the greatest Coulombic content to the least. Ion-dipole interactions are included here, but do not in the most formal sense belong to the list of intermolecular interactions. The term "ion" implies a formerly charged species, unlike a dipole, which infers a neutral molecule. However, for chromatographic discussion, ionic compounds may be encountered in both the mobile and stationary. phases.

Kaliszan defines the potential energy of the ion-dipole interaction as:

$$E_{i\text{-}d} = -W^2 \, (z \, \mu \cos \alpha \, / \varepsilon \, r^2) \qquad \{12\}$$

where z is the ion's charge, μ the dipole moment of the uncharge molecule, α the angle between a line r between the ion and the dipole's center. Relative electric permittivity, e, characterizes the ability of the solvent to pass a charge, and is high for dissociated solvents (81 F/m for water) and lower for less polar solvents (27 for ethanol, 8.8×10^{-12} for a vacuum). W is a constant which depends on the unit system used. The dipole moment μ is equal to:

$$\mu = q \, R \qquad \{13\}$$

where q is the charge magnitude and R the separation between charges.[210]

In practical terms, adding a less polar organic solvent to a mobile phase in which the solute-CSP interaction is dependent on an ionic salt in the mobile phase (such as the divalent cation Cu^{2+}) would decrease the ion-dipole energy ($E_{i\text{-}d}$) and decrease retention.

Dipole-dipole interactions occur between molecules which both possess a permanent dipole moment, as defined above. However, the degree of attraction or repulsion is determined by the orientation of the two molecules, and the population of the various orientations is controlled by the Boltzmann distribution, which in turn is heavily influenced by temperature. High attractive dipole-dipole interaction energy is favored when the molecules are oriented so that one positive dipole is near a negative dipole. At high temperatures, all dipole orientations are equally populated, and at low temperatures, high dipole-dipole interaction is favored. The overall relation is:

$$E_{d\text{-}d} = -W^2 \, (2/3kT) \, (\mu_1^2 \, \mu_2^2 \, / \, \varepsilon \, r^6) \qquad \{14\}$$

where W is the unit system constant, k is the Boltzmann constant, μ_1 and μ_2 are the two dipole moments, ε is electric permittivity, and r is the distance between the dipoles.

It should be noted that the above relationship suggests that CSPs which rely to a great extent on single-point dipole-dipole interactions may show increased enantioselectivity from lowered temperatures if a dipole-dipole is participating in the chiral selection mechanism.

Dipole-induced dipole interactions can exist between a permanent dipole molecule and a second molecule which may or may not be polar. The second molecule is polarized, inducing a dipole moment, which in this situation is not affected by temperature, since the induced moment cannot be disoriented from the direction of the inducing moment.[211] The interaction energy is then:

$$E_{d\text{-}id} = -W^2 \, [0.5 \, (\alpha_1 \, E_2^2 + \alpha_2 \, E_1^2)] \qquad \{15\}$$

where α is polarizability for molecules 1 and 2 (here assumed to be a scalar quantity), E_2 the electric field generated by molecule 2 (the dipole inducer), and E_1 the electric field for

molecule 1 (carrying the induced dipole). Atkins[212] defines polarizability as the dipole moment induced by an electric field of 1 v/cm, or more formally:

$$\mu_{induced} = \alpha \varepsilon_0 E \qquad \{16\}$$

where α is a coefficient of proportionality and has units of cm^3. Expressing { } in terms of m instead of energy, one sees:

$$E_{d\text{-}id} = -W^2 (\alpha_1 \mu_2^2 + \alpha_2 \mu_1^2) / \varepsilon r^6 \qquad \{17\}.$$

These dipoles are not influenced by temperature, as noted above, nor are they additive.

Finally, there are instantaneous dipoles which can exist between all molecules, neither of which necessarily exhibit a dipole moment. These London or dispersion forces arise from the fluctuating electron clouds surrounding every atom, which induce a momentary dipole moment in a nearby molecule. Although a complete calculation of all dispersion interactions requires a detailed analysis of wave functions of all excited states, an approximation is possible, since potential energy is proportional to the product of molecular polarizabilities, as in:

$$E_{disp.} = -W^2 (3/2) (I_1 I_2 / I_1 + I_2) (\alpha_1 \alpha_2 / \varepsilon r^6) \qquad \{18\}$$

where I1 and I2 are the ionization potentials for the two interacting molecules. Temperature is not a factor for E_d, since molecular orientation will not effect the random instantaneous dipoles.

Overall, the total potential energy for all the above van der Waals interactions are additive:

$$E_{vdW} = E_{d\text{-}d} + E_{d\text{-}id} + E_{disp.} \qquad \{19\}$$

and the dispersion term is usually much greater than the orientation ($E_{d\text{-}d}$) and induction ($E_{d\text{-}id}$) terms. For example, for 2-butanone at 40°C, the proportions are 78%, 8%, and 14%, respectively.

So far we have discussed only non-specific, low energy intermolecular interactions which contribute to diasteriomeric complex formation, the van der Waals forces. The next two types, hydrogen bonding and electron pair (charge transfer) donor-acceptor phenomenon, are about 10 times more energetic, and specific to certain functional groups. However, these interaction energies are still about 10 times weaker than covalent bonds.

Hydrogen bonding (a high energy form of dipole-dipole interaction), is extremely important for most CSP classes. The hydrogen bond develops when a proton is in close proximity to an electron pair donor or hydrogen bond acceptor group such as an oxygen atom (alcohols, carbonyls, ethers), a nitrogen atom (primary and secondary amines), a sulfur atom (thiol groups), a halogen, or the p-electrons in an aromatic or sometimes alkyne molecule. Hydrogen bonds are nearly linear, asymmetrical and equal to the distance between the proton donor atom and the proton acceptor. Bond energies can vary between 20 kJ/mol for O-H --- O to as high as 150 kJ/mol.

If the molecules involved in hydrogen bonding are represented as:

$$\mathbf{R - A \text{——} H\text{---}B - R'} \qquad \{20\}$$

where A-H is the proton-donating species and B-R' the more electronegative hydrogen acceptor, then there exists an asymmetry, as suggested above. Huheey[213] lists some typical values for calculated versus experimental bond distances for various hydrogen bonding situations, and the observed H---O distance (for the O——H---O complex) is only 1.70 Å versus the 2.60 Å calculated value. For N——H---O, the observed distance is 2.00 Å. The observed A——H distance in these two cases is 2.70 and 2.90 Å. It is important to keep these distances in mind when evaluating possible solute-CSP hydrogen bonding interaction sites.

The final type of interaction, and one very important in establishing diasteriomeric complexes for Pirkle-type CSPs, involves electron pair donation and acceptance. Here we are referring to an electron transfer (hence the synonym charge transfer interactions) between an

electron pair residing in a higher energy orbital (the donor) to a vacant, lower energy orbital (the acceptor). Although electrons may come from either the *n*, σ or π-orbitals, we will be concerned with only the π-electrons in reference to charge transfer in CSP-solutes complexes. To categorize the energy-levels for P-donor acceptor interactions, Kaliszan notes that the energy for the neutral benzene-1,3,5-trinitrobenzene case is -8 kJ/mol, making it fairly weak compared to some of the strong complexes formed between charged species, which can be as high as -188 kJ/mol.

Another component of the diasteriomeric formation scheme, which is important for steric hindrance analysis, is that of negative interaction or energy of repulsion. Huheey[214] notes that at very short distances the electron clouds begin to repel one another (Pauli exclusion principle). The relationship between repulsive energy and distance is:

$$E = +k / r^n \qquad \{21\}$$

where *k* is a constant and r is internuclear distance. The Leonnard-Jones function describes overall attractive-repulsive behavior between two molecules and is given by Kaliszan as:

$$E(r) = -(a / r^6) + (b / r^m) \qquad \{22\}$$

where m is between 9 and 12, and is the repulsive term. The attractive term is $-(a/r^6)$.

Table VI summarizes the various interactions, relative strengths and distances involved between the interaction molecules.

Table VI. A summary of molecular interactions important in forming diasteriomeric complexes.

Interaction Type	Relative Strength	Working Distances
Hydrogen Bond	Very Strong	Long range
Electron Pr. Donor-Acceptor	Strong	Moderately long range
Ion-Dipole	Strong	$1/r^2$, short range
Dipole-Dipole	Moderately strong	$1/r^3$, short range
Dipole-Induced-Dipole	Weak	$1/r^6$, very short range
Instant. Dip.-Induced-Dip.	Very Weak	$1/r^6$, extremely short range

After Huheey, ref. [215]. Note that Huheey also lists an ion-induced-dipole force, where

$$E = -0.5\ (Z^2\ \alpha\ /\ r^4) \qquad \{23\}$$

where Z is ion charge, α is polarizability, and r is distance.

3.2 Generalized Chiral Separation Mechanism

As outlined in Chapter II, the mode of chiral stationary phase separation is adsorption-desorption or liquid-solid chromatography, but involving two different adsorption complexes of different internal energies. Pirkle and Welch[216] described a series of possible adsorption equilibria which represented the CSP, enantiomeric solute and mobile phase by employing icons. Thirteen possible schemes were outlined, and a summary of the essential adsorption and desorption steps is shown in Figure 12. The significance of this work is the emphasis on the interaction of all three factors in determining the final equilibrium. Stationary phase, mobile phase and solute interact, resulting in an enantioselective separation if the difference in Gibbs free energy between the two diasteriomeric complexes is great enough.

Figure 12 summarizes all major facets of a chiral separation. Initially, solvent molecules, which in reality are usually a binary mixture, have adsorbed onto sites on both the CSP and solute. The interactions mentioned in the preceding section are reasonable for these mobile phase-CSP and mobile phase-solute associations. The stronger member of the mixture (usually an alcohol for normal phase and an alcohol or aprotic polar solvent for reversed phase situations) can be thought of as having similar interactions with the CSP as does the solute, and therefore has the ability to compete with the solute for interaction sites on the CSP. As the solute band begins its trip through the column, the first of many solute adsorptions takes place as the solute displaces a solvent species. A stronger and weaker diasteriomeric complex is formed, with unequal internal energies. Another solvent molecule can then selectively re-solvate the weaker solute-CSP complex, and some time later the stronger complex will be solvated. The difference in Gibbs free energy between the two complexes determines the final capacity factors, or difference in total time each complex is in existence, and hence the

difference in retention time and volume. The ratio of these capacity factors, α, determines the final enantioselectivty.

The majority of research has concentrated on the CSP-solute interaction, but it is obvious from the diagram that both the physical properties and structural characteristics, as well as concentration of the solute will intimately influence the degree of solute-mobile phase and CSP-mobile phase interactions.

3.3. Role of Temperature

As noted earlier in section 3.1, selectivity can be related to temperature, enthalpy, entropy and Gibbs free energy in the following manner:

$$\ln \alpha = -\Delta(\Delta H^\circ) / RT + \Delta(\Delta S^\circ) / R = -\Delta(\Delta G^\circ) / RT \qquad \{24\}$$

It is obvious from the expression that the enthalpy of adsorption is a function of temperature, but that the entropy is not. To optimize for maximum separation, then one must maximize the difference in enthalpy between the two complexes and minimize entropy differences, /obtaining the maximum free energy difference. To prevent excessive band broadening (low chromatographic efficiency), the enthalpy and free energy for each complex should be held to a minimum, since the larger ΔH° and ΔG° become, the longer the solutes remain on the column, and the greater the diffusion of the solute plug.

A given combination of CSP-solute-stationary phase may be enthalpy-driven, in which most of the total DDG° is due to the enthalpy term, in which case decreasing the temperature will improve the separation. Conversely, the majority of the free energy difference between the two complexes may be due to the entropy term. In this situation lowering the temperature may either not increase resolution, or may even decrease it due to deterioration in chromatographic efficiency. This efficiency loss is due to increased retention times (increased diffusion), and

poor kinetics of the mass transfer between mobile phase and stationary phase from the increased mobile phase viscosity.

The analytical approach used to determine enthalpy, entropy and Gibbs free energy for a given separation uses van't Hoff plots in which the natural logarithm of capacity factor or selectivity is plotted versus the reciprocal of temperature in degrees Kelvin. The slope of this plot is then proportional to enthalpy, and the y-axis intercept is proportional to entropy. This requires retention data at several temperatures for each CSP-solute-mobile phase combination. A large difference in slopes would then indicate an enthalpy-controlled situation, and a large difference in y-intercepts an entropy-controlled separation.

Although this sort of analysis has been common when studying normal and reversed-phase achiral systems, it is especially useful for racemic mixtures. Since enantiomers have equal internal energies, then the overall enthalpy of solute-solvent association-disassociation is equal, so that the overall $\Delta\Delta G°$, $\Delta\Delta S°$ and $\Delta\Delta H°$ values are only due to differences in the complex formation energy between the solute and CSP for a given mobile phase mixture.

A closer inspection of the van't Hoff plot of ln k' versus the reciprocal of temperature in degrees Kelvin is warranted at this time for two reasons. Firstly, some of the mechanistic inferences made in the Results section depend on van't Hoff plot data. Secondly, some conflicting claims have been made for the effect of reduced temperature on enantiomeric resolution, and generalizations are difficult. It will be instructive to examine in detail what result lowering temperature has on both the total resolution, and individually on capacity factor and selectivity.

Figure 13 shows two model van't Hoff plots to illustrate these various effects of lowered temperature. Plot 13a. shows an entropy-controlled separation, and is typical of, for example, the separation of two n-alkanes, a lower molecular weight X and a higher molecular weight Y, on a C_{18} reversed-phase, achiral column. Temperature is decreasing from left to

BASIC MECHANISM:

Adsorption-Desorption

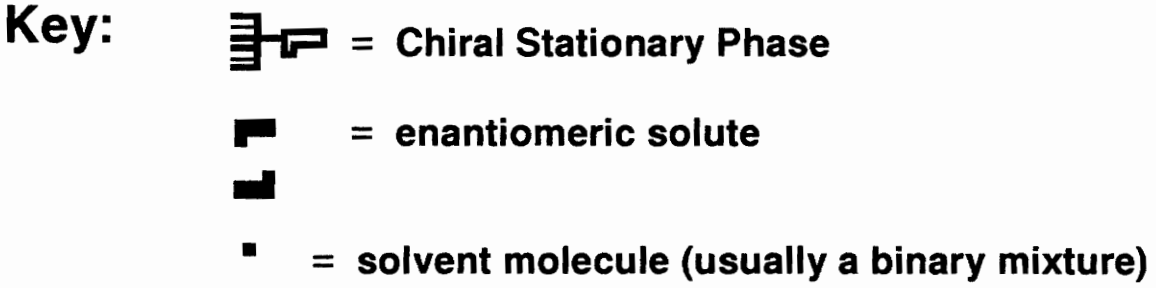

1. Solute Adsorption:

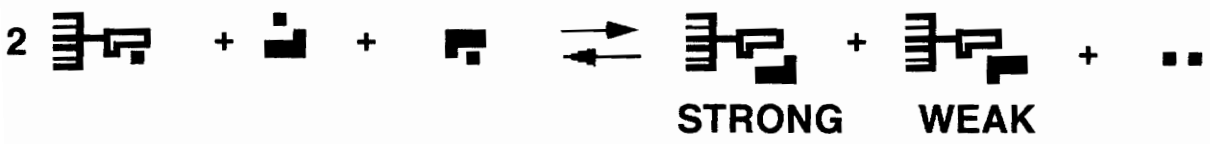

2. Solute Desorption:

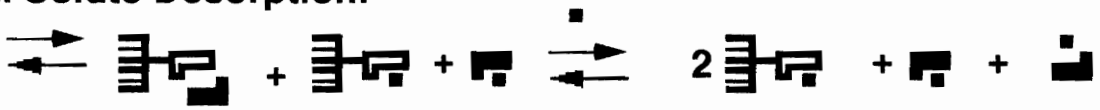

W. Pirkle, C. Welch, *J. of Liquid Chrom.*, 14(11), 2027-2042 (1991)

Figure 12. Basic adsorption - desorption equilibria

13 a.

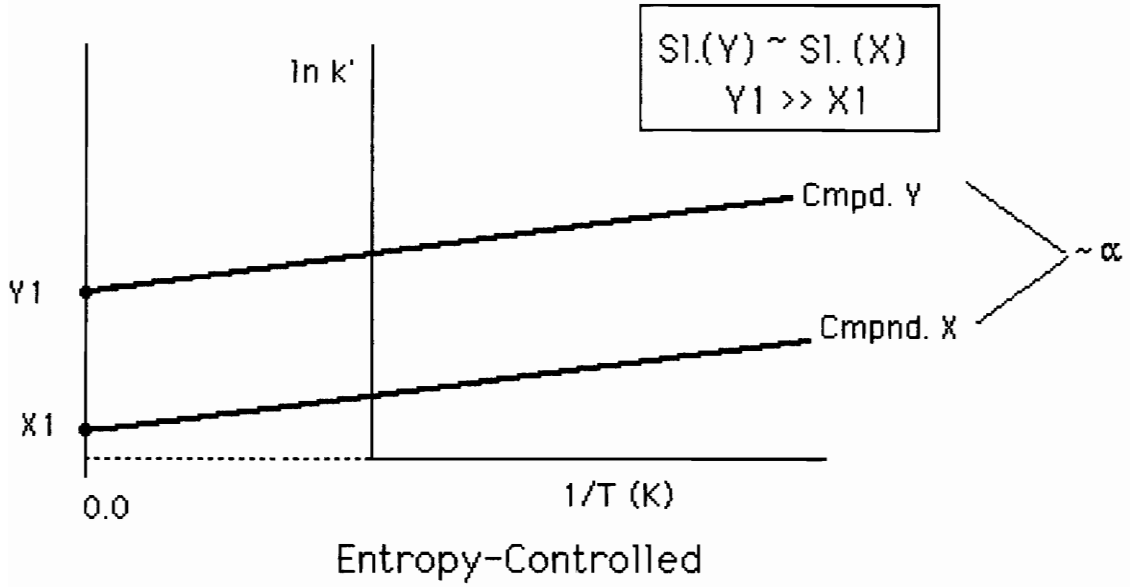

13 b.

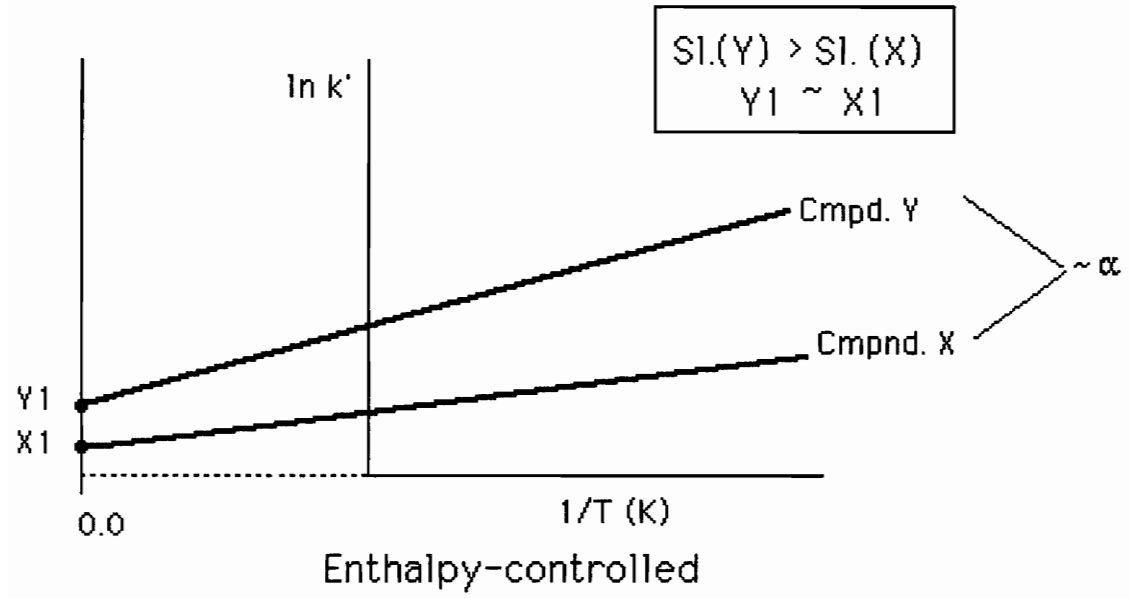

Figure 13. The entropy-controlled situation (a.), in which decreasing temperature does NOT increase selectivity, and the enthalpy-controlled situation (b.), in which selectivity improves as temperature decreases.

right, and the capacity factor (ln k') is increasing for both solute X and Y, but at the same rate, since the slopes are identical. Since enthalpy is proportional to slope, the enthalpies remain constant for both solutes as temperature decreases. The y-axis intercept, here designated by X1 and Y1, are not equal and therefore entropy, proportional to the intercept, is responsible for the difference in capacity factors and is controlling the separation. Selectivity k'_y / k'_x) is proportional to the distance separating the two lines and remains constant as temperature decreases. For the entropy-controlled separation then, whether the solutes be alkanes or enantiomers, selectivity is constant with decreasing temperature, and the difference in capacity factors accounts for resolution, which is a product of a capacity factor, selectivity and efficiency term (see Equation __).

For the enthalpy-controlled separation, Figure 13b., the selectivity does increase as the temperature decreases, as evidenced by the unequal and diverging slopes. The intercepts here are very nearly equal, but this is may not always be the case. For the model shown, the slope of the earlier eluting solute X is less than the later eluting Y, but the opposite could hold true. In addition, for some chiral solute-mobile phase combinations, reports of no increase or even decrease in the capacity factor of both peaks, but at unequal rates, have been noted.[217] Various possibilities exist, depending on the CSP, retention mechanism), solute and mobile phase, but any dissimilarity in the behavior of each enantiomer's capacity factor which increases their selectivity as temperature is decreased is an indication of an enthalpy-controlled separation. From the method development standpoint, if the separation is enthalpy-controlled, then temperature is a useful tool.

The van't Hoff plot models also illustrate the isoenantioselective temperature described by Galli[218]. and others. If the plots in 13b. are extended slightly to the left, they will cross. The temperature at the intersection of the two lines, where the capacity factors are equal, selectivity is one (no separation), and entropy and enthalpy are equal, is the isoenantioselective

temperature. The practical significance of this point is not clear, but it has been reported by several researchers and is characteristic of a given CSP-solute-mobile phase combination.

In summary, entropy-controlled separations are common for reversed-phase alkane homologues, and selectivity is constant. For enthalpy-controlled separations, the selectivity changes with temperature, and the separation can be optimized by choosing temperatures which produce the maximum selectivity. Capacity factors of the two enantiomers can differ in various ways, depending on the particular CSP-solute-mobile phase combination. Finally, by utilizing a van't Hoff plot of capacity factor as a function of the reciprocal of temperature, both quantitative values for Gibbs free energy changes, enthalpy and entropy can be derived, as well as qualitative information regarding the usefulness of temperature as an optimization tool.

3.4 Other Theoretical Method Optimization Considerations

We have discussed the possible effects on decreased temperature on capacity factor and selectivity, the thermodynamic terms of the master resolution equation (Equation {1}). Efficiency, the kinetic parameter, is of less importance in chiral separations than selectivity, and in the past various CSPs have not been known for extremely high plate counts.

As temperature is lowered, efficiency decreases due to the increased mobile phase viscosity and the concomitant increase in the rate of mass transfer of the solute to and from the mobile phase. The time required for a solute molecule to move through the more viscous mobile phase is increased, and increased band spreading results.

Plate height, H, is the column length divided by efficiency (N, number of plates), and should be minimized. Giddings, as shown by Synder and Kirkland[219], has identified five main contributors to plate height, or rate of band broadening:

$$H = 1 / (1/C_e d_p) + (1/(C_m D_p^2 u/D_m)) + C_d D_m/u + C_{sm} D_p^2 u/D_m +$$

(i, ii) (iii) (iv)

$$C_s D_f^2 u/D_s \qquad \{25\}$$

(v)

where (i) and (ii) are eddy diffusion and mobile phase mass transfer related terms, (iii) represents band spreading due to molecular diffusion, (iv) is the diffusion caused by mass transfer of the solute through a stagnant mobile phase layer, and (v) is the diffusion due to mass transfer through the flowing mobile phase. Generally, C represents a constant, d_p is the diameter of the stationary phase support particle, d_f is the stationary phase layer thickness, u is the mobile phase velocity, and D_m is diffusion in the mobile phase. This last term is important for our discussion of increased viscosity effects on band broadening.

Synder and Kirkland[220] use the Wilk-Chang equation to calculate D_m values:

$$D_m = 7.4 \times 10^{-9} (\psi^2 M_2)^{0.5} T / \eta V_1^{0.6} \qquad \{26\}$$

where ψ is the association factor for the solvent, M is the molecular weight of the solvent, T is the temperature in Kelvin, η is the viscosity, and V_1 is the molar volume of the sample molecule. Temperature is directly proportional to the diffusion coefficient, which appears three times in the above expression for plate height. In the diffusion expression, temperature is indirectly represented by viscosity.

To obtain a qualitative sense of the overall temperature effect on plate height, simply analyze the effect of decreased temperature on D_m and η. We know already that a temperature decrease results in a decrease in the rate of mobile phase diffusion. A decreased temperature also affects viscosity, and if we assume the mobile phase is a Newtonian fluid, Shaw[221] said that in the case of a simple capillary viscometer,

$$\eta = k \rho t \qquad \{27\}$$

where k is the viscometer constant, ρ is density, and t is time. Since density is equal to mass over volume, and volume is directly proportional to temperature, then as temperature

decreases, volume decreases, density increases, and by the above expression, viscosity increases. So D_m, mobile phase diffusion rate, then will be decreased directly by a decrease in temperature from the temperature term in its numerator, and will also be decreased by a decrease in temperature due to the increase in the denominator's viscosity term.

Returning to our temperature-plate height analysis, note the effect of decreased Dm (due to decreased temperature) in the three places it appears. First, for (ii), mobile phase mass transfer:

$$\textbf{(ii)} = C_m D_p^2 u \,/\, D_m \qquad \{28\}$$

This term increases as temperature decreases, increasing H and degrading efficiency.

Second, for (iii), molecular diffusion:

$$\textbf{(iii)} = CdDm \,/\, u \qquad \{29\}$$

Here the term does decrease, but in liquid chromatography molecular diffusion is very slow compared to gas chromatography, and is relatively an unimportant contributor to plate height and may neglected..

The third appearance of D_m in the overall plate height expression is for stagnant mobile phase mass transfer (iv):

$$\textbf{(iv)} = C_{sm} D_p^2 u \,/\, D_m \qquad \{30\}$$

Here again, as temperature decreases this term will decrease. The stationary phase mass transfer term D_s also will decrease with temperature, and is also in the denominator of the last term (v).

Overall then, peaks will broaden as the temperature is decreased Reviewing the master resolution equation again:

$$Rs = (k'/1+k')\,(\alpha-1/\alpha)\,(\sqrt{N}/4) \qquad \{31\}$$

we have possible improvement in total resolution from increased capacity factors and selectivity at lowered temperature, but realize a decrease from the efficiency term. The experimental question is, with a given CSP-mobile phase-solute triad, will the gains in

capacity factor and/or selectivity be offset by the definite loss in efficiency as the temperature is lowered? No generalized predictions can be reliably made for these thermodynamic factors, making empirical necessary, especially for chiral separations, where the retention mechanisms are much less well understood compared to older modes. In addition, because of the wide variance in CSP mechanisms, and the not infrequent existence of multiple, possibly competing retention mechanisms, experimental evaluation of temperature, solute and mobile phase effects on total resolution is required.

Flow rate effects on efficiency and resolution, like temperature effects on efficiency, can be predicted theoretically for chiral stationary phase separations. Although flow rate effects on efficiency are not identical for different CSP-mobile phase-solute combinations, generally the same trends are seen as in achiral chromatographic modes.

The typical van Deemter curve, a plot of plate (H) versus mobile phase velocity, is used to evaluate the degree of band broadening caused by increases in flow rate. A parabolic curve results[222], but the steepness of the ascending parabola as flow increases varies with the type of chiral selector, and of course the particle size. The inclusive plate height equation {25} shows that H is directly proportional to u, mobile phase velocity (which is directly proportional to flow rate for all terms except molecular diffusion). H is directly proportional to the square of particle size, which then has the greatest affect on band broadening, but cannot be changed to optimize a given separation. (Recently, however, one manufacturer, Daicel has begun offering some of its popular cellulose packings in both 10 and 5 μm sizes.)

If the proposed retention mechanism included kinetically slower processes, such as inclusion (host-guest) complex formation (versus faster attractive interaction-based complexes), then factors such as flow rate and temperature could affect the total number of times a given complex could form. Lowered temperatures slow molecular motion and may give solute species a better opportunity to interact with the inclusion complex site, increasing

capacity factors and possibly selectivity. In the same manner, slower flow rates, in addition to increasing efficiency, might also give rise to more host-guest complexations.

For a mixed or competing bi-mechanistic situation, in which one mechanism was of the inclusion complex and the other depended on attractive-repulsive interactions, changing flow rate, temperature and mobile phase composition could conceivably shift the balance from one mechanism to the other. Our results would seem to suggest this is the case for one of the test columns.

Mobile phase effects include both the type of alcohol or other strong solvent modifier and its percentage relative to the weaker solvent, if a binary mixture. In addition, CSP normal phase mobile phases frequently include a third component, such as acetonitrile, in small amounts to improve peak shape.

Regardless of the CSP type, the stronger solvent component competes for interaction sites with the solute molecules, as described in Section 3.2. For the single-mechanism R-dinitrobenzoylphenylglycine CSP, an alcohol such as 2-propanol competes with the solute for hydrogen-bonding interaction sites. Increasing the mole fraction of the alcohol decreases the capacity factors of the enantiomers, and as Zief, Crane and Horvath[223] found, increasing the alcohol's steric bulk increases selectivity in some situations. The general relationship of Soczewinski and Wachtmeister[224] holds true for normal and reversed-phase modes:

$$\log k'_{ij} = a_{ij}X + b_{ij} \qquad \{32\}$$

where k' is the capacity factor for a particular solute i on phase j, and a and b are constants characteristic of this solute-stationary phase, and X is the mole fraction of the stronger solvent. Many different statistical models for retention prediction are based on this relationship, often including other factors relating to stationary phase (number of carbons in the brush, or carbon coverage, for example) and solute structure, as noted in Chapter 2.

More specifically for chiral separations, Zief found that increasing modifier polarity, for Pirkle-type CSPs, also decreased capacity factors. His study did not find changes in selectivity with 2-propanol concentration changes, but our research came to a different conclusion.

Although commonly used, 2-propanol has a distinct disadvantage in terms of efficiency due to its high viscosity. The chlorinated hydrocarbons, acting as hydrogen acceptors, have lower viscosity.

3.5. Specific Mechanisms Suggested for DNBPG and Cellulose CSPs

Pirkle and many others have used a variety of approaches to study the mechanism responsible for the Type I DNBPG enantioselectivity. This CSP is probably the best characterized and longest used of the five major types. An (R)-DNBPG (Figure 1) was chosen to establish a benchmark CSP due to this large amount of experimental evidence concerning its mechanism.

A less well understood CSP, but one with a potentially greater range of solutes which can be separated without derivatization, is the Type II tris cellulose(3,5-dimethylphenylcarbamate) (Chiralcel OD, Figure 2). The generally accepted mechanism for this cellulose phase includes both the attractive-repulsive interactions between individual atoms (responsible for Type I retention), combined with a an inclusion (host-guest) complex which forms between the β(1,4-glucose) units, arranged in flat sheets (see Figure 6), and the solute. Cellulose CSPs without the three functionalized hydroxyl groups on the ring are well known, and are Type III CSPs, depending entirely on inclusion. The Chiralcel OD, then combines elements of both Types I and II to provide great versatility.

However, few in-depth studies have been done for the OD column, compared to the Pirkle types. Okamoto and Hatada[225,226], who developed many of these derivatized cellulose phases, have concentrated mostly on new cellulose types by coupling new groups to the carbohydrate ring and specific applications, rather mechanistic studies. A recent publication from Witte, et al[227] does attempt to link temperature, mobile phase composition and solute structure to some conclusions regarding retention mechanisms for a series of aminotetralins. This study is noteworthy for the variety of temperatures and solutes used, but rather disappointing in that only one polar mobile phase modifier was used (ethanol), and at only two concentrations. A more serious shortcoming for the mechanistic conclusions is that the authors ignored influence of the inclusion mechanism, only considering the attractive-repulsive interactions arising from π-π electron charge transfer and hydrogen bonding between CSP and solute. In addition, only resolution and capacity factor are discussed; their relationship as described by the resolution equation {1} is ignored.

Two important characteristics were noted in the De Zeeuw work, however. They found that aminotetralins which exhibited greater structural potential for π-π interactions (those having ethylphenyl or ethylthienyl substituents on the amine) with the CSP showed improved resolution as the temperature was lowered. But for another aminotetralin which depended upon hydrogen bonding (more energetic force) and had a primary amine, higher temperature resulted in increased resolution due to decreased band broadening, according to the authors. Their conclusion, that decreased temperature does not improve resolution for solute-CSP complexes which depend on hydrogen-bonding, is not proven by their data, which showed only two aminotetralin racemates which did NOT exhibit improved resolution at low temperatures. One of these, having a single phenol function, also shows a clear maxima in its resolution versus temperature data. The π-π interactions may be weaker energetically than hydrogen bonding, and perhaps enhanced at lowered temperatures, but the aminotetralin data does not show this.

A need still exists to determine what enantioselective mechanism for the Chiralcel OI column is affected by changes in temperature, mobile phase and flow rate. Experimentally, these variables are changed and mechanism information might then be inferred, but only if a well-characterized CSP-solute combination, subjected to the same set of variables, is availabl for comparison.

Our research depended upon the DNBPG column-TFAE combination to provide the baseline results, with an established mechanism. Both TFAE and another solute, trans-stilben oxide (trans-2,3-diphenyloxirane, Figure 4), which is not resolved on the DNBPG, separate easily on the Chiralcel OD. The DNBPG-TFAE complex depends on attractive-repulsive interactions only, while the OD-trans-stilbene oxide complex separates mainly through an inclusion complex. A multiple mechanism situation is represented by the OD-TFAE separation.

Figures 14 and 15 show two possible diasteriomeric complexes between the (R)-DNBPG stationary phase with (R)- and (S)-TFAE, respectively. Many interaction possibilitie have been proposed for the DNBPG-TFAE combination, but all are similar in that a π-π interaction is always shown between the electron-accepting dinitrobenzoyl group and the electron-donating anthracene. Hydrogen bonding is always proposed between the TFAE's hydroxyl hydrogen and a carbonyl on the CSP. The CF_3 group is also capable of acting as a negative end of another hydrogen-bonding group. The problem with many of the previous complexes shown in the literature has been the two-dimensional nature of the figures and the incompleteness; usually only two or three interaction sites are delineated.

Lipkowitz[228], as mentioned in Chapter II, has applied sophisticated molecular modeling software, based on quantum and molecular mechanics, to represent the DNBPG-TFAE complex. However, the figures resulting from the computations did not well convey t three-dimensional quality of the interaction, nor did they indicate exactly which groups and atoms were interacting.

We have used a version Allinger's[229] MM2 (molecular mechanics) program, as included in the Chem3D software (Cambridge Scientific Computing Inc., vers. 3.1) to initially construct a three-dimensional ball and cylindrical bond structure, which was then modified to achieve the lowest potential energy configuration using the "minimization" command. Ring closures, structural error and steric energy were minimized. Since the position of groups connected by single bonds, which can rotate, is set by the user and the conformation is not changed during minimization, the R and S-TFAE structure were built identically, except for the stereochemistry around the chiral carbon. The final bond lengths for all three structures ar listed in Appendix A.

The indicated molecular interactions were selected after working with plastic molecul models of the structures, then identifying the corresponding atom numbers in the Chem3D figures. Table VI summarizes the attractive and repulsive interactions shown by dotted and solid arrows, respectively, in Figures 14 and 15. Note that the (S)-TFAE complex, which elutes last and is therefore the more stable one, exhibits two more attractive interactions than does the (R)-TFAE, which elutes first.

The possibility of a mixed mechanism, or at least a situation in which the predominan mechanism will depend on solute, mobile phase and perhaps general chromatographic conditions such as temperature and flow rate, exist for the cellulose CSP. It should be possibl to utilize the two solutes and various conditions of temperature, flow rate and mobile phase t make inferences about which mechanism operates under what sort of conditions by examinir results of such experiments. Plots of resolution and the three constituents of the resolution equation, along with thermodynamic analysis using van't plots, can furnish at least qualitati evidence which supports or rejects the hypothesis of a mixed mechanism for the Chiralcel O column. In addition, basic optimization information can be obtained from the resolution vers temperature and mobile phase composition plots.

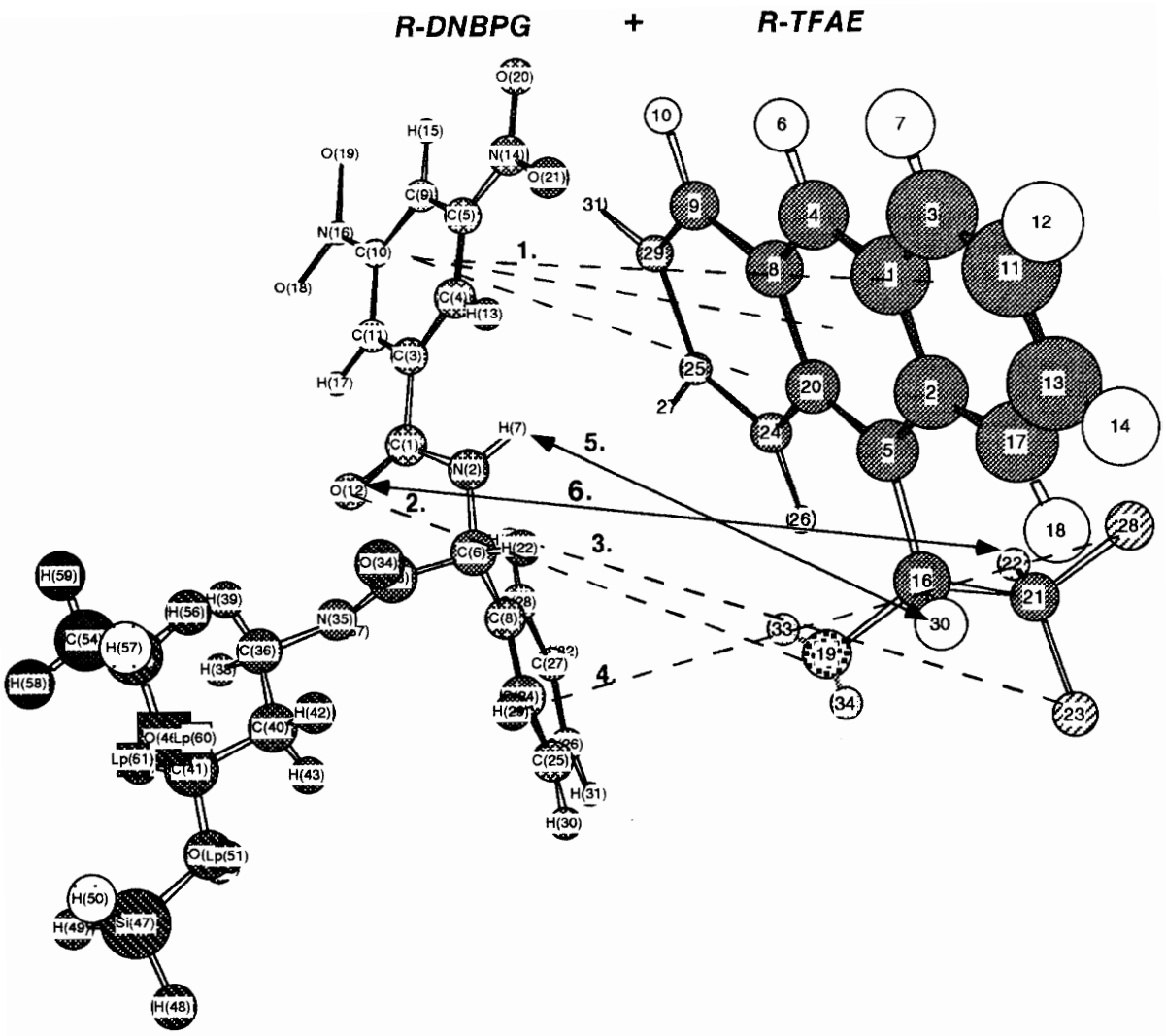

Figure 14. The proposed diasteriomeric complex between (R)-DNBPG and (R)-TFAE, based upon minimal energy conformations of each molecule as calculated by Chem3D software.

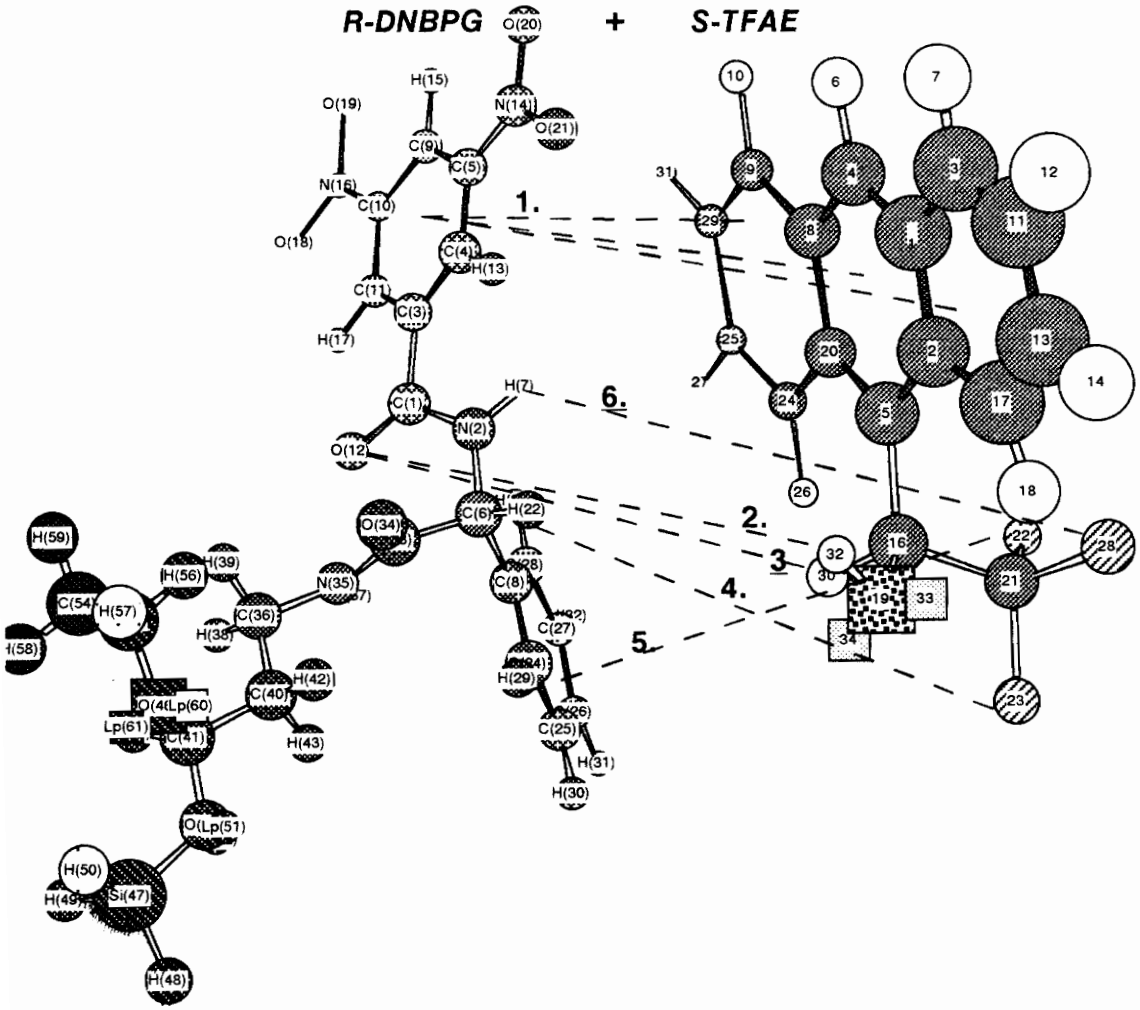

Figure 15. The diasteriomeric complex between (R)-DNBPG and (S)-TFAE shown with the attractive interactions 1 through 6.

Table VII Interactions between atoms for the (R)-DNBPG complexes with (R) and (S)-TFAE. The subscripts refer to the atom numbers in Figures 14 and 15. A "+" indicates an attractive interaction, a "–" a repulsive one.

Interaction Number:	**(R)-TFAE**	**(S)-TFAE**
1.	π-electron acceptor-donor, +	π-electron acceptor-donor, +
2.	O_{12} + H_{32}	O_{12} + H_{32}
3.	H_{22} + F_{23}	O_{12} + H_{30}
4.	H_{27} + F_{28}	H_{22} + F_{23}
5.	H_7 – H_{30}	H_{29} + F_{22}
6.	O_{12} – F_{22}	H_7 + F_{28}
TOTAL:	**6 Interactions, 4 attractive**	**6 interactions, all attractive**

3.6 Model Stationary Phase Studies Via Self-Assembled Monolayers

3.6.1 Self-Assembled Monolayer Theory

The previous discussion noted that some inferences are possible about chiral selection mechanisms from the chromatographic data. However, as was noted in the Introduction, hard evidence for or against a theoretical interaction between two particular atoms or functional groups requires some other kind of analytical approach.

Fourier Transform Infrared Spectroscopy was chosen as a method by which molecular information, especially concerning intermolecular hydrogen bonding, could be obtained. De Haseth's 1991 work with a TFAE–[BOC-L-Valine] complex in solution presented an excellent stating point, but lacked a significant element which was a part of the "real" chromatographic system: a solid support to which the chiral is attached. Such *ex situ* IR and NMR studies as de Haseth's lack a support, and the additional degrees of freedom afforded the complex in solution may distort the results, especially if enantiospecific differences between the two complex depend on steric hindrances, which may not be present in solution.

Together with Dr. Mark Anderson, who has experience with both self-assembled monolayers and various spectroscopic techniques used to evaluate surfaces, an *in situ* approach to investigate chiral retention mechanisms was chosen using a chiral functional group to model a CSP, and this group was to be a monolayer on a gold surface. The chiral molecule chosen was N-(BOC)-L-valine complexed with (R) and (S)-TFAE so that results could be compared to the de Haseth *ex situ* work.

As described in Chapter II, monolayer surfaces have been utilized in studies of many surface chemistry phenomena in which a well-characterized, single or multiple payer of molecules is required. Although never applied to modeling chromatographic surfaces, it would

seem to offer a promising method to overcome the difficulties in working with the complicated, difficult to characterized surface in a typical derivatized silica gel support liquid chromatography column. The disadvantage of using such a model involves the synthetic preparation and analytical confirmation of the monolayer, in addition to questions concerning how well such a surface mimics derivatized silica gel.

Sagiv's group at the Weizmann Institute compared adsorbed monolayer technology to the older Langmuir-Blodgett (LB) procedure for constructing a monolayer and noted that the self-assembly by adsorption is a fundamentally different process.[230] The self-assembly of amphiphiles by direct adsorption from a liquid solvent onto a surface was discovered by Bigelow and reported in 1946.[231] Self-assembly offers advantages in terms of surface layer stability, homogeneity and final structure compared to the LB method, as well as simplicity. Surfaces such as platinum, silicon, and oxidized silver and gold have been used as substrates since the early 1980s.

According to Sagiv et al, amphiphilic molecules (having a polar head group and non-polar tail portion) will adsorb to an appropriate surface, forming a single layer, oriented such that the non-polar tail is approximately 30° to the surface normal, with the polar head group interacting with the source. This interaction may be initially a physisorbtion process, and later chemisorption with covalent bonds. It depends on the nature of the substrate and head group, as well as the solvent and reaction conditions. Chemical activation of the non-polar surface must take place before another layer is added. Multilayers are achievable, using classic reaction strategies, but these may have to be modified somewhat. Polar groups such as aromatic and alkanethiols and disulfides on gold, fatty acids on silver and chlorosilanes on silicon.[232]

The physical and chemical adsorption of the monolayer is governed by basic potential energy and thermodynamic considerations, as given by Atkins.[233] Figure 16 shows that this process for chemisorption involves a greater negative enthalpy change, and has a greater

overall binding energy (ΔG), usually over 40 kJ/mol versus around 25 or less for physisorbed species. Since a decrease in enthalpy occurs when it is adsorbed onto a surface, and for the process to be spontaneous (-DG) DG must also be negative. Note that although a small activation energy is shown, Atkins also adds that many gas-phase adsorptions on metal surfaces "appear to be non-activated."[234] This is important for our work in that it is sometimes possible to react the same compound with a gold surface in either a solution (liquid phase) or gas phase environment, depending on the volatility of the surface-modifying agent. Due to the lower or non-existent activation energy, a gas phase process is preferable from a thermodynamic viewpoint. In addition, some evidence exists that for some compounds, any liquid solvent present can prevent chemisorption, and that the only successful method is a gas phase deposition, especially in cases where a reactive intermediate (an acid chloride, for example) is being added in building up multiple monolayers.[235]

The kinetics of adsorption are in general governed by the Langmuir isotherm relationship, which relates the rate of filling of adsorption sites to the gas pressure above a surface. The sticking probability (rate of adsorption of molecules divided by rate of collision of molecules with the surface) decreases as the surface sites are filled, expressed formally as molecules per square centimeter. The fractional cover or θ is defined by Atkins as the number of adsorption sites filled divided by the number of sites available.[236] The Langmuir isotherm then is defined as:

$$\theta = \mathbf{K}p_A / (1 + \mathbf{K}p_A) \qquad \{33\}$$

where $K = k_a/k_d$, the rate of adsorption divided by desorption, and p_A is the pressure of the adsorbing species.

In practice, self-assembling monolayer adsorption in the liquid phase seems rather insensitive to concentration of the adsorbing species, although few rigorous studies have been made. Bain, Evall and Whitesides in 1989[237] concluded that thermodynamics control the composition and structure of alkylthiol monolayers adsorbed onto gold surfaces from solvents

of various polarities. They did not quantitatively evaluate the adsorption isotherms, however. Thiol adsorption is favored over disulfide, and they proposed a two-step process of physisorption followed by chemisorption. Simple equilibrium expressions do not explain the composition of monolayers formed from mixed solutions. In polar solvents, adsorption of the less polar component is favored, and in non-polar solvents, adsorption of the more polar component is favored, supporting the conclusion of thermodynamic control over the process. The same conclusion was reached by Shaw for bulk solution adsorption of various fatty acid solutions in toluene and water onto silica gel and charcoal.[238]

Shaw also gives the appropriate form of the Langmuir and Freundlich equations which describe solution adsorption:

$$x/m = (x/m)_{max}\, a\, c \,/\, (1 + a\, c) \qquad \{34\}$$

and:

$$x/m = k\, c^{1/n} \qquad \{35\}$$

where x is the amount of solute adsorbed by a mass m of solid, c is the equilibrium solution concentration, with a, k and n as constants.

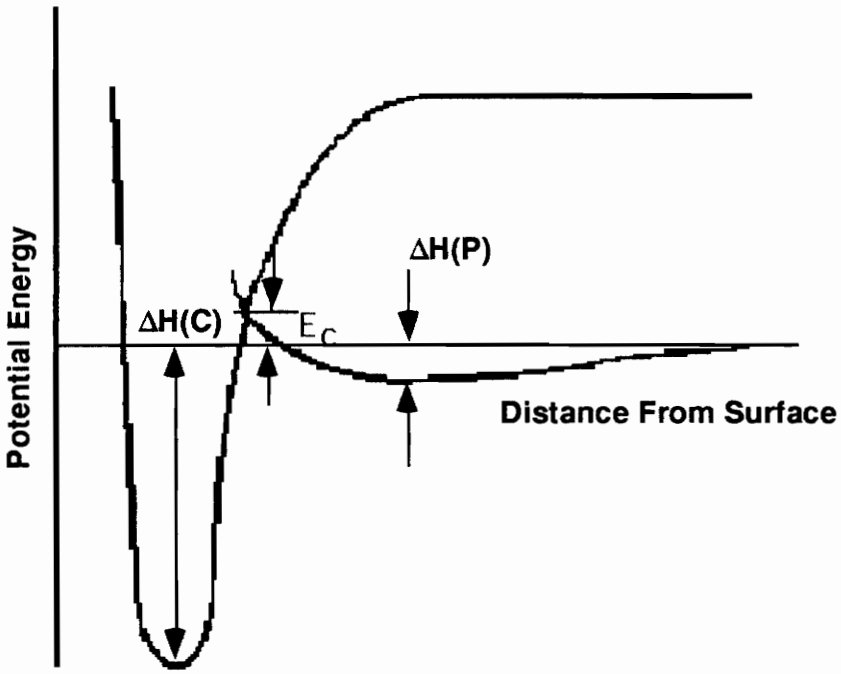

Figure 16. The potential curves for physisorption [DH(C)] and chemisorption [DH(P)] are shown, as well as Ec, the chemisorption activation energy.

After Atkins, p. 939.

3.6.2 Summary of Surface Modification Strategies

The original strategy was to create a model chiral stationary phase using chemistry which was very similar to that which has been utilized for silica gel-supported CSPs. A hydroxyl surface, obtained from solution phase deposition of 4-hyrdoxythiolphenol (4-HTP), would be analogous to the silanol surface of silica gel. Rogers et al synthesized BOC-L-valine CSPs on silica gel supports in 1987.[239] This was the first scheme we attempted, using a 4-amino-dimethylmonomethoxysilane (see Figure ?) to furnish a primary amine, which then could theoretically be linked to the valine using a peptide condensing reagent N-ethoxycarbonyl-2-ethoxy-1,2-dihyroquinoline (EEDQ).[240,241,242] However, after successfully attaching the thiophenol layer, the silane did not react reliably, probably requiring more vigorous conditions.

The next series of experiments eliminated the silane, instead using 4-aminothiophenol (4-ATP) directly. Again, the first monolayer was established, but the valine condensation was unsuccessful. A liquid-phase coupling of the 4-ATP and BOC-L-valine was also attempted, but the reactive thiol group interfered with a biphasic extraction step using an aqueous layer.

The final series of attempts featured a bimolecular thionyl chloride nucleophilic substitution reaction to form an acid chloride from a carboxylic acid group, which then can be reacted with the valine, producing an anhydride.[243,244] We decided on two different strategies, both using 11-mercaptoundecanoic acid (MUA) to provide a carbon "brush" to function as a spacer, and to provide the thiol on one end, for attachment to the gold surface, and the carboxylic acid at the other to form the acid chloride.

The approach tried first was to oxidize the MUA with iodine and potassium iodide, forming the disulfide, which was then made into a di-acid chloride and then coupled with BOC-L-valine. Liquid phase deposition was then performed.

Since thionyl chloride is volatile, we also performed a vapor phase reaction with the gold surface having a liquid phase deposited layer on MUA. While still under vacuum, since the thionyl chloride is very water reactive, we flooded the surface with a valine solution in the aprotic, moderately polar solvent methylene chloride. Efforts to react the acid chloride surface with valine in the vapor phase failed, probably due to its low vapor pressure.

Although ethanol has been used traditionally for liquid phase alkylthiol and disulfide deposition, we preferred dried methylene chloride without the acidic proton. The more polar groups attached to the non-polar alkyl chain in our experiments could have associated too well with ethanol, discouraging surface adsorption. Ethanol did not work well with the 4-HTP, and was not used thereafter. In addition, the acid chloride intermediate and anhydride product molecules are both water sensitive, so every effort was made during the preparation to keep out water, which is very difficult with ethanol. Finally, the IRRAS experiment is also water sensitive, and we obtained much better spectra at every stage of the preparation when the slide was kept evacuated in a desiccator.

3.6.3. FTIR-Reflectance Absorbance (IRRAS)

Of the two spectroscopic techniques used in this research, Infrared Reflection Absorption Spectroscopy (IRRAS) and Polarization Modulation-IRRAS (PM-IRRAS), the former is instrumentally easier to set and run, but more demanding in that good spectral results depend on having a reference sample and a sample compartment purged of residual water and carbon dioxide.

The IRRAS method has been used extensively for monolayer characterization, including functional group characterization, spatial arrangement of the groups, and coverage.[245] Griffiths and de Haseth[246] note that the signal intensity of the R-A (reflectance-

absorbance) spectra depends on both the grazing angle of the incident beam and the reflectivity of the metal surface upon which the monolayer sample is attached. The thickness of a film that will give the same signal intensity for an R-A spectrum as that produced using a conventional transmittance method and a 10 mm film is:

$$\textbf{Thickness } (\mu m) = 2\ d\ /\ 10 \cos \alpha \qquad \{36\}$$

where d is 3.5 μm and α is the angle of incidence. The practical effect is that as the angle increases, the minimum thickness required for an acceptable signal-to-noise ratio decreases, so that very thin (1 nm) monolayers can be analysed. As a comparison, the thickness of the polystyrene test film supplied with IR spectrometers is about 50 μm.

Two other factors also make possible very thin film analysis. A highly reflective gold (over 90% of the incident light is reflected), silver, platinum or polished silicon wafer surface is required. Porter[247] gives a detailed of the dependence of the mean square electric field (MSEF) upon the reflectivity of the surface media and the influence of the air/media interface for electrical vectors in the x, y and z planes. Generally, Ex and Ey are negligible for all incident angles, with Ez for the air/gold interface at its maximum for an incident angle of 79. The other parameter which is taken advantage of is the intensity enhancement of light polarized parallel to the surface (S-polarized light) compared to light polarized perpendicular to the surface (P-polarized). Griffiths claims the use of the P-polarized incident beam can result in up to a 25x improvement due to the constructive interference between the S and P-polarized beams. This is due to the fact that S-polarized light is reflected 180° out of phase, and destructive interference occurs at the metal surface, making the reflected s-polarized light intensity zero. P-polarized light is reflected 90° out of phase, and constructive interference takes place.[248]

For acceptable results for monolayers on metal substrates, then, a highly reflective surface (gold preferably), a high incidence angle (80° or higher), and P-polarized light are

required. In addition, the use of Fourier Transform instruments is a given to provide adequate sensitivity. Monolayer analysis is not possible with a grating instrument.

3.6.4 Polarization Modulation FTIR (PM-IRRAS)

Figure 17, from Buffeteau[249] shows the details of a Polarization Modulation IRRAS experiment. The IRRAS spectrum of a compound *d* adsorbed on a metallic surface can be represented by:

$$\mathbf{A\ (d) = 1 - R_p(d) / R_p\ (0)} \qquad \{37\}$$

where $R_p(d)$ represents the absolute reflectivity of a p-polarized beam from the reacted surface and $R_p(0)$ represents reflectivity from the blank surface (typically a freshly oxidized surface).

For very thin films, or surfaces with many interfering bands (such as water), many scans are required over many minutes to obtain an acceptable S/N. Small changes over this time in the instrumental parameters, as well as changes in the sample compartment atmosphere, make it difficult to obtain a good spectrum.

The PM technique takes advantage of the fact that incident S-polarized beams give no MSEF for interactions with the surface (no absorption from surface-bound species occurs), but the molecules in the bulk layer (either a gas or liquid above the surface) absorb *both* S and P-polarized light. Thus we have a situation in which we can select the desired P-polarized signal for the surface species from the combined S and P-signals representing both the bulk and surface species. This is achieved electronically with a photoelastic modulator (ZnSe P.E. Module. in Figure 17), which switches between S and P polarization at some preset rate, generating, after further signal processing, the differential reflectivity spectrum:

$$(\Delta R/R) = (R_p - R_S) / (R_p + R_S) \quad \{38\}$$

where R_p and R_s are the P and S-polarized reflectivities.

The practical results are a significant increase in sensitivity to the surface-bound species of interest, together with a much decreased sensitivity to the interfering bands from any gas (CO_2 and H_2O) or liquid (in our case the solvent used for the enantiomeric solute) present in the bulk layer above the surface. In addition, Buffeteau notes that now a true in situ, long-term monitoring of the surface is possible, enabling surface reaction kinetics to be studied in real-time.[250]

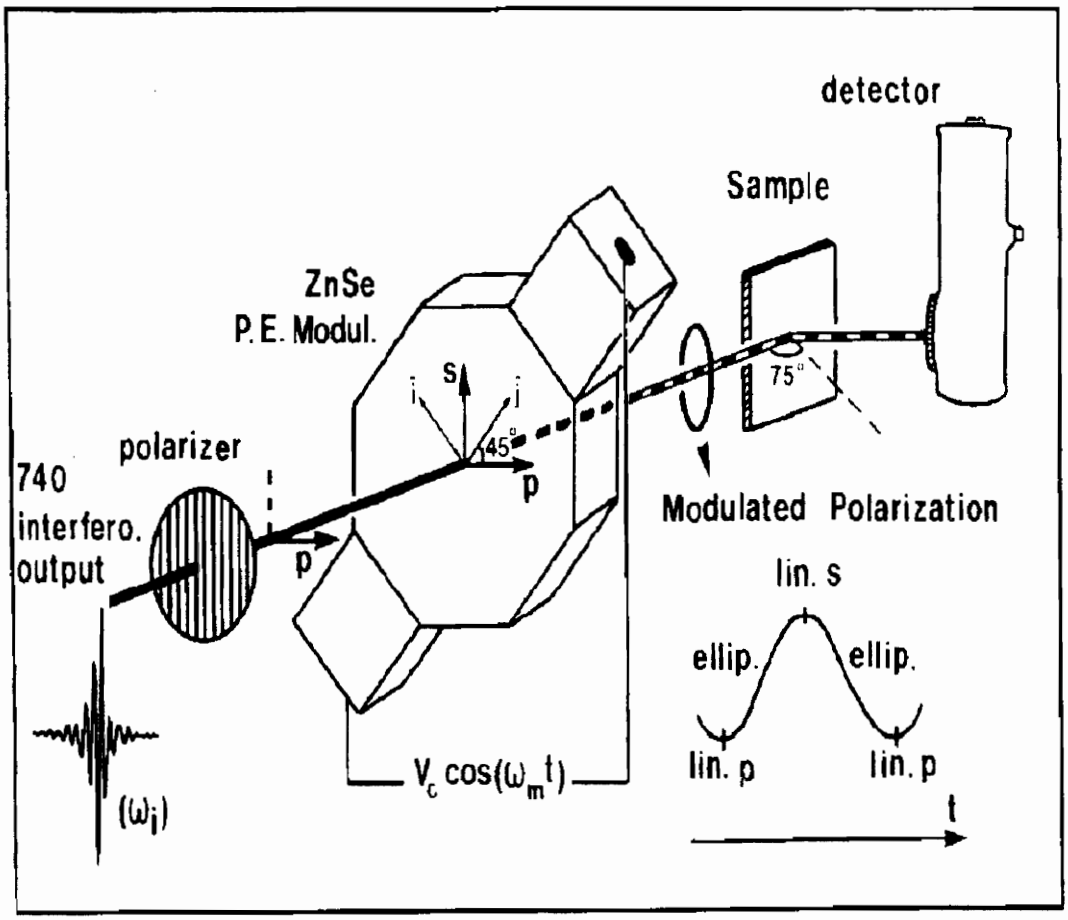

Figure 17. This is a generalized representation of the PM-IRRAS experiment.

After Buffeteau et al, ref. 249.

CHAPTER IV

EXPERIMENTAL

4.1 Early Optimization Studies

Instrumentation and Solutions

All chromatography was performed with Hitachi equipment (Hitachi Instruments, Mito, Japan). A Hitachi Model 655 isocratic pump, and Model 655 variable wavelength UV-visible spectrophotometric detector with a 3 µl flow cell were used without modification. Wavelength used was 254 nm unless stated otherwise. The injector valve used for most of the experiments was a Rheodyne Model 7120 (Rheodyne, Cotati, CA) with a 5 µl loop. A Hewlett-Packard Model 3394 Inkjet integrator-plotter (Hewlett-Packard, Avondale, PA) received a 0 to 1 volt analog signal from the detector .

Temperature control of the column was maintained with a 30 cm-long plastic column water jacket (Alltech Assoc. Inc., Deerfield, IL) attached to a Lauda RM-6 circulating/cooling bath (Brinkmann Instruments, Westbury, NY). Deionized water served as the circulating heat transfer fluid for temperatures between 25 and 3.3°C, and a 1:1 ethylene glycol-water mixture served adequately for temperatures as low as -30°C. As shown in Figure 25, the mobile phase reservoir, a glass 1-liter bottle, was placed in a plastic dish pan and surrounded with ice and water in order to cool the mobile phase before it reached the column jacket. A polystyrene foam lid was shaped to fit over the top of the pan, surrounding the reservoir, to further help maintain constant temperatures. A thermometer was used to monitor the bath temperature, adding ice or water to achieve the desired bath temperature. The temperature of the mobile phase inside the reservoir was also checked to ensure adequate equilibration time when the

system temperature was changed. All tubing downstream of the injector (1/16" O.D., 0.007" I.D.) was insulated with scraps of foam rubber and aluminum foil to minimize temperature gradients. The injector body and the tubing and connections on the inlet and outlet sides of the column jacket were also insulated in a like manner.

Test solutes of (R)- and (S)-2,2,2-trifluoro-1-(9-anthryl)ethanol (Figure 3), plus the racemic mixture (Aldrich Chemical, Chicago, IL) were made up at the concentration of 30 mg/ml (w/v) in HPLC-grade hexane (J. T. Baker, Phillipsburg, NJ). The other test compound, trans-stilbene oxide (Aldrich Chemical), was also prepared in hexane at 500 μg/ml w/v), the higher concentration being necessary to obtain similar peak heights without attentuation adjustment. As can be seen in Figure 4, the trans-stilbene oxide lacks TFAE's anthracene substructure, a highly sensitive UV chromophore. To all of these mixtures was added HPLC-grade toluene (J. T. Baker) at a level of 200 μg/ml (w/v) to function as a void volume marker. Although Pirkle recommends the use of 1,3,5-tertiarybutyl benzene[251] (TBB) as an absolute indicator of zero retention by the 3,5-dinitrobenzoylphenylglycine (DNBPG) column, our goal was not absolute measurement of void volume. Toluene retention time was compared to TBB for both the DNBPG and cellulose-based columns (Chiralcel OD) used in the optimization studies and found to give be statistically equal.

The chiral stationary phase columns used were an (R)-N-(3,5-dinitrobenzoyl) phenylglycine (DNBPG, J. T. Baker, Phillipsburg, NJ) and a cellulose tris(3,5-dimethylphenylcarbamate, trade name Chiralcel OD) made by Daicel Chemical Industries Ltd., Tokyo, Japan and distributed in the U.S. by J. T. Baker. The structures of these CSPs are shown in Figures 1 and 2, respectively. Both were packed in 25 cm long by 4.6 mm I.D. stainless steel (SS-316) tubes and used silica gel as the support material. The DNBPG column features a covalently bonded stationary phase and 5 μm particles. The Chiralcel OD has a more fragile coated or adsorbed stationary phase on 10 μm silica gel. Because of its non-bonded nature, and the solubility and morphological properties of the cellulose, there are both pressure

and mobile phase constraints upon the use of the Chiralcel column. The covalent DNBPG (there are ionic varieties available) has only the usual silica gel pressure limitation (about 5,000 psi)252 and no constraints for solvent useage.

The latest J. T. Baker recommendations for the Chiralcel OD[253] warn against using any chlorinated solvent, ketones, toluene, acetonitrile over 1% and water over 10% because of the solubility of the cellulose. Our Chiralcel OD was rinsed with 5 column volumes of hexane at the end of each day, although we were using the recommended 2-propanol/hexane mobile phase.

As noted earlier, J. T. Baker HPLC-grade hexane and 2-propanol were used in a 70:30 proportion for all runs in the initial study (25 to 3.3°C). One or two liter batches were made by measuring individually the appropriate volumes using a graduated cylinder, then combining, using a sonicating bath to ensure complete mixing, and degassing, of the viscous alcohol. Since the mobile phase was predominantly the non-polar hexane, in which gases have a very low solubility, no constant helium purge was necessary. This method proved satisfactory for all hexane-propanol mixtures; bubble formation in the pump or detector cell was not a problem.

Early on it was noticed that different lots of 2-propanol effected the capacity factor and selectivity due to the differences in water content. This was first discovered upon opening a new, sealed 4-liter bottle of alcohol and seeing as much as a 50% increase in capacity factor results for the Chiralcel OD column. Similar, but less severe effects were noted for the DNBPG column also. (See Chapter IV for bar graph results.of the effect of varying amounts of water in IPA.) After deciding upon a lot which gave similar results to the original, we were always careful for keep the bottles tightly sealed and to make up fresh batches of mobile phase weekly.

Data Handling

A microcomputer spreadsheet program was used to calculate the results for capacity factor (k'), selectivity (α), efficiency (N) plate height (H), and resolution (R) for each of the enantiomers separated in each injection. Since approximately 960 peaks were analysed for the complete 25 to 3.3°C part of the research, a fast, semi-automated method of data reduction was required.

To avoid manual measurement of each peak, the area-to-height ratio, automatically calculated by the integrator, was used to obtain an expression for N, number of plates, that the spreadsheet program could utilize. Raw data consisted of five values from the integrator report for each injection: t_0, t_{r1}, t_{r2}, $(A/H)_1$ and $(A/H)_2$, where (A/H) is the integrator-calculated ratio of peak area divided by height. Initially, the spreadsheet Quattro (Borland International, Scotts Valley, CA) running on an IBM-XT clone (Data Fox 88-2, 20 megabyte hard drive, 640K RAM, Intel 8088 processor, DOS 3.1, from Data Fox, Phoenix, AZ) was used to generate data sheets which were then inspected for errors. The individual k', α, N, H and R values for each of six replicate runs per given temperature and flow rate, for each solute on each of two columns, was then manually entered into Cricket Graph (version 1.3.2, (Computer Associates International, Islandia, NY), running on a Macintosh IIsi computer (40 megabyte hard drive, 5 megabytes of RAM, Motorola 68030 processor, Operating System 6.07, Apple Computer, Inc., Cupertino, CA) where X-Y plots were generated.

The procedure for obtaining an expression for efficiency, N, and subsequently resolution, R, is derived from the basic definition of N, as detailed by Bidlingmeyer and Warren[254] :

Assuming a Gaussian peak shape:

$$N = t_r^2 / \sigma 2 \qquad \{39\}$$

By definition:

$$\text{Area} = \sqrt{2\pi}\ \sigma\ h \qquad \{40\}$$

where A is peak area, s is the standard deviation, and H is the peak height.

Rearranging:

$$\sigma^2 = A^2 / 2\pi\ h^2 \qquad \{41\}$$

Substituting for σ^2 and rearranging:

$$N = 2\pi\ [t_r / A/h\ )]^2 \qquad \{42\}$$

For resolution:

$$R_S = \Delta t_r / 0.5\ (W_1 + W_2) \qquad \{43\}$$

where W is the width at base of peaks 1 and 2.

And for N (basic def.):

$$N = 16\ (t_r / W)^2 \qquad \{44\}$$

and

$$W = 4\ t_r / \sqrt{N} \qquad \{45\}$$

Substituting for W in R expression:

$$R_S = \Delta t_r / 0.5\ (4\ t_{r1} / \sqrt{N_1}) + (4\ t_{r2} / \sqrt{N_2}) \qquad \{46\}$$

Simplying:

$$R_S = \Delta\ t_r / 2[(t_{r1} / \sqrt{N_1}) + (t_{r2} / \sqrt{N_2})] \qquad \{47\}$$

The expressions for adjusted retention time ($t_{r'}$), capacity factor ($t\ r'_2 / t\ r'_1$), plate height in μm (L, column length in μm, divided by N) and selectivity (k'_2 / k'_1) are all standard.

Each injection was checked for reasonable A/H ratios, as a noisy baseline or a temporary anomaly can produce errors in the peak detection algorithms and thereby produce incorrect areas for a given peak. If any problems were found, the peak height and area were determined manually by measurement with a metric ruler. These errors sometimes occurred when running at very low flow rates and temperatures, which gave an exceedingly large peak width.

Table VIII. The simple Quattro spreadsheet program, which is nearly identical to the formulas used for a later Excel version (Excel 4.0, Microsoft Corp., Redmond WA), appears below in.

Column:	Variable:	Formula:
A	Temperature	RAW DATA
B	Flow Rate	"
C	t_0	"
D	t_{r1}	"
E	$(A/H)_1$	"
	t_{r2}	"
G	$(A/H)_2$	"
H	t'_{r1}	$D2-$C2
I	t'_{r2}	$F2-$C2
J	k'_1	$H2/$C2
K	k'_2	$I2/$C2
L	N_1	2*@pi*(($D2/$E2)^2
M	N_2	2*@pi*(($F2/$G2)^2)
N	H_1	250000/$L2
O	H_2	250000/$M2
P	α	$I2/$H2
Q		($F2-$D2)/(2*(($D2/@SQRT($L2)) + ($F2/@SQRT($M2))))

Experimental Procedure

Six replicate injections were made for each solute, at each flow rate (0.2, 0.5, 0.7, 1.0, 1.2, 1.5, 1.7 and 2.0 ml/min), at each temperature (initially 26, then 25, 20, 15, 10, 3.3°C) on each of the two CSPs described above, the DNBPG and the OD. Injections were begun at the highest temperature, doing a complete set of temperatures and solutes for one column, then switching to the other column. A 25 µl Hamilton syringe was rinsed with the 70:30 hexane-propanol mobile phase whenever the solute was changed, and the injected volume was always at least 15 µl, flushing the loop with 3x its capacity. Data was processed and inspected daily in case any runs produced unreasonable results due to the previously mentioned baseline and/or incorrect integration problems.

Calculations based on Meyer[255] were made to ensure that no more than a 1% increase in band broadening was occurring because of excessive extra-column volumes for the injector loop, detector cell or tubing. The volumes calculated to produce a 1% increase for these areas, with the volume used for the experiments in parentheses were:

Injector, flow rate of 0.2 ml/min (worst case) - 21 µl (5)

Detector, 21 µl inj., 0.2 ml/min flow ---------- 10.5 µl (3)

Tubing length, 0.2 ml/min, V_R =4.3 ml --------106 cm (74)

where V_R is the retention volume for a trans-stilbene oxide peak at 0.2 ml/min flow rate.

4.2 Sub-Zero Optimization Studies

Instrumentation

All parts of the HPLC system described above were unchanged, however a mobile phase heat exchanger was added to improve the pre-cooling of mobile phase. Generally, more insulation was added to both HPLC tubing and connections, and to the plastic tubing connecting the circulating bath to the column jacket. Figure 25 shows the complete apparatus.

Figure 27 shows the heat exchanger details. A 3 meter length of 1/16" by 0.04" stainless steel HPLC tubing was cut, coiled and placed inside a plastic column jacket made for 12 to 15 cm-long columns (Alltech Assoc., Deerfield, IL). Mobile phase output from the pump is plumbed into the heat exchanger, then to the injector valve. All tubing downstream from the heat exchanger jacket, as well as the jacket itself, is insulated. Cooling fluid (1:1 ethylene glycol/water) is delivered from the outlet of the column jacket through 0.25" O.D. plastic tubing to the heat exchanger jacket, and then routed back to the bath. The 1/16" O.D. tubing was chosen because it matched the jacket compression fittings, designed for standard HPLC tubing, and the large 0.04" I.D. provided a thin wall tube in which heat transfer could take place more quickly than with 1/16" tubing.

To test the performance of the heat exchanger, the device illustrated in Figure 26 was installed in the mobile phase tubing in front of the column jacket. It consists of a stainless steel "T" connector with 1/16" compression fittings. The bottom of the end opening was drilled out to provided a 1/16" passage clear through the connector, versus the constriction present in a normal compression fitting. A 1/16" O.D. thermocouple (Omega #CPSS-1160-12, Omega Engineering Inc., Stamford,CT) was inserted through the drilled out opening and secured with a ferrule and nut. The thermocouple was connected to a digital thermometer (Omega #HH-25TC) with factory calibration. A 70/30 hexane/2-propanol mobile phase was pumped through

the system at various flow rates. Temperature readings of the mobile phase were taken, after allowing time for equilibration, and compared with the temperature readout on the circulating bath.

Experimental Procedure

Similar procedures were employed with this series of studies, using both DNBPG and Chiralcel OD columns, and the TFAE and trans-stilbene oxide test probes. The first series of sub-zero work involved temperatures between 0.0 and -30°C, with 3 repetitions at each of 3 flow rates (0.5, 1.0 and 1.5 ml/min.). The important difference was in the mobile phase composition. It was decided that a **20%**, 2-propanol, 80% hexane mixture, versus the previous 30% 2-propanol, be used for these low temperature studies due to the greatly increased viscosity, and subsequent loss of efficiency, of 2-propanol at very low temperatures. Another reason was to prolong column life by decreasing the amount of polar modifier used.[256]

This decision had an unexpected result, which later proved to be very interesting.. In general, both capacity factors and overall resolution trends for R versus temperature plots were effected by this mobile phase change, and the effects were solute and CSP-specific.

A later batch of runs was made between +25 and -25°C, also at 20% alcohol, to verify the unexpected results for the Chiralcel OD column. A total of 3 repetitions were done at one flow rate, 0.7 ml/min, for all temperatures and solutes, with runs at 0.2, 0.5, 0.7, 1.0 and 1.2 ml/min at 25, 0 and -15°C for trans-stilbene oxide to generate van Deemter curves. The higher flow rates were not used due to the higher pressures at these very low temperatures, and the fragility of the cellulose (Daicel recommends a sustained maximum of only 750 psi.).

4.3 Mobile Phase Studies

Experimental Procedure

The initial reason for undertaking mobile phase experiments, aside from the fact that very little in-depth work had been done by chromatographers with chiral stationary phases, was a dramatic change in capacity factors when a new lot of 2-propanol was used.

Four separate studies with various mobile phases and solutes were completed. The first involved adding small amounts (<0.5%) of water to a 70/30 hexane/2-propanol (Lot B40615) mobile phase and plotting the resulting k', H, a and resolution versus the v/v% of water in the mobile phase. The initial step was to dry Molecular Sieve 5A for 6 hours at 200°C. After cooling, 100 g of Molecular Sieve was added to 1 liter of the premixed 70/30 hexane/2-propanol and the mixture stood, tightly sealed, for 24 hours. A 0.45 μm, 45 mm diameter Teflon filter (Gelman FP) was used to filter out the fines. The same mobile phase mixture was also prepared from undried hexane and Lot B40615 of 2-propanol for comparison. Small, 100 ml aliquots of the hexane/alcohol mobile phase were mixed with HPLC-grade water, using Eppendorf calibrated adjustable pipets (Brinkmann Instruments Inc., Westbury, NY) to give solutions with 0.011, 0.016, 0.021, 0.026, 0.066, 0.096, 0.0186 and 0.375% (v/v) water content. No miscibility problems were encountered due to the high alcohol content and the small amount of water added. Both TFAE and trans-stilbene oxide were separated on the Chiralcel OD column, with 2 runs each at 0.5, 1.0 and 1.7 ml/min flow rates. Plots of master resolution equation parameters versus water content were then constructed.

The second and third studies, done at different times, involved evaluating the changes in selectivity and resolution caused by differing amounts (30, 25, 20, 15, 10, 7.5, 5 and 2.5%, v/v) of 2-propanol in the predominantly hexane mobile phase. The test solute was held constant, with TFAE the choice, and 6 repetitions per condition.. Temperature and flow rate

were also constant at 25°C and 0.6 ml/min, and the column used first was the DNBPG, the best characterized of the two. The third and later study used the same design, but substituted the Chiralcel OD column, and only 3 repetitions per given mobile phase, and dropped the 2.5 and 5% levels due to excessive elution times (over 1 hour). The OD study was completed for both 25 and 5°C temperatures.

The fourth part of the mobile phase investigations involved changing the solute structure in an effort to determine what of any easily determined structural parameters could be correlated with retention. This experiment was a limited attempt at QSERR (Quantitative Structure Enantiomeric Retention Relationship), done with in collaboration with Scott Stauffer of the VPI Laboratory Automation Group. Solutions of TFAE and trans-stilbene oxide, as previously described, and racemic propranolol at 100 µg/ml in hexane, were separated at 30, 25, 20, 15, 10, 7.5 and 5% levels of 2-propanol in hexane. A fourth compound, acetylacetamide cinnamic acid methyl ester (AACA-ME), was also used, for a total of four compounds. The AACA-ME was synthesized by Dr. Brian Hanson's VPI group and was originally brought to our group for determination of enantiomeric purity. Six replicate injections were made for the TFAE and trans-stilbene (as noted above), and three injections at each condition were made with the propranolol and AACA-ME. Flow rate was 0.6 ml/min and temperature was constant at 25°C.

The usual chromatographic parameters were calculated for the results, and plots of natural logarithm of capacity factor versus percentage of isopropanol were made. A linear regression model was fitted to the plots and the slope determined. The structural descriptors were calculated for TFAE, trans-stilbene oxide and propranolol using an Environmental Protection Agency program SPARC.[257,258] We were unable to successfully run the program for AACA-ME without producing an error message; the reason was not clear. This program has since been revised, but we were not able to obtain a copy.

These descriptors which were thought most likely to correlate with capacity factors were α, the Taft-Kamlett hydrogen donor index, which gives an index to the amount of hydrogen-bonding free energy which is due to proton donating groups, and b, the Taft-Kamlett hydrogen acceptor constant.[259] In addition to the these, two other parameters called average molecular polarizability and molecular volume were also calculated by SPARC. The first three have been used successfully to predict appropriate chiral stationary phases for a particular enantiomeric structure and previous separation.[260] The molecular volume is calculated from the volume of a specific structural fragment, corrected for the number and size of fragments attached to it, and further corrected for shrinkage due to dipolar interactions, and expansion due to ordering by hydrogen bonding, and is given for 25°C. More information can be found in the SPARC manual or the Karickhoff[261] work.

Solubility of these solutes in hexane and octanol was also computed by SPARC, and is shown in Table IX.

To determine correlation between these structural descriptors and the mobile phase modifier percentage, each was plotted versus the slope from the corresponding ln k' versus percent alcohol curves. This technique has been used with success previously in QSRR studies of reversed-phase systems by Kaliszan[262] and Jinno[263], among others. According to Kaliszan, the logarithm of capacity factor is a linear function of the mole fraction of the strong solvent and two constants (slope and intercept), which are characteristic of a given solute and stationary phase. This is termed the Soczewinski-Wachtmeister relationship.

4.4 Model CSP Experiments

4.4.1 Substrate Material and Surface Preparation

One inch square glass slides, with a 50 Å-thick layer of chromium attached by an evaporative process, was purchased from Evaporated Metal Films Inc. (Ithaca, NY). The chromium functions as a binder for the overlying 1000 Å-thick gold surface layer.

Cleaning of the surface is necessary immediately prior to immersion in the solution containing the compound for adsorption. A zero-valence surface state was achieved by holding the slide with a disposable polypropylene forceps and immersing in a stirred and heated (120-130°C) solution of 75% concentrated sulfuric acid and 25% hydrogen peroxide (30%) for 2 minutes. The hot substrate was then immediately rinsed with 20 to 30 ml of HPLC-grade water (J. T. Baker, Phillipsburg, NJ) followed by 20 ml of HPLC-grade acetonitrile (J. T. Baker), then immediate drying under a stream of filtered, dried helium or nitrogen. The surface was visually inspected for sheeting after the water rinse, and inspected for homogeneity and streaks after the drying step. If satisfactory results were obtained, then the slide was immediately placed in the deposition solution. Slides destined to be used for background scans in the shallow grazing angle FTIR-RA analysis were stored in plastic boxes and scanned within one hour.

The "piranha" cleaning solutions were always disposed of after each use, and fresh slides were always used. Approximately one out of every five slides had a poorly coated gold layer and showed surface imperfections, or even partial loss of the gold layer, after removal from the cleaning solution. These were discarded.

Although literature procedures suggest absolute ethanol as a cleaning agent[264] , or optimally the use of surfaces with freshly vapor deposited gold layers,[265] the best procedure for our purposes was to use the very pure acetonitrile, rather than the ethanol, which was not

available as an absolute, HPLC-grade. We did not have access to gold vapor deposition equipment.

4.4.2 Liquid-Phase Monolayer Deposition

Solutions of the compound to be adsorbed on the gold surface were between 1 and 25 millimolar concentrations in GC/MS-grade methylene chloride (J. T. Baker) and were stored in wide-mouth, 250 ml glass jars with PTFE-lined plastic screw top lids. The solutions were kept for a maximum of two weeks before discarding.

The freshly cleaned and dried slides were immediately placed in the deposition solution and left at room temperature for 1 to 2 hours, after which forceps were used to hold the slide for removal and cleaning with 5 to 10 ml of methylene chloride, followed by drying in nitrogen or helium. Storage was in polypropylene boxes placed in an evacuated desiccator, with indicating calcium chloride (DriRite) in the bottom. It appears that the use of a desiccator helps to reduce the number of water bands when performing the shallow grazing angle FTIR-RA experiment.

The final, and successful attempt at attaching the N-tert.(BOC)-L-valine to the surface of the slide involved first depositing a monolayer of 11-mercaptoundecanoic acid (MUA), which was prepared as a 10 millimolar solution in methylene chloride. Immersion time was 60 to 80 minutes. The MUA was synthesized from 11-bromoundecanoic acid (available from Aldrich) by Dr. Mark Anderson (VPI &SU) using an established procedure.[266] Following characterization by FTIR-RA, the slide was placed in the glass reaction vessel for vapor phase deposition of thionyl chloride.

Other compounds deposited onto the gold substrate in earlier work included 4-hydroxythiolphenol (4-HTP, Aldrich Chemical Co.), which was prepared at a concentration of 25 millimolar in methylene chloride. Deposition time was 2 hours at room temperature. A 25 millimolar solution of 4-aminothiophenol (4-ATP, Aldrich) in methylene chloride was also

used, with a deposition time of 2 hours at room temperature. The 4-aminopropyl-dimethylmethoxy-silane (Hüls America Inc., Piscataway, NJ) was also used, at a concentration of 2% (v/v) in methylene chloride, and deposition time was 30 minutes at 50°C, with curing at 90°C for 30 minutes. The MUA-disulfide solution was made at a concentration of 1 millimolar (due to the small amount available) in methylene chloride. The BOC-valine-disulfide solution was 5 millimolar in the same solvent.

The solution phase synthesis product, described below, which attempted to make a disulfide compound with tert.-BOC-L-valine groups attached at each end, was dissolved in HPLC-grade chloroform (Fisher Scientific) at a 5 millimolar level, and a 3 hour immersion time at room temperature was used.

4.4.3 Liquid-Phase Synthesis of Di(11-N-tert.-(BOC)-L-valine)undecanoate sulfide)

The oxidative coupling of 11-mercaptoundecanoic acid to the disulfide was accomplished by titration with iodine/potassium iodide[267], followed by reaction with thionyl chloride, then coupling to N-tert.(BOC-L-valine).

•Oxidation of Thiol:

A 206 mg aliquot of the MUA noted above was added to 20 ml of HPLC-grade chloroform in a 50 ml beaker with a magnetic stir bar. A 1% iodine /2% potassium iodide (Fisher Scientific) solution in HPLC-grade water was added drop-wise to the stirred MUA via a 50 ml buret. A total of 13.9 ml of this solution was required to completely react with the MUA, as indicated by the onset of a very slight pink-purple cast to the solution. This compares to a calculated volume of 10.8 ml, based on exactly 1% iodine. Our solution was probably less than 1%.

The reacted mixture was transferred to a 125 ml glass separatory funnel and the bilayer allowed to settle, after which the lower chloroform layer was drawn off and washed twice with water, then dried by percolating through anhydrous magnesium sulfate (Fisher Scientific) placed in a Whatman # 1 filter paper. The chloroform was evaporated under dry nitrogen, and the resulting yellow powder weighed 165 mg after drying.

Recrystallization was in initially 10 ml of hexane, which was warmed in a 70°C water bath and chloroform added drop-wise (about 5 ml) until the solution was clear. This solution was placed at 4°C for 1 hour, then carefully decanted and filtered through a Whatman #1 filter cut to fit a 7.5 cm Büchner funnel. About 150 ml of cold (0°C) hexane was used to wash the product, after which the filter paper was dried at room temperature, the white product washed off the paper and flask with chloroform. A 130 mg yield of off-white powder resulted. Yield: 63%.

TLC Characterization:

Silica gel TLC plates (Baker Flex-Gel IB-F, J. T. Baker) were eluted with a 95:5 chloroform-glacial acetic acid mobile phase, developed using a 1.27% (w/v) iodine, 3.25% (w/v) sodium azide in 12.5% ethanol/water[268],solution, then heated to bring out the color using a heat gun. The final Rf value was 58.2, with one spot..

$^{+}$H-NMR Characterization:

Two samples submitted to the VPI Analytical Services NMR lab were analyzed in deuterated chloroform on the Bruker 400 MHz instrument . The results confirmed that the starting material, 11-mercaptoundecanoic acid (MUA) had oxidized to the disulfide. The spectra were very similar, with a broad methylene singlet peak at 1.28 ppm, a sextet at 1.6 to 1.68 ppm (1.56 to 1.64 for the MUA), a triplet at 2.31 to 2.37 (2.30 to 2.35 for MUA), and

finally the diagnostic triplet for the disulfide at 2.65 to 2.70, versus a quartet at 2.46 to 2.54 for the MUA.

•Reaction to Form Acid Chloride, Coupling with N-tert.(BOC)-L-valine:

An 11 millimolar solution of the above disulfide was made using 100 mg (0.23 millimoles) of solid with 25 ml of chloroform. 50 ml of methylene chloride was added to a dry, 500 ml three-neck round bottom flask placed over a magnetic stir plate.flask. About two equivalents, or 30 µl (44 millimoles) of thionyl chloride (Eastman Kodak) was quickly mixed with 1 ml of methylene chloride and 1 drop of dimethylformamide as a catalyst, then added to the stirred flask under nitrogen purge. The disulfide mixture was placed in an addition funnel, the mixture stirred, and the solution added drop-wise to the stirred mixture. A tap-water cooled condenser with a DriRite-filled drying tube was place in the condenser top. No sign of a reaction was noted and after two hours, another 100 µl of thionyl chloride was added and the mixture was gently refluxed another 3.5 hours, at which time 1 ml of the mixture was removed and added to 2 ml of concentrated cold ammonia. A precipitate formed, indicating the presence of the acid chloride. The refluxing was stopped and a vacuum distillation, using a water aspirator, was used to remove the solvent and excess thionyl chloride (boiling point 79°C at 760 mm). Another 40 ml of chloroform was added to the flask, and 0.44 millimoles (100.5 mg in 10 ml of chloroform) of N-tert.(BOC-L-valine) was added drop-wise to the stirred mixture in 10 minutes. The mixture was gently refluxed 9.5 hours, after which the chloroform was evaporated under vacuum. An impure, off-white oily solid resulted, was dried under vacuum overnight, and finally yielded 389 mg. The substance initially had a distinctive, spearmint-like odor, which vanished after one week after storage in a vacuum desiccator.

$^{+}$H-NMR Characterization:

A complex spectra resulted from the 400 MHz analysis, yielding a quartet at 0.91 to 1.00 ppm, a quartet from 1.27 to 1.33, a small quartet at 1.44 to 1.66, triplets at 2.31 to 2.37 and 2.65 to 2.70, a doublet at 2.89 and 2.97, and a very complicated multiplet between 3.99 and 4.13 MHz.

4.4.4 Vapor-Phase Synthesis of MUA-Acid Chloride, Coupling to N-tert.(BOC)-L-Valine

A freshly oxidized gold substrate was immersed in a 10 millimolar solution of 11-mercaptoundecanoic acid in methylene chloride for 80 minutes, washed with the same solvent then dried. After FTIR-RA characterization to establish the probable success of the liquid-phase deposition, the slide was placed in a glass reaction vessel, attached to a glass vacuum manifold and manometer, designed especially for vapor-phase modification of monolayers (see Figure 24). The apparatus was evacuated to about 300 millitorr, and left undisturbed to 20 minutes to remove volatile contaminants, then purged and evacuated three times with dry nitrogen, and finally evacuated and left 10 minutes, after which the valve to the gold slide reaction vessel was closed. Next a 10 µl Hamilton Model 701 GC syringe (Hamilton Co., Reno, NV) was used to inject a total of 25 µl of neat thionyl chloride (Eastman Kodak, Rochester, NY) through a teflon-coated septum into the headspace above the gold substrate. The low pressure immediately caused vaporization of the acid chloride. After 20 minutes, the reaction vessel valve was opened and the excess thionyl chloride and any HCL (reaction product) allowed to be drawn off into the dry ice/acetone cooled trap. No nitrogen purge was used to prevent any moisture from entering with the nitrogen, which could react with the freshly prepared acid chloride surface. N-tert.(BOC)-L-valine (Sigma Chemical Co., St. Louis, MO), at a concentration of 300 millimolar in methylene chloride, was added through the

septum using a 250 µl Hamilton 1725 gas tight syringe. Initially 250 µl of this the solution was sprayed into the headspace above the slide, but this did not produce FTIR bands indicating that the valine had reacted with the acid chloride, probably because of the amino acids relatively low vapor pressure.The successful method required spraying 500 µl of valine solution directly onto the surface of the slide, then allowing 60 minutes for the reaction to proceed, after which time the reaction flask was evacuated, then the apparatus purged with nitrogen three times. After returning to ambient pressure, the slide was removed and immediately washed with dry (stored over sodium sulfate) methylene chloride, then dried with nitrogen.

4.4.5 Spectroscopic and Other Analytical Techniques

°Infrared Reflection-Absorption Spectroscopy

IRRAS, or FTIR-RA (Fourier Transform Infrared-Reflection Absorption) spectroscopy served as the primary analytical tool for characterizing the modified gold surfaces. It is a fast, convenient technique but requires a clean gold surface for a background spectrum, and is subject to carbon dioxide and water interferences, the latter a particularly difficult problem in the humid summer months. The polarization modulation (PM-IRRAS) experiment, discussed below, requires peripheral electronic equipment and alignment of the components on an optical bench, but does not need a blank slide and can be "tuned" so that interfering water and solvent bands are eliminated, thus allowing an examination of a solution-surface interface, the key experiment for our research.

IRRAS analysis was done using a Nicolet Model 710 FTIR (Nicolet Instrument Corp., Madison, WI) equipped with a Balston Type 75-60 system (Balston Filter Products, Haverhill, MA) to eliminate water and carbon dioxide in the sample chamber. A wire-grid polarizer (Cambridge Physical Sciences, Cambridge, MA) was placed in the sample compartment to provide p-polarized incident light, which enhances sensitivity compared to an unpolarized

beam. A Spectra-Tech Model FT-80 Fixed Grazing Angle Specular Reflectance accessory (Spectra-Tech Inc., Stamford, CT) was placed in the sample compartment. This is a platform designed to hold the flat gold substrate in a horizontal position, with gold mirrors to direct the source beam at an 80°angle incident to the surface. The aperture was 7 mm, and the polarizer was placed in a slot on the left end of the platform. For most measurements, data collection parameters were set to provide a 4 cm^{-1} resolution using 256 scans at a velocity of 40 cm per minute. Detection was by a mercury cadmium telluride (MCT) module at liquid nitrogen temperature.

Final spectra were absorbance (as a ratio of the sample and a freshly cleaned gold surface blank) versus wavelength in reciprocal centimeters. Samples were dusted with a stream of dry nitrogen before scanning, and were allowed remain in the sample compartment between 15 and 30 minutes, depending on weather conditions, to purge water and carbon dioxide. Signal-to-noise levels for IRRAS surface measurements are low due to the very small amount of sample that is producing the absorbance for a monolayer, which is typically on the order of 1 nanometer in thickness.[269]

• Polarization Modulation IRRAS

The overall components of the PM-IRRAS experiment are shown in Figure 17. The theoretical advantage of using modulated polarized light is the ability to further reduce digitization noise by suppressing the interferogram's centerburst amplitude, although techniques other than PM have been used.[270] Our instrument used a Hinds Model PEM-80 ZnSe photoelastic modulator (Hinds Instruments Inc., Hillsboro, OR) to modulate the beam from the FTIR. Modulation frequency was 73 kHz, with the beam incident on the sample as described above. As shown in Figure 19, a CaF crystal is placed between the beam and the sample to compensate for reflections from the two unequal intensity beams of polarized light.[271] This modulated signal must be demodulated, then filtered to produce an interferogram

with an intensity proportional to the difference between the p and s-polarized light (I_p - I_s), thereby achieving constructive interference and amplification of an otherwise very weak signal. This process is accomplished with an EG&G Princeton Applied Research Model 5204 Lock-In Analyzer (EG&G Princeton Inc., Princeton, NJ) doing the demodulating.,The signal is then input to the A/D (analog to digital) converter within the FTIR, then output to the workstation to produce the final spectrum, either a difference (I_p - I_s), or sum (I_p + I_s).

The final experiment to evaluate the (R) and (S)-TFAE complexes with the model chiral stationary phase (BOC-L-valine) attached to the gold substrate was done using a 50 ppm deuterated chloroform solution of each enantiomer, placed on the gold surface. The trapezoidal calcium fluoride crystal was then positioned to intercept the beam. After proper alignment of the optical bench, measurements were made with slightly changed data collection parameters to accommodate the PM technique.

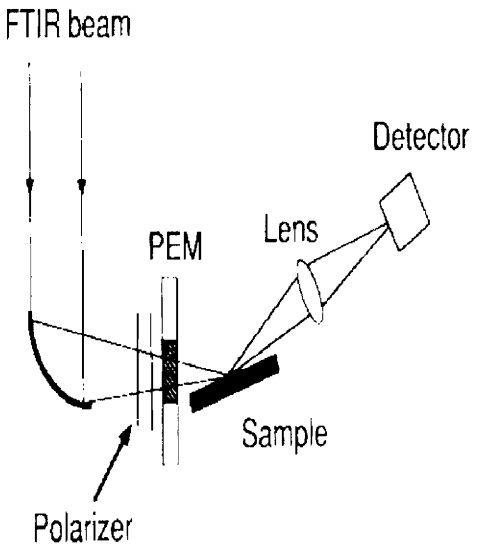

R. M. Corn, et al, *Anal. Chem.* **1991**, *63*, 55-60

Figure 18. The general optical setup for the polarization modulation FTIR experiment is shown.

(After ref. , Corn 1991.)

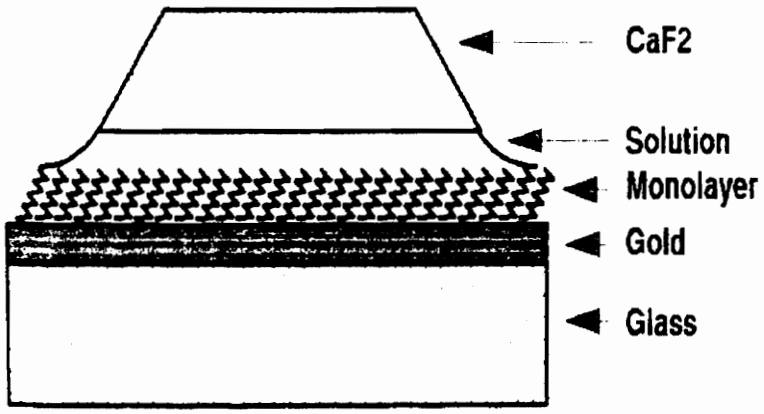

Figure 19. Proposed configuration for the PM-IRRAS measurements of (R) and (S)-TFAE-model CSP complexes.

After ref. 23, M. R. Gatin, PhD. dissertation, VPI & SU, 7/92.

• X-Ray Photoelectron Spectroscopy

Surface analysis for elemental confirmation was done in VPI & SU's Surface Analysis laboratory using a Perkin Elmer PHI 5300 instrument featuring a MgKα achromatic X-ray source (1253.6 eV). Power was set at 400 watts using a 15 KeV beam voltage, with vacuum levels typically around $1x10^{-7}$ Torr. The 1" x 1" gold slides were cut into fourths (1/4" x 1/4"), and taped to the sample holder with double-sided cellophane adhesive tape. The beam struck a surface of 1 x 3 mm dimensions after proper alignment prior to starting the analysis. Calibration used the gold $4f_7$ orbital, with an 83.8 eV energy.

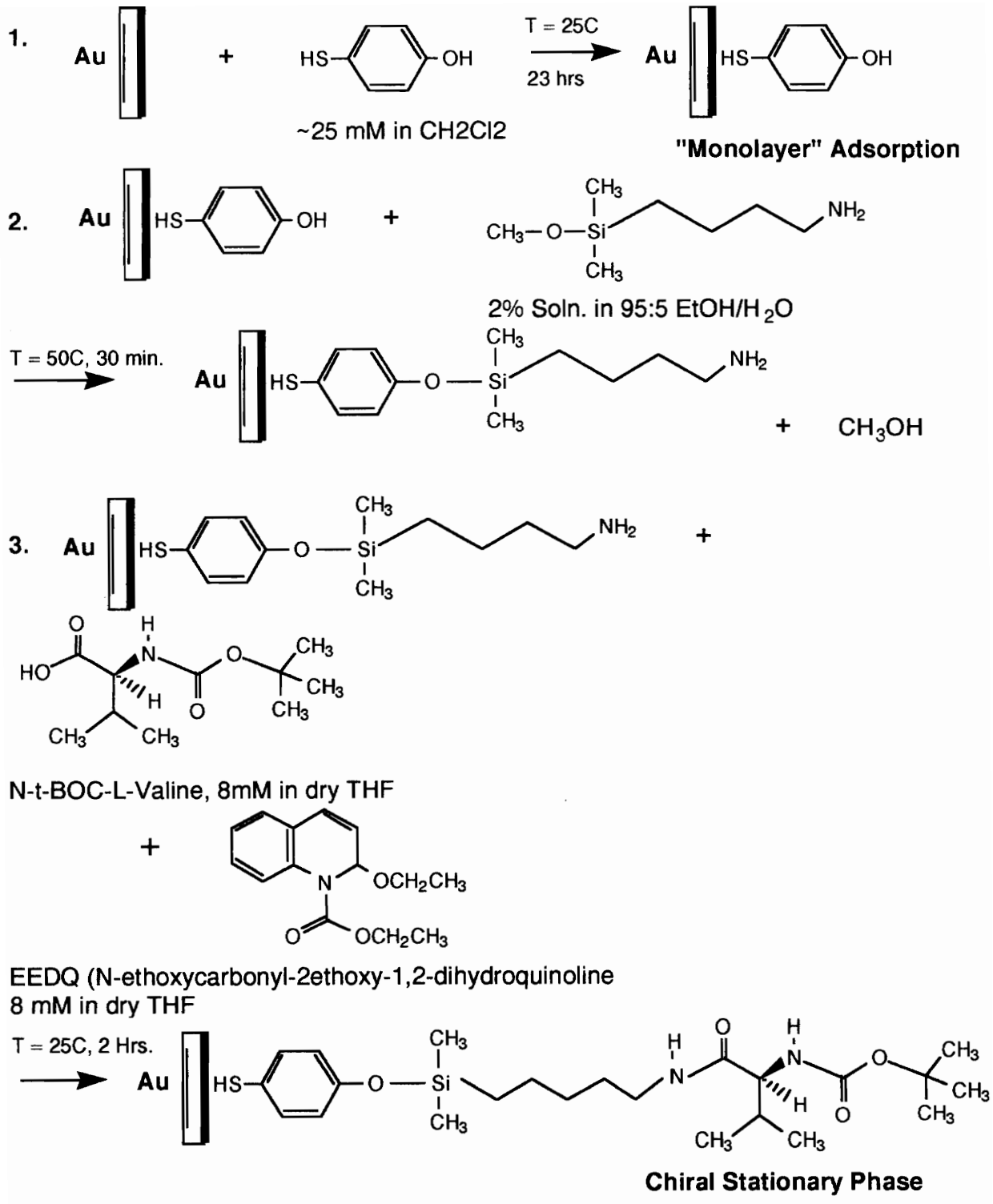

Figure 20. The first three steps of the first synthetic strategy using methoxysilane.

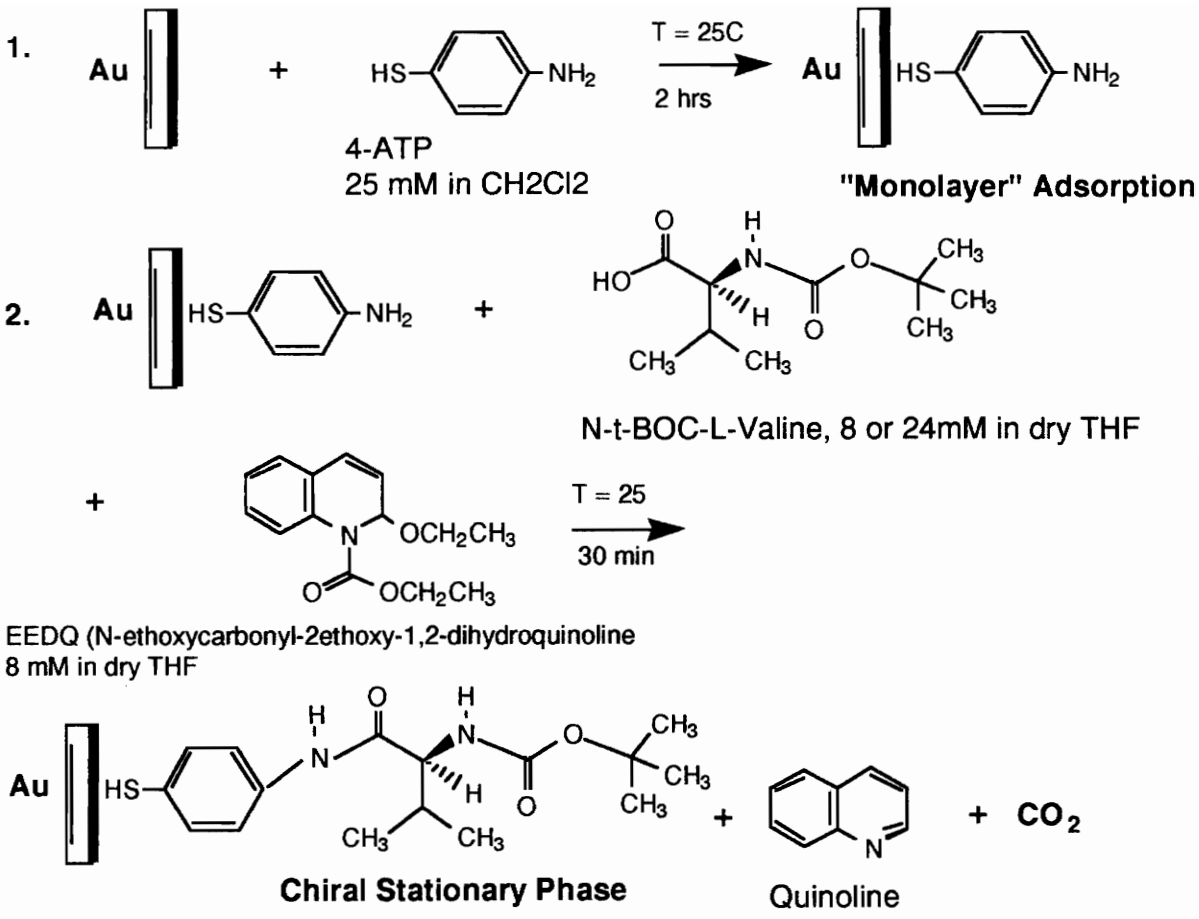

Figure 21. The alternative synthetic scheme without the silane group is outline above..

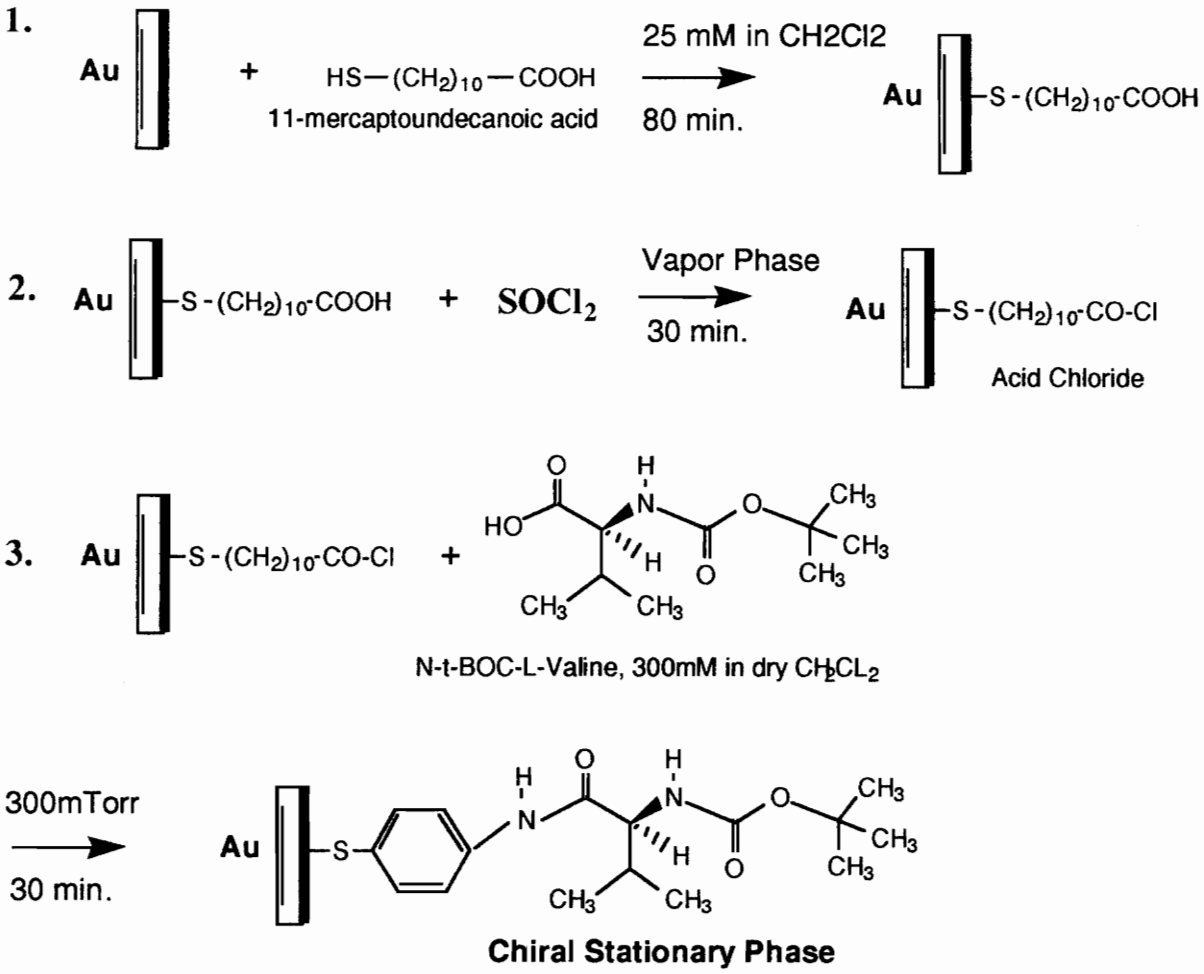

Figure 22. Here is outlined the combined vapor phase, evacuated liquid phase scheme which was successful in depositing a (BOC)-L-valine surface.

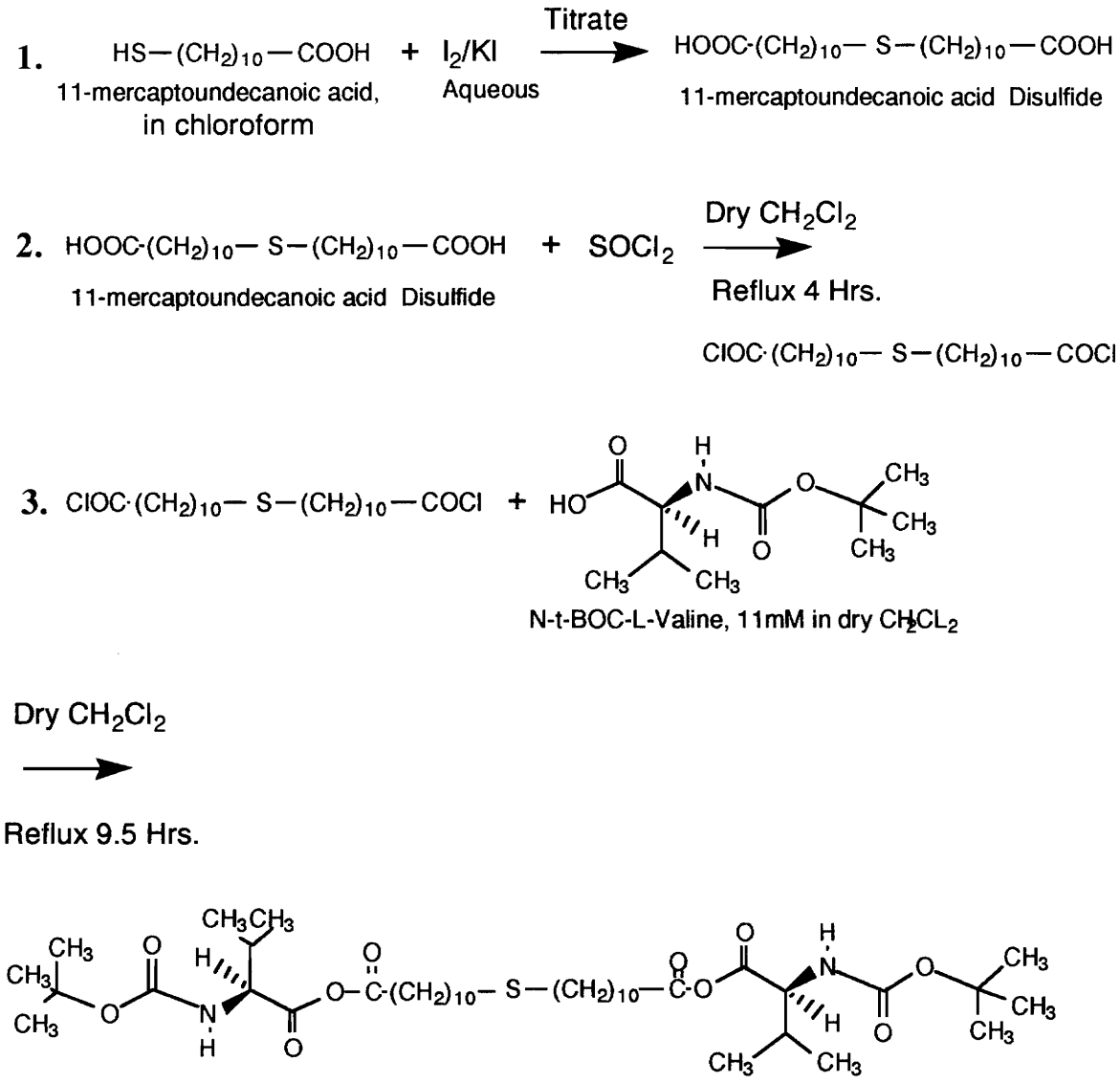

Figure 23. This illustrates the synthetic steps involved in preparing the disulfide-linked BOC- valine in solution,

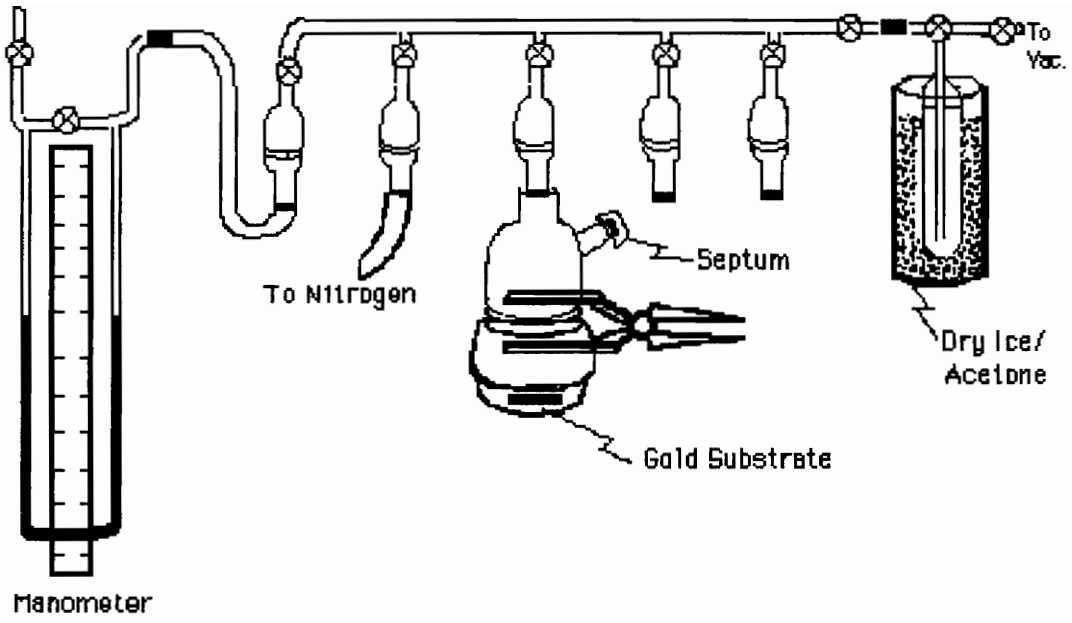

Figure 24. The vacuum manifold used for vapor phase deposition is shown, along with the glass vessel specially designed for reacting gold-coated slides. This same apparatus was also used for reacting the acid chloride surface with liquid BOC-valine.

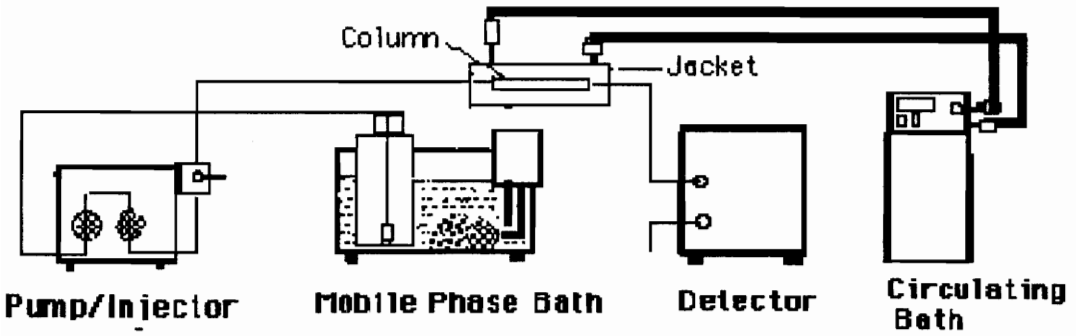

a.

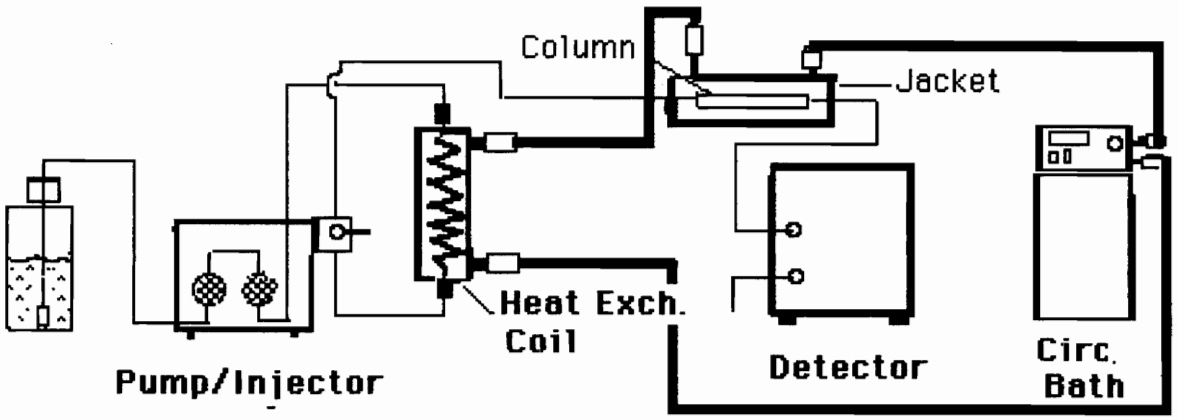

b.

Figure 25. Evolution of HPLC apparatus and temperature control equipments. 25a shows the early plastic tub bath for cooling the mobile phase; 25.b includes the 0.040-inch, 3-meter length of tubing coiled inside a column jacket used to condition the mobile phase before it entered the injector and column.

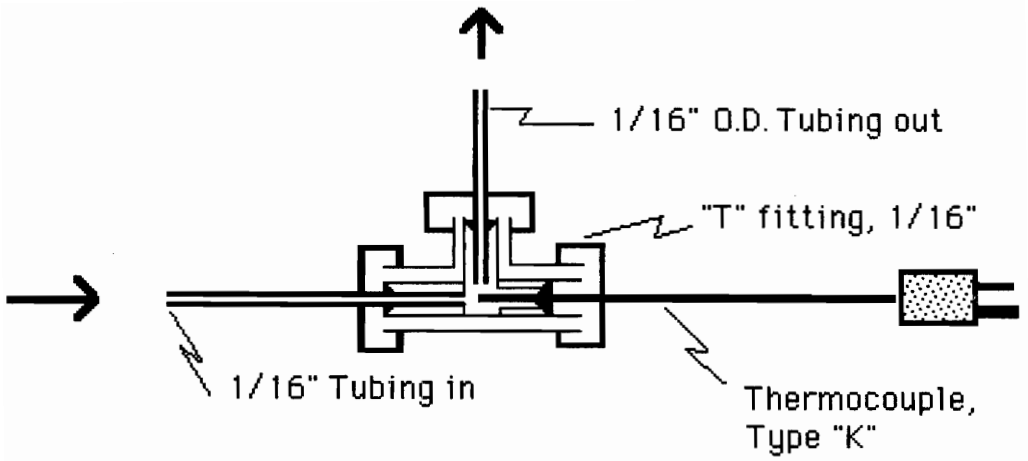

Figure 26. Apparatus for measuring mobile phase temperatures.

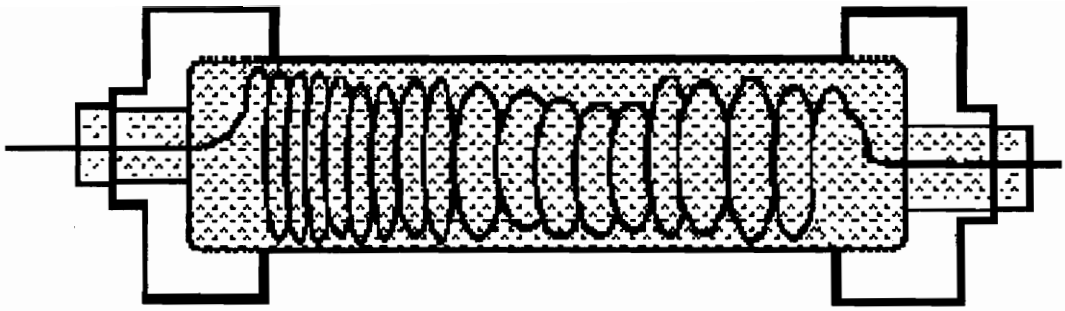

Figure 27. Heat exchanger used to pre-condition mobile phase temperature.

CHAPTER V

RESULTS AND DISCUSSION

5.1 Initial Optimization Studies

5.1.1 TFAE on DNBPG

The first group of experiments which evaluated the effect of temperature and flow rate upon the resolution equation parameters involved both the TFAE and trans-stilbene oxide (t-stil.) solutes separated on a Pirkle-phase dinitrophenylglycine (R-configuration, DNBPG), and a Type II cellulose Daicel Chiralcel OD (3,5-dimethylphenylcarbamate) stationary phase, using exclusively a 70:30 hexane-2-propanol mobile phase. The mobile phase composition is important to note because of its effect on the overall trends in selectivity and resolution, which change for the sub-zero temperature studies done with a 20% alcohol modifier, described in a later section..

The well characterized Pirkle column provided us with a baseline of data for temperature, flow and later mobile phases changes. Knowing that the DNBPG enantioselective mechanism depended almost exclusively upon attractive and repulsive interactions, we could then compare results for the cellulose OD column and make some mechanistic conclusions by inference.

This section will briefly describe the trends seen for capacity factor, selectivity, plate height and finally total resolution for temperatures between 26 and 3.3°C, and for flow rates between 0.2 and 1.7 ml/min. In most cases, each data point shown in figures 30 to 33 represents the mean of six replicate injections. Generally, the data exhibited more uniform

behavior over the temperatures selected, and there were fewer outlier points, than corresponding data for the Chiralcel OD, shown in Section 5.1.2.

Figure 28 is a van't Hoff-type plot of the natural logarithm of capacity factor versus the reciprocal of temperature in degrees Kelvin. As described in Chapter III, Theory, the y-intercept of this plot is proportional to the entropy of desorption of the solute from the chiral stationary phase, but note that this value is extrapolated from a zero-value of the x-axis, corresponding to absolute zero. The slope is proportional to the enthalpy of desorption. The many lines represent least squares regression models for each of the flow rates, and indicate, as would be predicted from theory, that flow rate has no affect on k'. (Analysis of variance, performed by StatView, showed no significant effect of flow rate on capacity factor at the 95% confidence level.) In addition, since six runs were made at each flow rate and temperature, the reproducibility is good. Correlation coefficients ranged from 0.975 to 0.99.

Several points are immediately obvious from the qualitative shape of the plots for $\ln k'_R$ and $\ln k'_S$. First, the vertical separation (a large difference in y-intercepts exists, and so entropy control is apparent) is proportional to selectivity (α), and since the lines are almost parallel (nearly, but not quite equal slopes), this separation is entropy-controlled over the given temperature and flow rate range. Also, the magnitude of the capacity factors are less than zero for the DNBPG. Overall, capacity factors are increasing as the temperature decreases from left to right across the plot, so that the overall resolution is being helped by this increase in k' as the temperature is lowered.

Figure 29 tells us that selectivity, the ratio of the capacity factors for the R and S-TFAE enantiomers, is also increasing as the temperature decreases. If the lines in Figure 28 were extended farther to the right (in the direction of lower temperature), they would diverge somewhat, predicting the selectivity behavior seen in Figure 29. Again, separate least squares estimates were made for each flow rate, and the effect of flow rate upon selectivity was not

significant at the 95% level. So for the second term in the resolution equation, lowering temperature has a positive effect on final resolution.

Figure 30 shows us that for the kinetic term, plate height, lowered temperature has a positive effect on H, and therefore negative effect on N, the efficiency term in the resolution equation (H = L/N). Again, this is in line with our common-sense expectations concerning molecular activity at low temperatures, and the resulting peak width increase will partially offset gains made in the capacity factor and selectivity terms. Although the van Deemter plot (HETP versus average linear mobile phase velocity) is not shown, we can see from the three curves that lower flow rates give decreased band broadening (increased efficiency).

To discover the net effect upon resolution, we refer to Figure 31. This data from the DNBPG column forms a convenient map for the chromatographer doing a method optimization for this column and a similar solute and mobile phase. Maximum resolution is achieved at minimum temperatures and flow rates, showing that indeed the gains made for capacity factor and selectivity overcome the worsened efficiency at lower temperatures. As for the effect of flow rate, it is apparent from Figure 30 that the attractive-repulsive interactions, especially the low energy charge transfer complexes, are very sensitive higher flow rates, producing much more band broadening as the flow rate increases.

Early on in our research, after obtaining the above results, it was tempting to over generalize this conclusion for other CSP-solute-mobile phase combinations. As we shall soon see, it is a mistake to oversimplify the complex interdependence of these three factors.

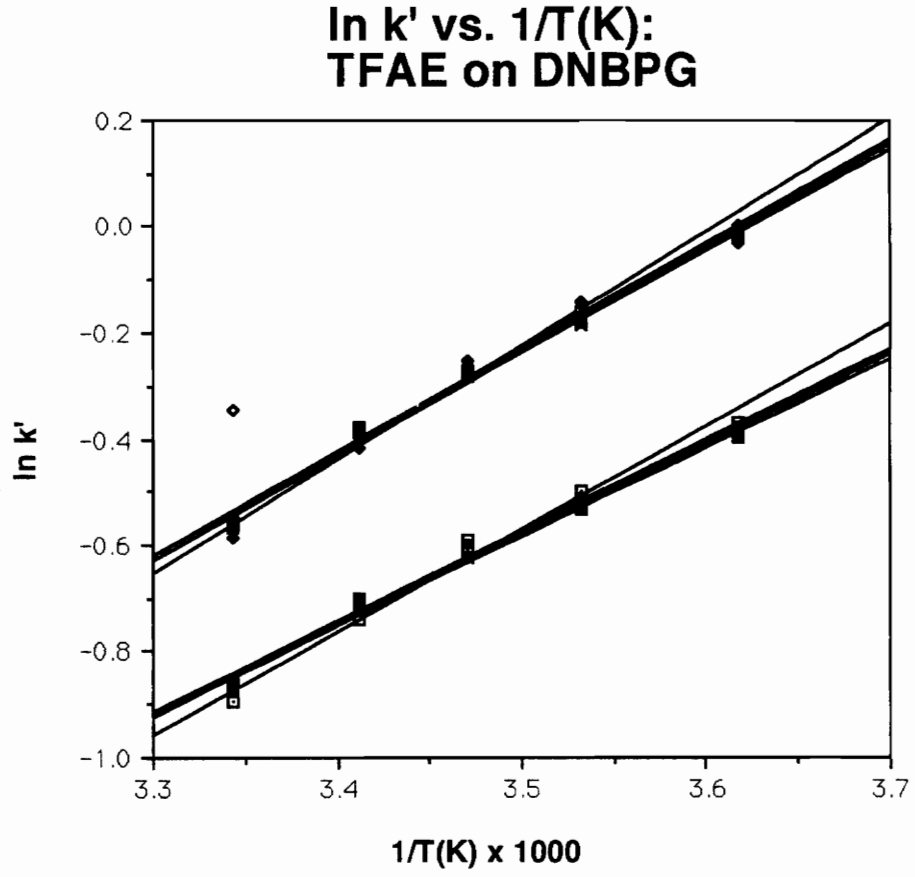

Figure 28. The van't Hoff plot for TFAE separated on DNBPG between 3.3 and 26°C, and at flow rates between 0.2 and 1.7 ml/min. Lines represent the individual linear regression model for each flow rate (3 replicates each) ; correlation coefficients ranged from 0.985 to 0.997.

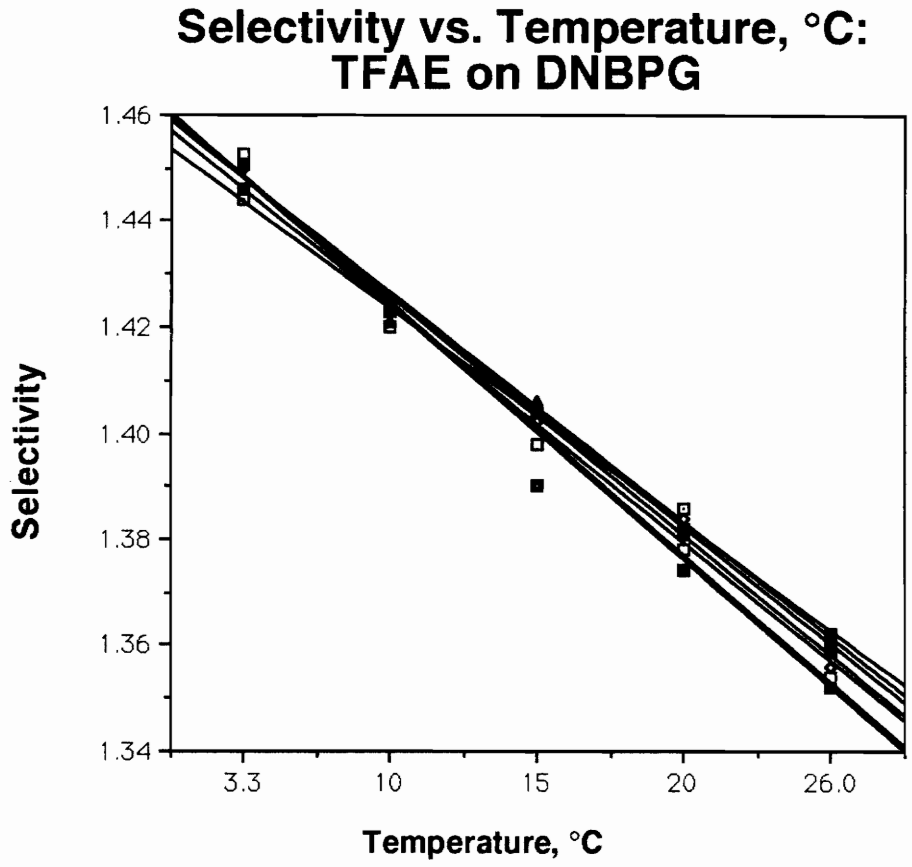

Figure 29. Selectivity (α) versus temperature, for flow rates of between 0.2 and 1.7 ml/min. Lines represent the individual linear regression model for each flow rate (3 replicates each) ; correlation coefficients averaged 0.990 and ranged from 0.975 to 0.995.

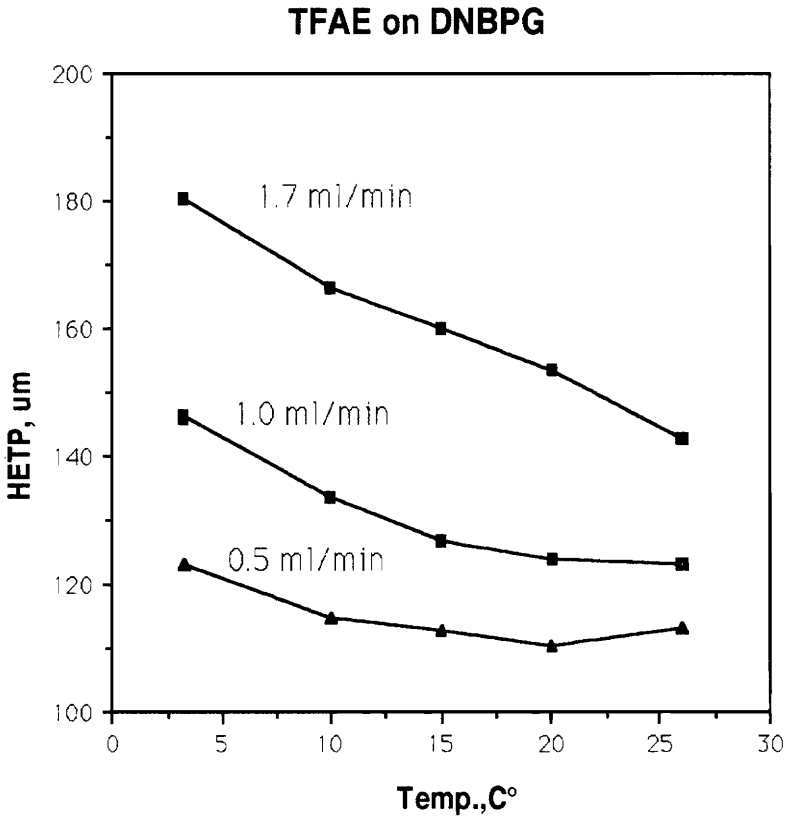

Figure 30. Plate height versus temperature is shown for three different flow rates. Each data point is the mean of six replicate injections.

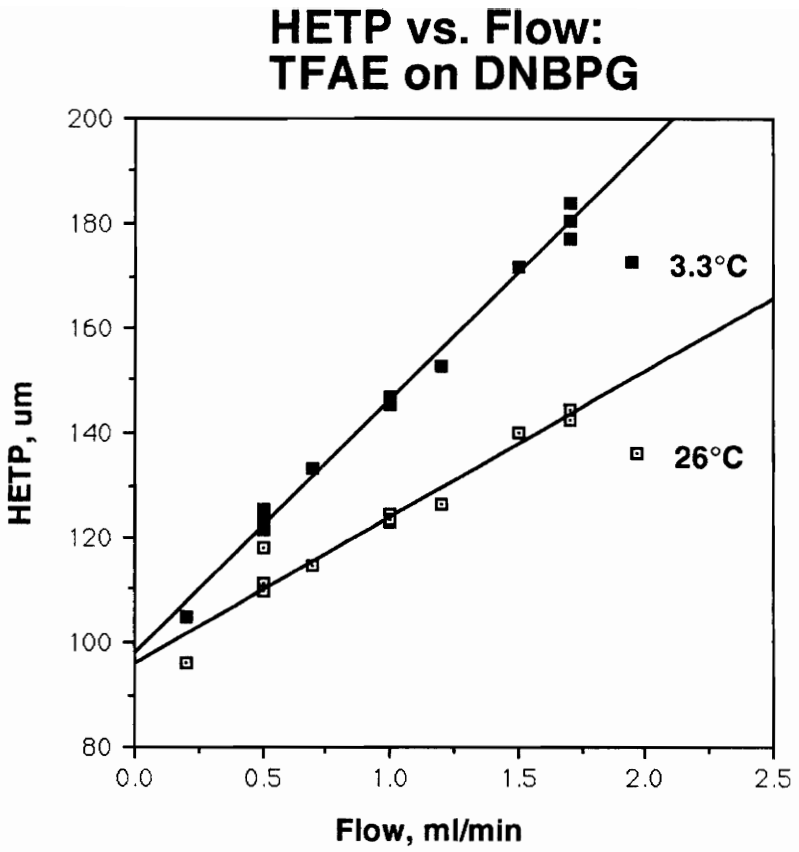

Figure 31. Plate height is plotted versus flow rate for the separation of TFAE on DNBPG. Note that the curves are more linear than those for TFAE on cellulose (Figure 35), and the effect of temperature upon the slope is much more pronounced compared to the cellulose CSP.

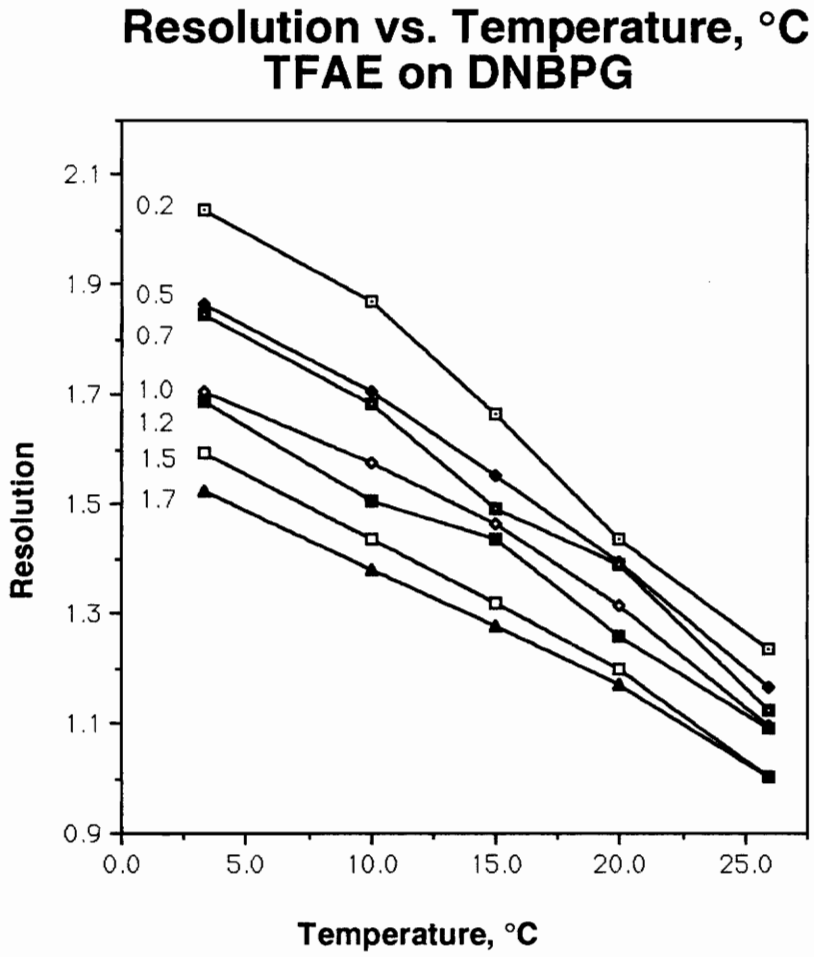

Figure 32. Resolution versus temperature is shown for seven flow rates. Each point represents the mean of six replicate injections.

5.1.2. TFAE and trans-Stilbene Oxide on Chiralcel OD

We applied the same methods to the mechanistically more complex cellulose CSP, featuring 3,5-dimethylphenylcarbamate groups attached to each six-member carbohydrate ring (see Figure 2). Both inclusion complex and attractive-repulsive interaction mechanisms are structurally possible, but it has not been clear from the research done by others if these mechanisms operate separately, simultaneously or are in competition and influenced by solute and chromatographic separation conditions.

The strategy here was to compare OD results with the baseline DNBPG column in order to find mechanistic evidence for or against the above possibilities. The two solutes differ structurally, and these differences may be characterized quantitatively by some physical-organic indices, which are shown in Table IX. The most significant differences between the solutes are indicated by the bold-faced values for α, hydrogen-donating n-index, and solubility in hexane and octanol for trans-stilbene oxide versus TFAE. Since trans-stilbene oxide has no acidic proton, its a index is zero, and is more than 400-times more soluble in the alcohol as is TFAE. Due to its lower overall polarizability (2.36 versus 2.90 for TFAE), it is also more soluble in hexane. Overall, we have for trans-stilbene oxide a smaller (molecular volume is 187 versus 207 ml/mol), non-acidic, less polar molecule which is more soluble in both components of the hexane alcohol mobile phase than is TFAE.

The numerical results from Table IX then support qualitative observations based on comparison of the two molecular structures. In addition, the DNBPG stationary phase has high indices for both hydrogen donor and acceptor sites per molecule, as the attractive-repulsive interaction theory requires for the polar interaction sites. On the basis of Table IX alone, one might suppose that a trans-stilbene oxide racemate would be difficult to separate on the Pirkle column, and indeed this is the case. Even as low as -30°C, the trans-stilbene oxide peak is only just beginning to show a splitting; at all lower temperatures only a single peak is evident.

Table IX. Solute and CSP Physical Properties

Property	Units	DNBPG	TFAE	t.-Stil. Oxide	Propranolol
Polarizability	$Å^3$/mol	3.93	2.90	2.36	3.13
α, Taft-Kamlett H-donor sites	# sites/mol	0.939	0.548	**0.000**	0.455
β, Taft-Kamlett H-acceptor sites	# sites/mol	1.98	1.05	0.466	1.25
Molecular Vol.	ml/mol	270	207	187	223
Solubility in Hexane	moles/L	NA (Bonded Phase)	1.5×10^{-6}	**1.10**	1.1×10^{-6}
Solubility in octanol	moles/L	NA (Bonded Phase)	0.0113	**4.289**	0.0106

Values were generated by the EPA "SPARC" program (Performs Automated Reasoning in Chemistry, U.S. EPA, Athens, GA)

The solubility differences become important when we analyze the results of sub-zero temperature studies in which the mobile phase used contained only 20% alcohol, and in the mobile phase studies when the percentage of alcohol was varied.

Figure 33 shows three chromatograms which are representative of the three possible separations: TFAE on DNBPG, TFAE on Chiralcel OD and trans-stilbene oxide on OD. Note that, although the temperature is lower (but the flow rate is higher) for the 10 μm particle size OD separations, there is more tailing of the second peak compared to the 5 μm particle size DNBPG column. This difference was a constant at all conditions, and is due both to the difference in column efficiency due to particle size, and more to the point a difference in separation mechanisms. In any chromatographic mode where there exists multiple, and usually competing separation mechanisms, an increase in band broadening will be evident.

Figure 34 shows the two van't Hoff plots for TFAE and trans-stilbene oxide separated on the Chiralcel OD column. Each cluster of points making up the four curves represents six repetitions at each of three flow rates (0.5, 1.0 and 1.7 ml/min), for a total of 18 injections per cluster. The lines through these points are the least squares linear regression fit through the means at each temperature.

There are several interesting points of comparison between these van't Hoff plots and that for TFAE separated on the DNBPG column. First, the magnitude of the capacity factor values for S-TFAE (k'_2) is greater for the OD column compared to the Pirkle (Figure 28, all values for k'_1 (R-TFAE) and k'_2 are less than zero), but note that the OD column's k'_1 values are MORE negative, and the slope is much less steep, than for the corresponding curve for DNBPG. Overall, this qualitatively indicates that a more energetic complex is forming between the TFAE molecule and the OD column compared to the TFAE-DNBPG complex. We shall see in the next section that the enthalpy, entropy and overall free energy differences,

when quantitatively evaluated, will support our observational argument from Figures 28 and 34.

Moving next to the plate height contribution to resolution, we see in Figure 35 the van Deemter curves for TFAE separated on the cellulose column at both temperature extremes, 3.3 and 25°C These two curves are shown to (1) graphically demonstrate the negligible effect of lowered temperature on plate height for the OD column (in contrast to the DNBPG situation), and (2) to show the rapid increase in plate height (loss in efficiency) for the TFAE solute as the flow rate is increased. Contrast the increase in plate height at 3.3°C at low flow rates for TFAE (Figure 35) with the almost overlapping curves for 25 and 3.3°C for trans-stilbene oxide on Chiralcel OD, shown in Figure 36. Each point represents six injections .

Mechanistically, these results suggest that a difference exists for the CSP-solute interactions for cellulose versus those for DNBPG, which displayed more sensitivity to lowered temperatures (Figure 31). Since the Pirkle phase depends much more on π-π charge transfer interactions, which are weaker than hydrogen bonding an inclusion complex types, it follows that temperature would have a greater effect for DNBPG separations. Figure 31 is shown with points connected by a least squares *linear* regression (correlation coefficients of 0.992 and 0.956 for the 3.3 and 26°C plots, respectively), rather than the 2° polynomial models used for the Chiralcel OD van Deemter plots of Figures 35 and 36. The striking effect of temperature on the DNBPG plate height is very apparent, with the slope values of 48.5 mm per 1 ml/min for 3.3°C, versus 27.7 mm per ml/min for 26°C underlining how temperature sensitive this separation is. In contrast, the cellulose column van Deemter curves, using the polynomial model, show virtually overlapping 3.3 and 25°C plots for both TFAE and trans-stilbene oxide.

In summary, plate height , the kinetic term of the resolution equation, is more temperature dependent in a more linear manner for the TFAE-DNBPG complex than is the

TFAE-Chiralcel OD complex due to a single versus multiple mechanism separation, respectively.

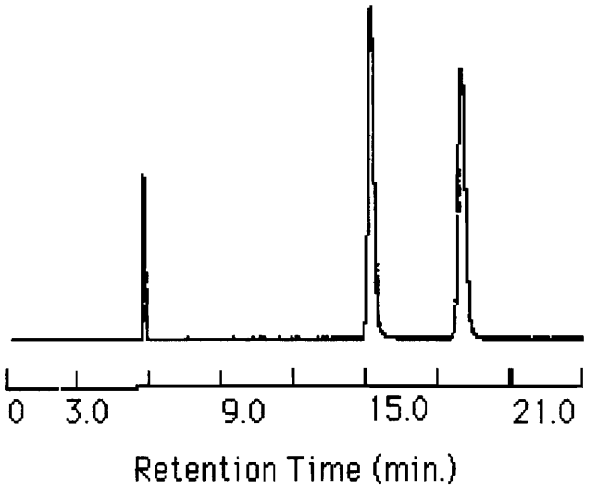

a.

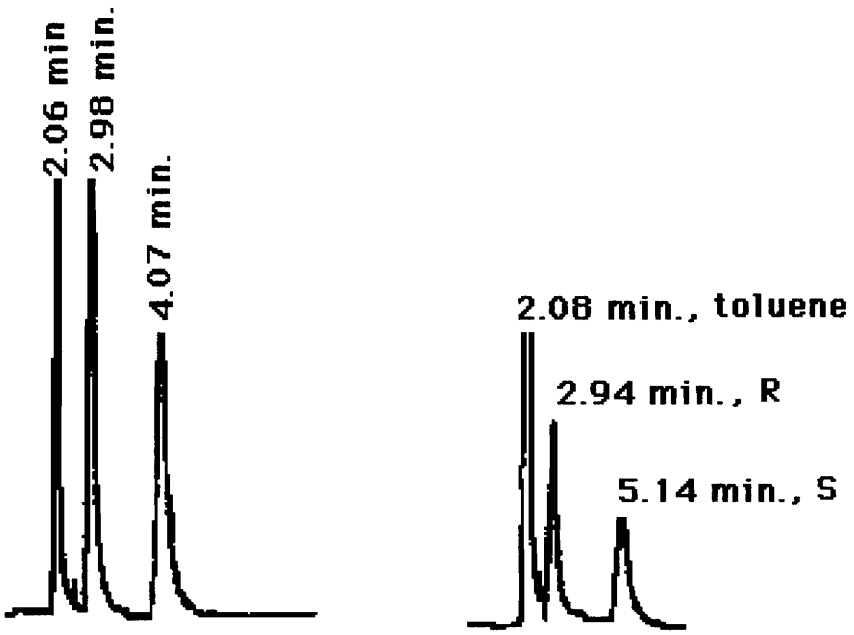

b. c.

Figure 33. (a.) TFAE on DNBPG, (b.) TFAE on OD, and (c.) t-Stil.Oxide on OD. Conditions: a. 90/10 hexane:IPA, 0.5 ml/min, ambient temp.; b. and c. 70/30 hexane:IPA, 1.7 ml/min, T=3.3°C.

k'(t-S) > k'(TF)

30% IPA

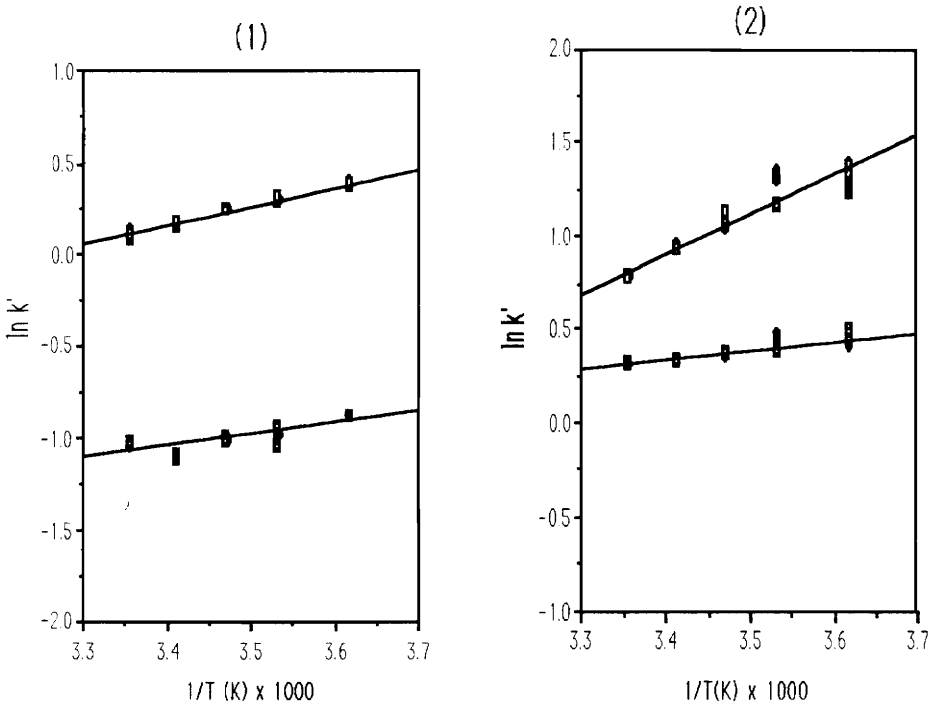

34 a. **34b.**

Figure 34. On the left (34a.) is shown the van't Hoff plot for k'_1 (bottom) and k'2 (top) for TFAE separated on Chiralcel OD. On the right (34b.) is trans-stilbene oxide resolved on the same CSP, with the first eluting peak curve at bottom and the later eluting peak's curve at top. Note the entropy-controlled conditions (nearly equal slopes) for TFAE, but the enthalpy-controlled (unequal slopes) separation for trans-stilbene oxide.

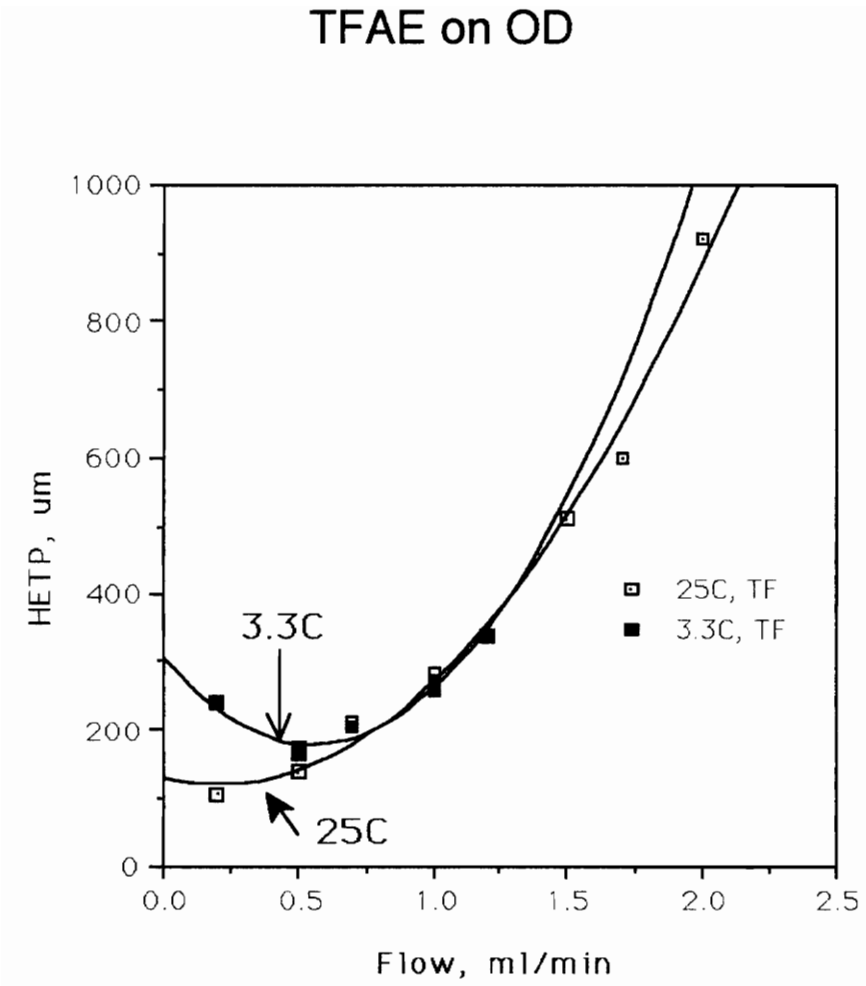

Figure 35. Height equivalent to a theoretical plate (HETP) versus flow rate is plotted for the separation of R and S-TFAE on the Chiralcel OD column. Data for both the low and high temperature extremes are shown.

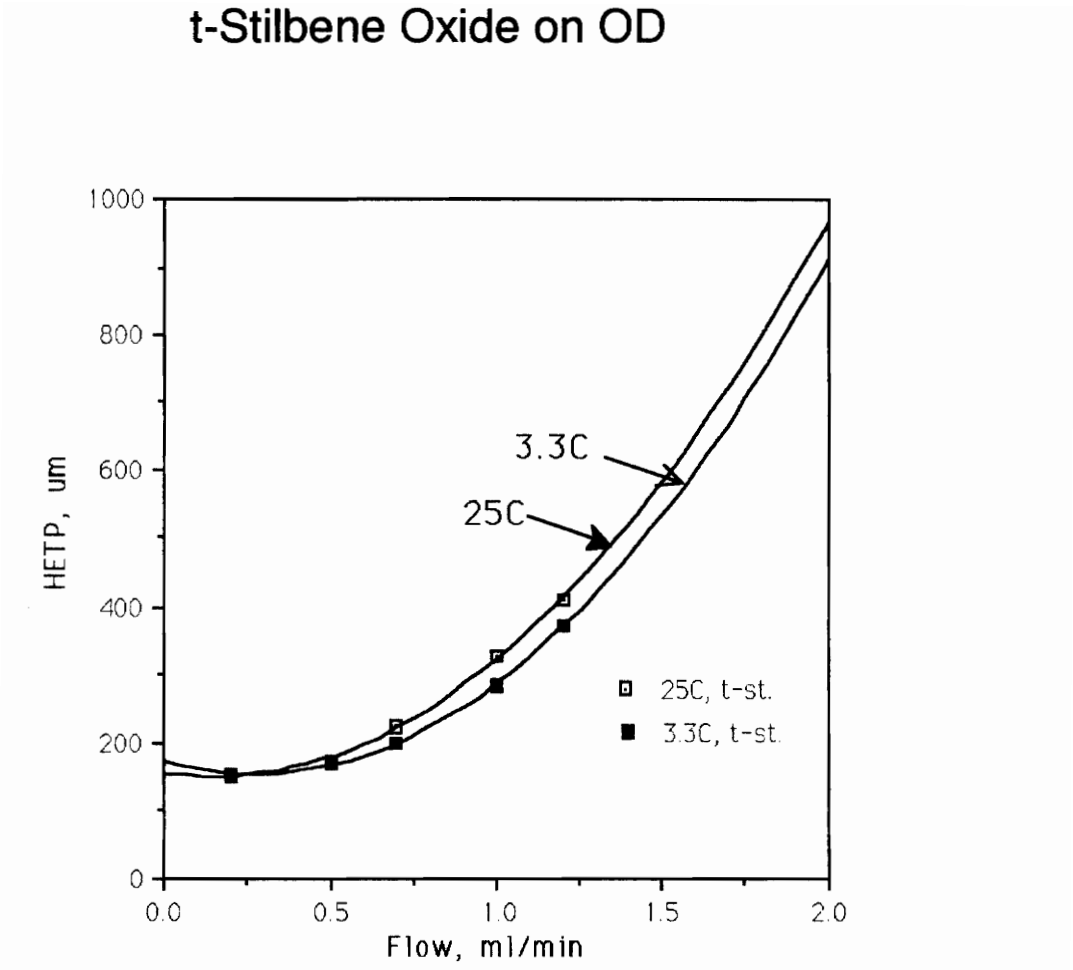

Figure 36. HETP is plotted versus flow rate for trans-stilbene oxide separated on Chiralcel OD. Note the similarity for the 3.3 and 25°C curves at very low flow rates, compared to the increase in plate height for TFAE at 3.3°C (Figure 34).

Finally, we shall compare all three column-solute combinations in terms of selectivity versus temperature, noting that in Figure 37 three distinct levels of selectivity emerge. As selectivity is directly proportional to the difference in Gibbs free energy between the two enantiomers, we can relate these three selectivity levels to the CSP-solute complex strength, and therefore to the enantioselection mechanism.

The TFAE-DNBPG combination gives the lowest selectivity values, which conforms to the postulated single-mechanism consisting of lower energy charge transfer interactions between the aromatic rings, and hydrogen bonding. The stereospecific interactions are influenced by temperature, as evidenced by the change in slope. It appears that both charge transfer and hydrogen bonding interactions are stereospecific, as the selectivity is increasing with lowered temperature, but we know that hydrogen bonding interactions are usually too strong to be affected by temperature, whereas charge transfer effects are not.[272] This would suggest that, although most researchers attribute the enantioselective interaction to hydrogen bonding, that in this case it is a combination of hydrogen bonding and charge transfer effects.

The separations done on the cellulose column feature greater magnitudes of selectivity, in keeping with the theory of two possible modes of interaction, attraction-repulsion by the carbamate groups and an inclusion complex mechanism provided by the flat, parallel layers of glucan units (see Figure 6). Since we know that the trans-stilbene oxide requires some sort of inclusion mechanism for enantioselectivity (there was no separation on the DNBPG), it can be concluded that this inclusion complex is of a higher energy than the attractive-repulsive interaction separating TFAE on the DNBPG column, since selectivity is higher (2.5 to 3 versus less than 1.5).

The third case, that of a TFAE separation on cellulose, shows the highest selectivity of all, and again this can be related to mechanisms. TFAE separates both on the Pirkle and cellulose columns, and is capable of participating in both hydrogen bonding and inclusion

interactions by virtue of the polar CF_3 and OH groups and the aromatic anthracene group, which is known to insert into cyclodextran inclusion cavities. TFAE then shows the highest complex energy due to the possibility of multiple enantioselective retention mechanisms with the cellulose column.

Flow was not a statistically significant influence on selectivity in all cases shown in Figure 37. The 0.7, 1.0 and 1.7 ml/min injections at each temperature overlapped completely except for the trans-stilbene case. The data was thoroughly checked, and the decreased precision at the lower temperatures is "real", with each given flow rate/temperature data point being the mean of six injections.

A possible explanation for this "noisier" data, seen for other plots using the Chiralcel OD, may be instability in the fragile cellulose column bed, compared to the more robust bonded silica gel of the Pirkle column. Another possibility for this particular data set may be pressure fluctuations caused by intermittent blockage of the injector port, which was not discovered until many months after the experiment was completed. McGuffin et al[273] examined the effect of pressure in reversed-phase systems in 1991 and found it to influence retention. Recently[274], using an *in situ* laser-induced fluorescence technique, they proved that increasing temperature produces increasing capacity factors with all other conditions held constant. Thus our pressure fluctuations, whatever the cause, would have resulted in more variability in the capacity factor-derived selectivity plots.

The final resolution versus temperature plots for TFAE and trans-stilbene oxide on the OD column are shown in Figures 38 and 39. Paralleling the trend for selectivity, the TFAE data is less noisy, and features statistically significant negative slopes (slopes are non-zero at the 95% confidence level), indicating that lowered temperature does improve separation. However, if we compare the linear regression slopes for TFAE on both OD (Figure 38) and on DNBPG (Figure 32) for the 0.5 ml/min flow rate, we note that the resolution improvement on the Pirkle CSP amounts to 0.031 resolution units per degree centigrade decrease, whereas for

the Chiralcel CSP the improvement is only 0.024 units per degree. For both CSPs, the resolution improves at a faster rate as the temperature is lowered at lower flow rates, because of the enhanced efficiency term.

The shallower slopes of the resolution versus temperature curves for both solutes on Chiralcel OD further supports the hypothesis of a mixed mechanism because of the more temperature-sensitive attractive-repulsive interactions of the Pirkle column compared to the relatively temperature insensitive inclusion complex and hydrogen bonding interactions possible for cellulose.

Tables Xa and Xb are numerical summaries of the plotted data for capacity factor, selectivity and resolution, expressed as the mean plus and minus the Student t-table value times the standard deviation divided by the square root of the number of repetitions $(n)^{275}$, listed in column 1 of both tables. Xa includes data for the TFAE separated on DNBPG, and Table Xb summarizes the results for both TFAE and trans-stilbene oxide separated on the Chiralcel OD phase. Note that data for both columns covers only the 1.0 ml/min flow rates, but that it is representative for all flow rates in terms of selectivity and resolution.

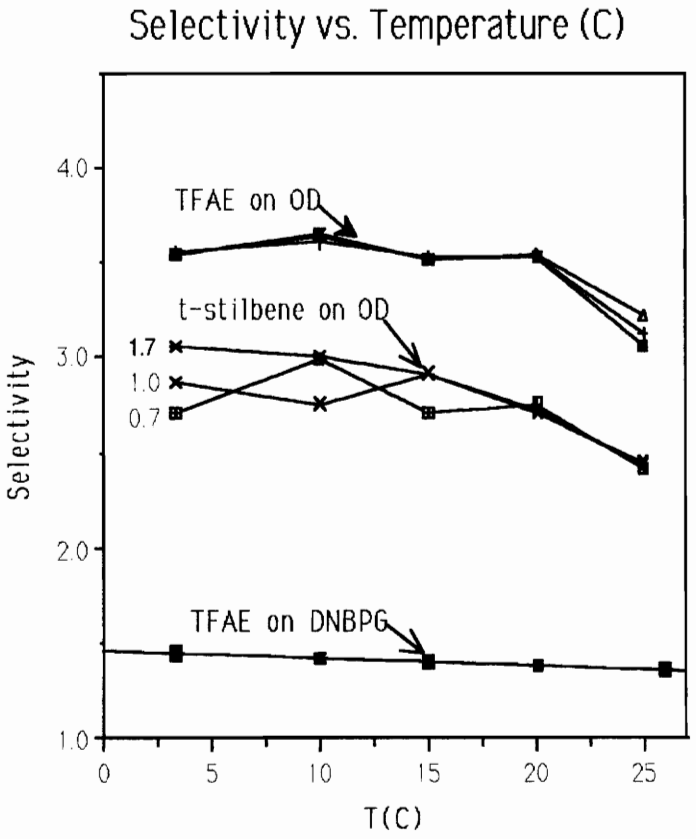

Figure 37. Selectivity versus temperature is plotted for the three CSP-solute combinations using a 30% IPA/hexane mobile phase. Each cluster of points represents six replicated injections at 0.7, 1.0 and 1.7 ml/min flow rates.

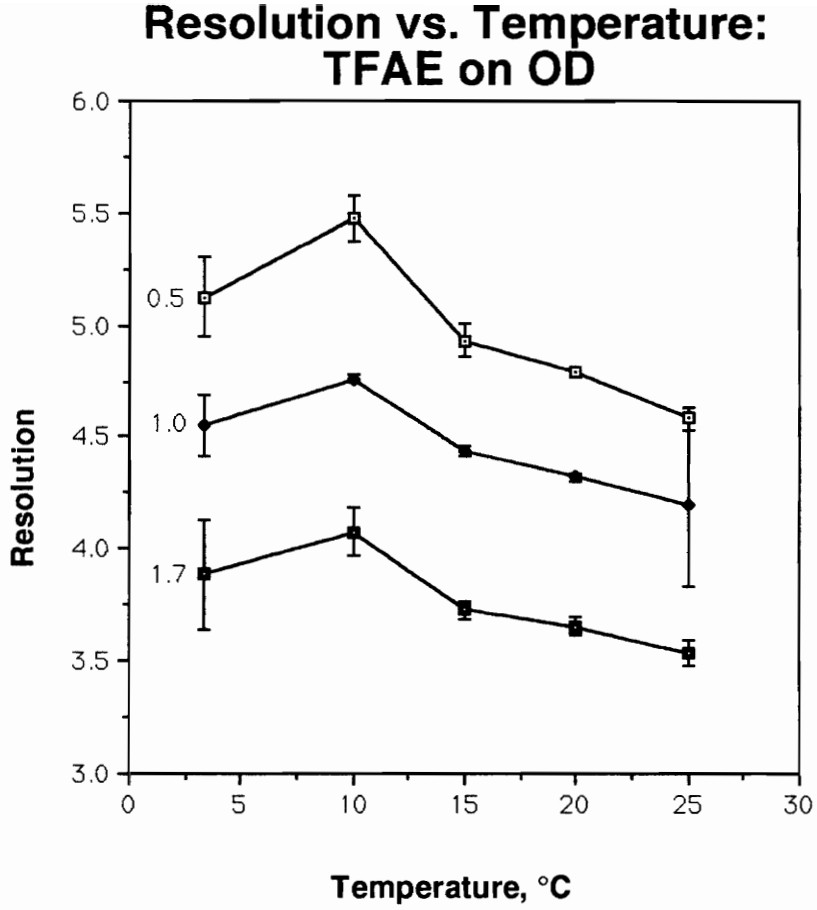

Figure 38. The separation of TFAE enantiomers on Chiralcel OD is shown. Each point represents six chromatographic injections. The three plots refer to flow rates of 0.5, 1.0 and 1.7 ml/min. Error bars represent a 95% C.I. and are calculated as per reference 279 [Mean ±(t) (Std. Dev.)/√n)]

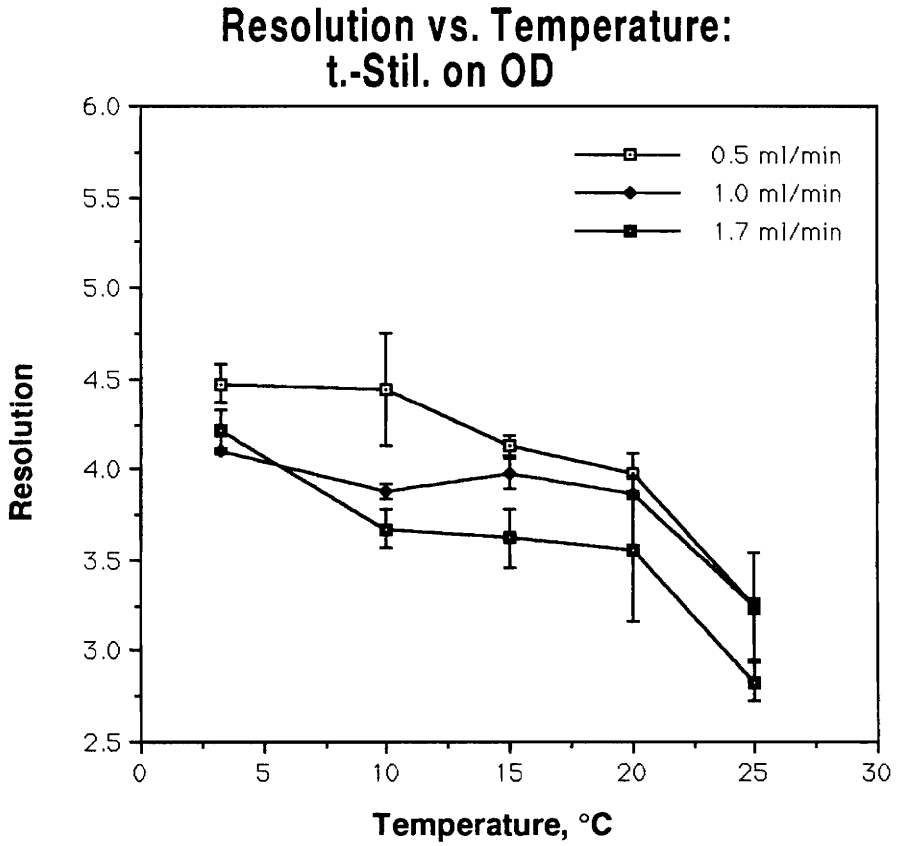

Figure 39. The plot of resolution versus temperature for trans-stilbene oxide enantiomers on a Chiralcel OD stationary phase is shown. Note that the 1.0 ml/min flow rate plot does lie in the middle, but that it crosses the lower-lying 1.7 ml/min plot at the 3.3°C point. (Error bars as per Figure 38.)

Table Xa. Summary of measured parameters at 1.0 ml/min flow rate for the DNBPG column, with TFAE as solute.

n	T (C)°	k', R iso.	k', S iso.	α	R
3	26	0.42±.004	0.57±.005	1.36±.014	1.09±.048
3	20	0.49±.005	0.68±.001	1.38±.0061	1.32±.007
3	15	0.55±.005	0.77±.005	1.40±.011	1.46±.005
3	10	0.59±.003	0.85±.008	1.42±.008	1.58±.064
3	3.3	0.68±.005	0.98±.005	1.45±.009	1.71±.032

Error is equal to the mean $\pm t(s/\sqrt{n})$, at a 95% C.I.*n* is the number of runs. (From ref. 279.)

Table Xb. Summary of measured parameters at 1.0 ml/min flow rate for the cellulose (OD) column.

Solute	n	T (C)°	k',R iso.	k',S iso.	α	R
TFAE	6	25	0.35±.003	1.08±.004	3.06±.001	4.20±.36
	6	20	0.33±.002	1.17±.003	3.54±.014	4.32±.013
	6	15	0.37±.001	1.29±.004	3.52±.007	4.44±.024
	6	10	0.37±.002	1.36±.008	3.64±.015	4.76±.016
	6	3.3	0.42±.006	1.48±.001	3.55±.005	4.55±.014
t-stil.	6	25	0.32±.002	0.80±.003	2.45±.01	3.24±.041
	6	20	0.34±.003	0.94±.009	2.72±.012	3.86±.023
	6	15	0.36±.003	1.06±.011	2.92±.021	3.98±.090
	6	10	0.48±.002	1.32±.003	2.75±.006	3.88±.045
	4	3.3	0.42±.003	1.25±.001	2.96±.019	4.12±.017

5.2 Sub-Zero Optimization Studies

Several sets of studies were conducted using temperatures below 0°C to probe the lower limit of resolution improvement possible by lowering column temperatures. The first experiment spanned a range of 0 to -30°C, and used a 20% alcohol modifier with hexane in order to reduce band spreading at such low temperatures, since 2-propanol's high viscosity would be an even bigger problem at such low temperatures, and the subsequent chromatographic band broadening at the previous 30% concentration would be excessive. We did not anticipate any changes in the capacity factors for individual enantiomers which would change the overall resolution versus temperature trend, but indeed an interesting change did occur.

The low temperature runs were repeated for the Chiralcel OD column, but included temperatures from 25 to -25°C for this second set of data. It was difficult to join curves generated from the original 25 to 3.3°C data to the later 0 to -30° data because of magnitude changes caused by column aging. HPLC columns change over time and use; this was much more of a problem with the non-bonded cellulose CSP than with the Pirkle phase, however. The results presented in this section were generated from the later +25 to -25 series of injections, with a plot s for the DNBPG column between .0 and -30°C only.

Figure 40 summarizes both trans-stilbene oxide and TFAE results for ln capacity factor versus 1/T plot for the Chiracel OD column, and Figure 41 shows the corresponding plot for TFAE on the DNBPG column. The striking aspect of the OD column results is that the capacity factor for trans-stilbene oxide with a 20% IPA mobile phase is now ***less*** than that for TFAE with a 30% alcohol modifier. There would be an elution order change if both of these compounds were being separated in the same run. This effect can be explained by reviewing

20% IPA: k'(t-Stil.) ≤ k'(TF)

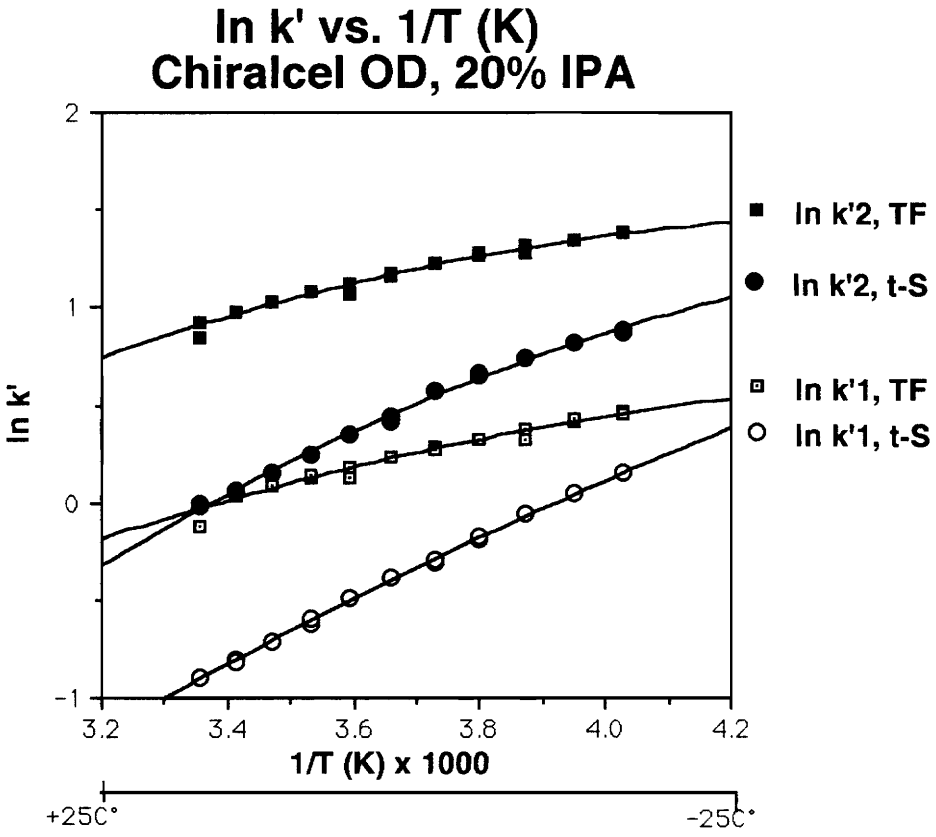

Figure 40. Plotted are logarithms of capacity factors for trans-stilbene and TFAE separated on the Chiralcel OD column at temperatures between +25 and -25°C. Each point represents three flow rates (0.5, 1.0 and 1.5 ml/min), with three replicate injections per rate. Lines are second degree polynomial regression fits, in contrast to the apparent linear behavior modeled for the 3.3 to 25°C runs (Figure 34). Note the reversal of ln k' magnitude compared to the 30% IPA mobile phase.

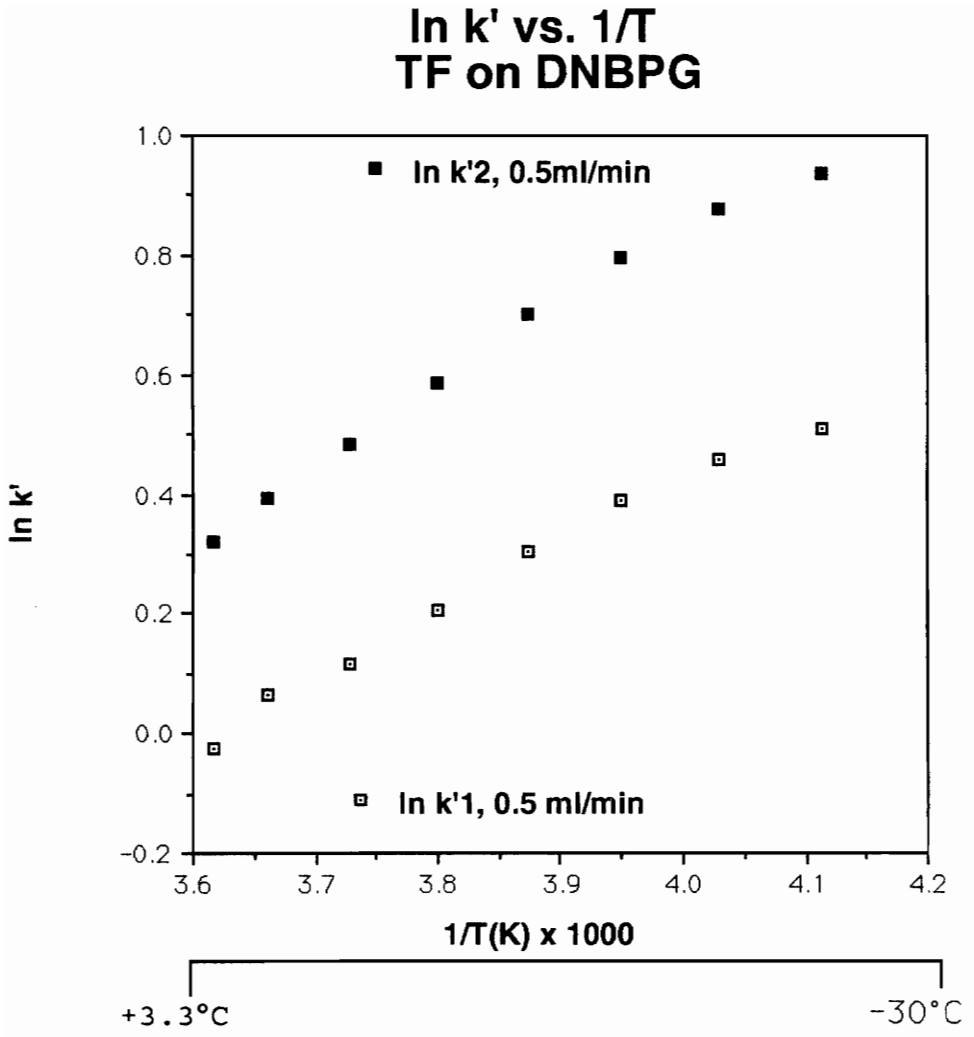

Figure 41. Here is the analogous plot to Figure 40, for TFAE on DNBPG, showing the results for 0,5 ml/min flow rate between +3.3 and -30°C. Each point is the mean of three injections.

the solubility data (Table IX) and keeping in mind the three elements involved in the general separation mechanism (Figure 12), we can argue that the decreased alcohol concentration is responsible for the increased amount of time that TFAE is spending in contact with he stationary phase (increased capacity factor). We know that TFAE is more soluble in octanol than in hexane (0.011 versus 1.5 x 10^{-6} moles per liter, respectively), and therefore when the alcohol concentration in the mobile phase drops from 30 to 20%, the TFAE can remain in contact with the CSP for a greater period of time, increasing its capacity factor. It is more difficult to make a similar argument for the trans-stilbene oxide, since it has high solubility in both mobile phase constituents.

Figure 42 shows the overall reduced plate height (for the first eluting enantiomer) versus temperature plots for all three solute-CSP combinations for a 0.5 ml/min flow rate and 20% alcohol modifier. Each data point is the mean of three injections. The TFAE separation on DNBPG includes temperatures from +3.3 to -30°C; the OD column data is for a +25 to -25°C range.

The reduced plate height *h* , versus normal plate height H (or HETP) is simply H divided by the silica gel particle size in micrometers, which normalizes band spreading for columns of different particle sizes. By using *h*, the differences between the solute-CSP combinations are due only to the differences in kinetics arising from the various retention mechanisms at work in each case. The overall ranking agrees with the theoretical discussion of the possible *number* of interactions between solute and CSP, with the simplest case of trans-stilbene oxide on OD (inclusion complex only) exhibiting the least amount of band broadening. Next we have the TFAE on the Pirkle phase DNBPG, where several types of attractive-repulsive interactions may occur, specifically charge-transfer and hydrogen bonding. Finally, the TFAE separated on Chiralcel OD, featuring inclusion complex, charge transfer and hydrogen bonding interactions which combine to produce the greatest overall resolution (see

Figures 37 and 38) also exhibits the poorest efficiency (highest h) at low temperatures. Note also that even at 25°C, neither of these CSPs show a reduced plate height value of only 7 to 8, which is mediocre in comparison to the 2 to 3 of a well-packed reversed-phase column.

Generally, there must be a distinction made between the number of possible interactions forming a diasteriomeric complex between the CSP and solute, which affect the kinetics of the separation, and the strength of these interactions, which influence the thermodynamic parameters of capacity factor and selectivity. Both the number and interaction strength interact to produce a final enantioselectivity, and both are influenced by temperature and mobile phase composition.

The selectivity behavior of the two stationary phases is remarkably dissimilar at low temperatures and a 20% alcohol mobile phase. Figure 43 shows the behavior for separations of TFAE and trans-stilbene oxide on Chiralcel OD column, with decreases in selectivity, especially for trans-stilbene. In contrast, selectivity linearly increases as the temperature drops when separated on the DNBPG column, as seen in Figure 44.

Finally, overall resolution versus temperature is shown in Figure 45 for the cellulose column, and in 46 for the Pirkle. Here is a profile that we have not yet seen so clearly: the trans-stilbene oxide resolution increases to a maximum, than begins to decrease at very low temperatures as the plate height begins to increase (see Figure 42). For the TFAE-OD case, the sharp increase in band broadening negates the increased selectivity (Figure 44) and capacity factor (Figure 41), producing a steadily decreasing resolution as the temperature drops. In addition, the very high k' values also are contributing to the increased plate height, since more broadening occurs for longer retention times. Compare this with the gain in resolution with lowered temperature for a ***30%*** alcohol mobile phase, as shown in Figure 38.

Finally, the previously nearly linear resolution versus temperature curves for various flow rates in the 3.3 to 25°C (Figure 32) obtained at 30% alcohol and 70% hexane, is now

much less linear at the lower flow rates, and a resolution peak occurs near -10°C for the 0.3, 0.5 and 0.7 ml/min flows. The 1.0 and 1.2 ml/min curves are still increasing in resolution at -20°C, the lowest experimental temperature. Solubility factors can again aid in explaining this be behavior. At 30% IPA, resolution varies between slight over 1 and 1.75 for all flow rates, but upon going to the 20% alcohol mobile, resolution values jump to between 2 and 4.75 for the same 3.3°C temperature. We postulate that the TFAE's decreased mobile phase solubility allows more time in contact with the CSP, and alters the fundamental adsorption equilibria. Mechanistically, the role of charge transfer interactions, more temperature sensitive because of its lower energy, may become amplified by this change in mobile phase.

These results are unusual for reversed-phase HPLC separations, where essentially one mechanism is responsible for separations, and changes in mobile phase and temperature primarily affect the capacity factors obtain, and where efficiency is more important in comparison with selectivity. For chiral stationary phases, the opposite situation exists.

The balance of the three equilibrium factors (CSP, solute and mobile phase) is easily altered by changes in any of the three or by temperature, producing drastic changes in overall resolution behavior. This makes generalizations, which might be useful to guide method development, rather risky, as we noted earlier. After finishing the first batch of temperature studies, the inclination was to conclude that lowered temperature always increased resolution, but solute and mobile phase factors complicate the situation considerably.

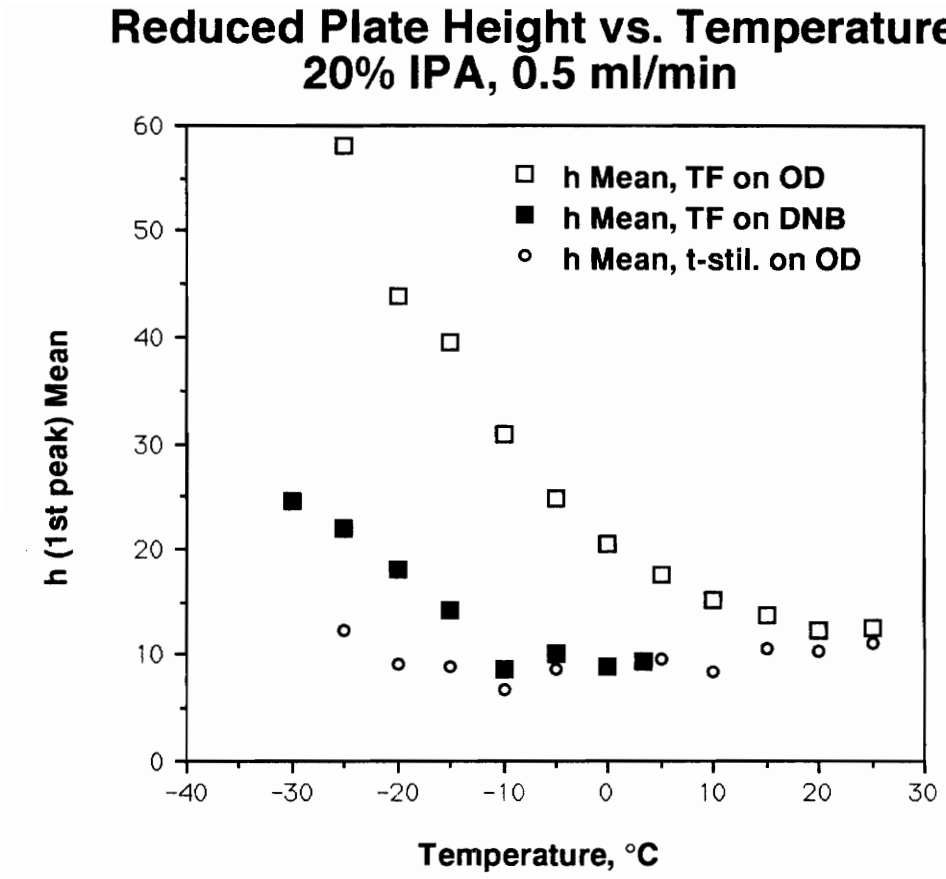

Figure 42. The reduced plate height (HETP/particle size) of the first eluting isomer is plotted versus temperature at a flow rate of 0.5 ml/min and an 80:20 hexane-2-propanol mobile phase. Note that the plate height, or rate of band broadening, follows the proposed number of solute-CSP interactions from low (trans-stilbene oxide on OD) to high (TFAE on OD).

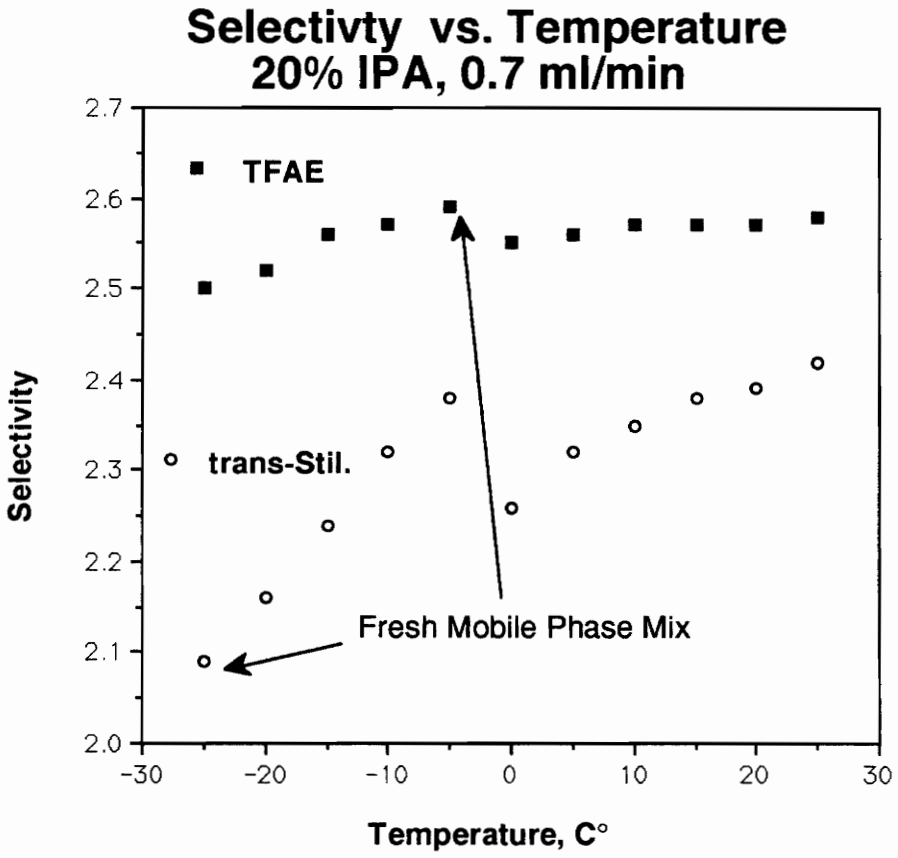

Figure 43. Selectivity versus temperature for both solutes on the Chiralcel OD with a 0.7 ml/min flow rate and 20% alcohol modifier. The break in both curves is caused by the use of a fresh batch of mobile phase, which used a different lot of 2-propanol containing a different amount of water. (See Section 5.3, Mobile Phase Studies.) Compare the decrease in trans-stilbene selectivity here to the increase at 30% alcohol, Figure 37.

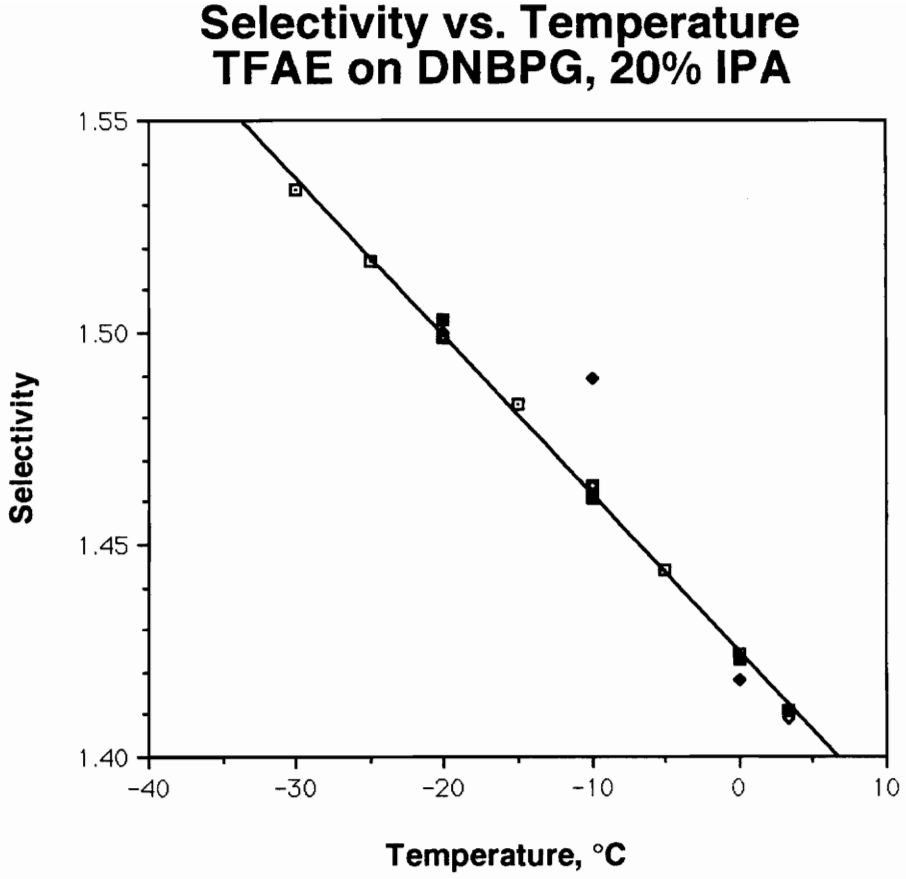

Figure 44. Selectivity for TFAE enantiomers separated on DNBPG with 20% alcohol modifier at 0.3, 0.5, 0.7, 1.0 and 1.2 ml/min flow rates. Compare the linear increase in selectivity with decreasing temperature seen here with the decreasing TFAE selectivity shown in Figure 43.

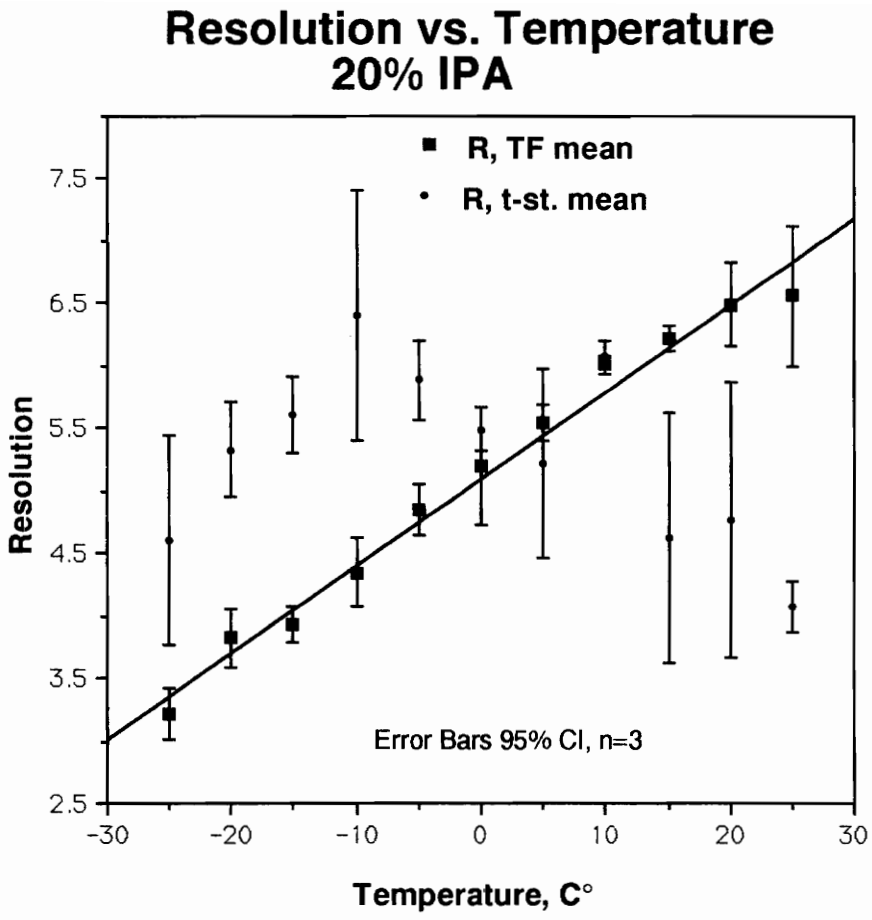

Figure 45. Resolution is plotted as a function of temperature, with error bars representing a 95% CI, and calculated according to reference 279. Flow rate is 0.7 ml/min.

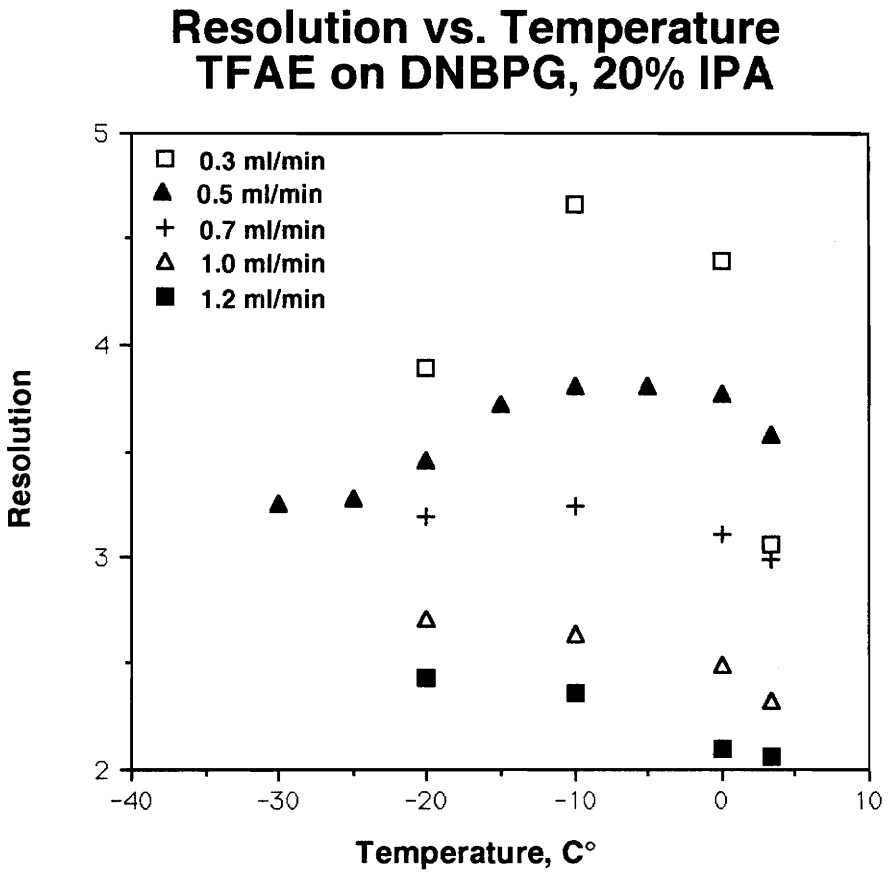

Figure 46. Resolution of TFAE on DNBPG using a 20% alcohol mobile phase and at flow rates of 0.3, 0.5, 0.7 1.0 and 1.2 ml/min.; each data point is the mean of three injections.

A thermodynamic analysis of the temperature data described so far can quantitate some of the changes in chromatographic behavior we have observed qualitatively. Table XI below is a summary of various enthalpy and entropy values calculated as described in Chapter II, Theory. The slope error, as calculated from the analysis of variance table from each linear regression model (StatView software), gave a final enthalpy error range of between ±3 and 25% 30 to 135 cal/mole), depending on the individual chromatographic results.

The enthalpy and entropy values for TFAE separated on DNBPG are all negative, indicating an ethalpy-controlled situation, and there is a slight decrease when moving from 30 to 20% alcohol modifier. In contrast, the Chiralcel OD column shows a change from negative to positive $\Delta\Delta H°$ and $\Delta\Delta S°$ values when the mobile phase is changed, indicating a change from enthalpic to entropic-control. This has implications for method development: if the entropy term is predominant (Equation 24), and the enthalpy term positive, then the separation is under entropic control and decreasing temperature will not be helpful. For the TFAE on Chiralcel OD, with positive enthalpy and entropy terms (boldfaced in Table XI) at 20% IPA, we have seen that the resolution becomes much worse at low temperatures (Figure 45). The same holds true for trans-stilbene oxide, which goes from a very negative to a highly positive enthalpy, and exhibits an inverted parabolic resolution versus temperature curve in Figure 45.

Table XI. Thermodynamic quantities for the preceding chromatographic separations.

		ΔH°: cal/mole		ΔS°: cal/mole K			
Solute/CSP	% IPA	ΔH°1	ΔH°2	ΔS°1	ΔS°2	ΔΔH°	ΔΔS°
TF/DNB	20	-544	-639	-1.97	-2.14	-95	-0.17
	30	-844	-960	-3.24	-3.48	-117	-0.24
TF/OD	20	-366	-352	-1.25	-0.71	**+14.0**	**+1.77**
	30	-314	-513	-1.59	-1.67	-199	-0.08
t-Stil/OD	20	-790	-700	-3.10	-2.35	+90.0	+1.49
	30	-232	-108	-0.604	-3.22	**-848**	**-2.62**

Enthalpy Error: ±3 to 25% (30 to 135 cal/mol), 95% C.I.

5.3 Mobile Phase and Solute Studies

5.3.1 Mobile Phase Study Background

The second major part of the optimization research involved varying the 2-propanol modifier in the mobile phase. Although other alcoholic and halogenated hydrocarbons have been used, as Zief[276] described, and can have certain selectivity advantages for a particular CSP-solute combination, the most commonly used modifier is 2-propanol. It is miscible with hexane, the usual weak mobile phase component, and is useful in solvating many of the more polar solutes which otherwise could not be separated in a predominantly hexane-based solvent system. Its high viscosity is a disadvantage, particularly at lowered temperatures.

As described in a preceding section, the need for a mobile phase study became apparent after a change in lots of alcohol significantly changed capacity factors (see Figure 47).The capacity factor for S-TFAE (k'_2, TF) was particularly variable. A comparison of the label analyses for the three lots revealed slightly different amounts of water present, and even more important was the fact that these different jugs had been exposed to the moisture-containing ambient atmosphere for various periods of time. Since water, when dissolved in IPA and subsequently the mobile phase, would be an extremely effective polar modifier, we decided to vary the amount of water in the mobile phase to confirm this theory.

Figure 48 shows the results of the effect of varying amounts of water in a dried 30% IPA/hexane mobile phase (see Chapter IV, Experimental, for details). Both resolution and selectivity curves could be modeled with a logarithmic function, with correlation coefficients of 0.937 and 0.981, respectively. It is obvious that small changes (0.01% of the mobile phase) in the water content of an alcoholic modifier, whether caused by absorption of water from the atmosphere or from initial production conditions, can have significant effects on a chiral

assay's effectiveness, a particular concern if the analysis must meet daily system suitability standards which include capacity factor and resolution requirements.

5.3.2. Alcohol Mobile Phase Studies

We next varied the amount of 2-propanol in hexane, using the DNBPG column and TFAE initially. This combination produced smooth, logarithmic curves for capacity factor, selectivity and resolution versus 2-propanol concentrations between 2.5 and 30%. The plot for plate height produced a linear relationship, with plate height increasing with an increase in 2-propanol. Figure 49 shows the results for final resolution. versus % IPA at 25°C, 0.6 ml/min flow rate, with six injections per condition. The conclusion is that the polar modifier content can strongly affect all components of the resolution equation, and has been neglected as an optimization tool. Too often in the application guides only a 90:10 hexane-isopropanol recommendation will be given, with no mention of possible alternatives. This mixture is a good starting point, but if there is some evidence of enantiomeric separation, then the method may be tuned by varying the modifier. The increase in efficiency with decreased alcohol percentages is especially interesting.

The last mobile phase experiments tested the effect of various isopropanol concentrations on the separation of TFAE on the cellulose column. Since we had found such diverse behavior in past comparisons, it was deemed unwise to extend the conclusions regarding mobile phase optimization from the Pirkle column to the cellulose CSP due to the different possible retention mechanisms.

In addition to TFAE, we also separated three other racemic mixtures: trans-stilbene oxide once more, propranolol and a chiral amino acid derivative, acetylacetamide cinnamic acid methyl ester (AACA-ME), synthesized by Dr. Brian Hanson of the VPI faculty. The latter two structures are shown in Figure 50. Physical-organic structural indices for propranolol are given in Table IX, but not for AACA-ME due to repeated failures of the SPARC software

when this structure was input. The version used was an early one, but several requests to the EPA in Atlanta for an updated program went unanswered, as did requests for additional background material detailing the SPARC calculations.

Figure 51 is a plot of the capacity factor of the second eluting peak versus percentage of isopropanol in the mobile phase, a flow rate of 0.6 ml/min, temperature of 25°C, with three replicate injections per condition. All four solutes are plotted to demonstrate the effect of structure on retention. Logarithmic curves are fitted to each solute curve to give a quantitative aspect to the differences in curvature. TFAE and propranolol are both similar in the Taft-Kamlett α and β indices, and in their calculated solubilities in hexane and octanol (see Table IX). These compounds have very similar capacity factor behavior in Figure 51, so it can be concluded that their interaction mechanisms with the CSP are also similar, consisting of inclusion complex, π-π charge transfer and hydrogen bonding. The trans-stilbene oxide and AACA-ME have much smaller capacity factors and seem to form a second grouping. Their structures are somewhat similar, lacking the large π-electron donating ring systems and hydroxyl groups (a hydrogen donating group) of the previous two molecules. Although the AACA-ME, with its two carbonyl groups and secondary amine, would seem to have greater hydrogen bonding possibilities, the AACA-ME retention is less than that of trans-stilbene oxide above 10% isopropanol concentrations, but greater at 10% and below. The polar alcohol modifier is evidently competing strongly for the AACA's hydrogen bonding sites at higher alcohol concentrations. The AACA is may also be participating in a host-guest (inclusion) complex with the cellulose by means of its phenyl ring.

Figure 52 details the relationship between 2-propanol concentration and plate height of the second eluting enantiomer for the four solutes (conditions as above). In contrast to the behavior for TFAE on the Pirkle CSP, here we see an *increase in plate height* as the alcohol content is decreased, opposite to the Pirkle column behavior. Again, the analyst must not make optimization strategy generalizations using data from one type of CSP,and then apply it to

another. For the cellulose column, a viscosity decrease with isopropanol decrease does not seem to be significant in reducing plate height, as with the DNBPG. Other factors, such as solubility considerations, are at work.

Resolution of each of the four solutes is plotted versus alcohol percentage in Figure 53. The order, from high to low resolution, is TFAE, trans-stilbene oxide, propranolol and bringing up the rear, with very low resolution values, is AACA-ME. This order is identical to that for selectivity versus alcohol content (not shown), and is represents the relative energies of interaction between the solute and CSP. Although not easily predictable from its structure, the amino acid is the most difficult to resolve, having lower capacity factor and selectivity than any of the other solutes. In addition, its selectivity actually decreased with decreasing alcohol content.

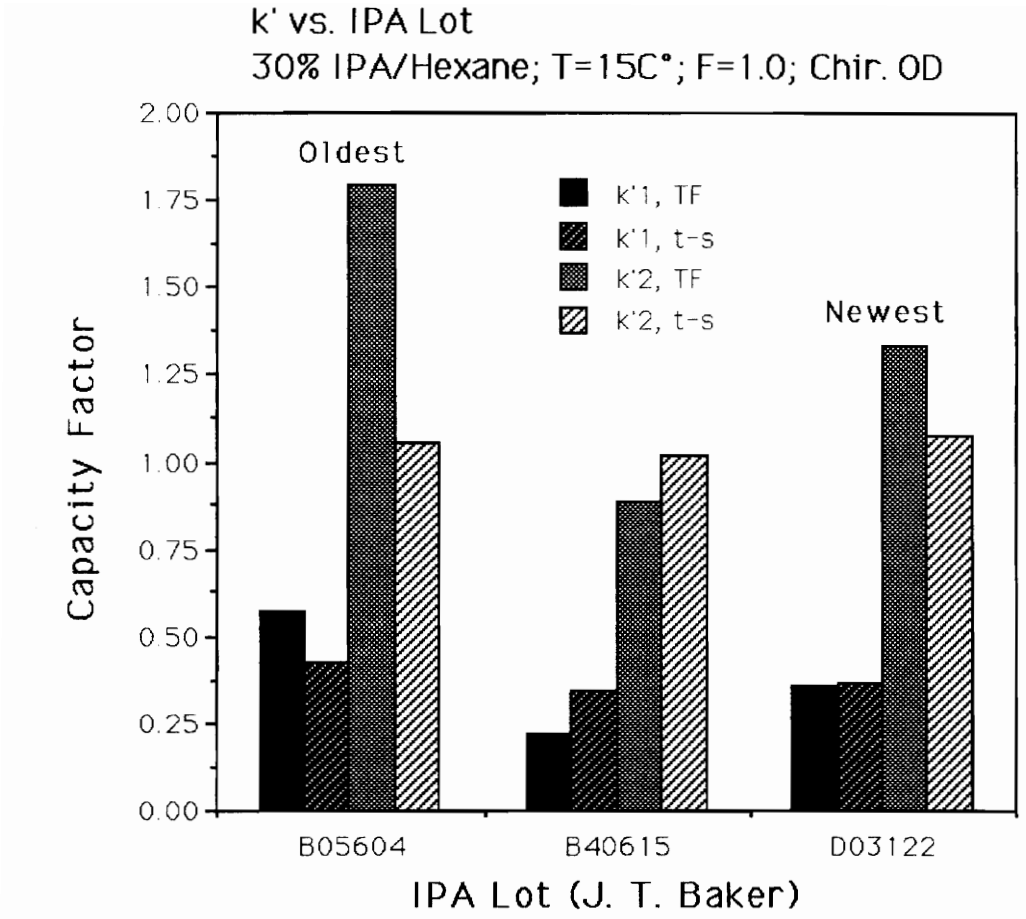

Figure 47. Shown above is the variation in capacity factors obtained using several different lots of 2-propanol (IPA). Conditions for these runs were 15°C, 1.0 ml/min flow rate, the Chiralcel OD column, 30% IPA/hexane mobile phase and the TFAE and trans-stilbene oxide solutes.

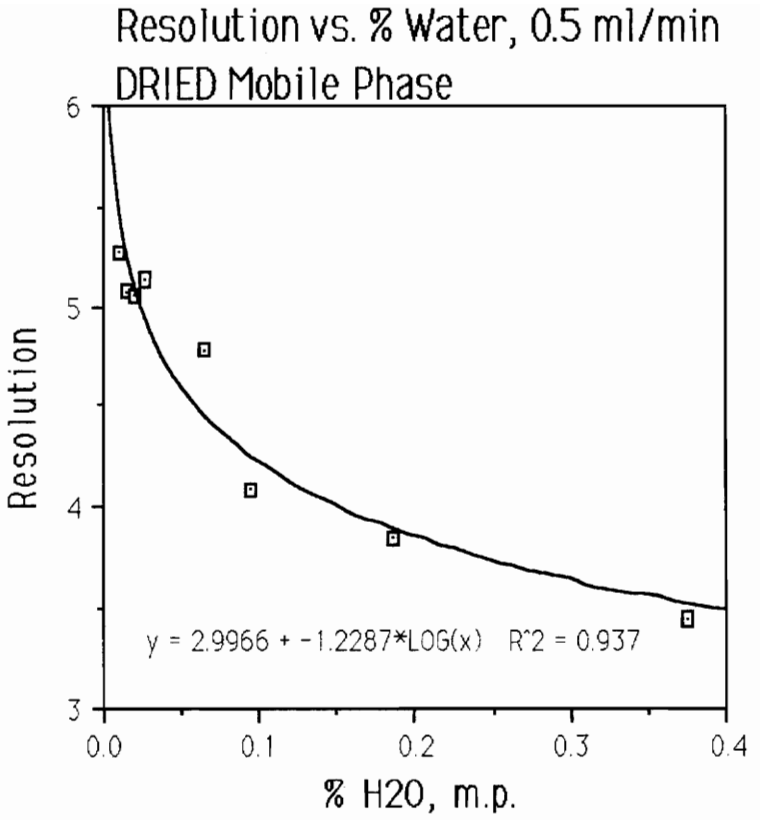

Figure 48. The results of a water titration study shown as a plot of resolution versus percentage of water in the mobile phase, which had been dried previously. Two injections were made for each data point shown., the solute was TFAE and t the column a Chiralcel OD.

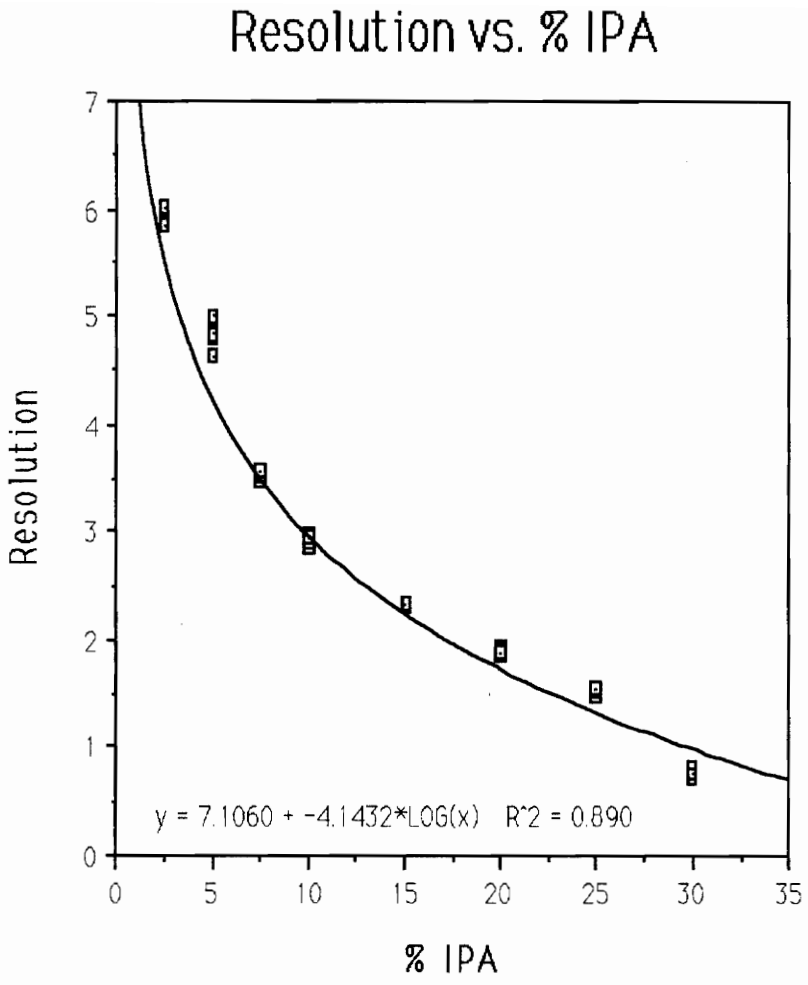

Figure 49. Resolution of the TFAE racemic mixture is plotted versus the mobile phase alcohol content for a flow rate of 0.6 ml/min, a temperature of 25°C, with six injections per condition.

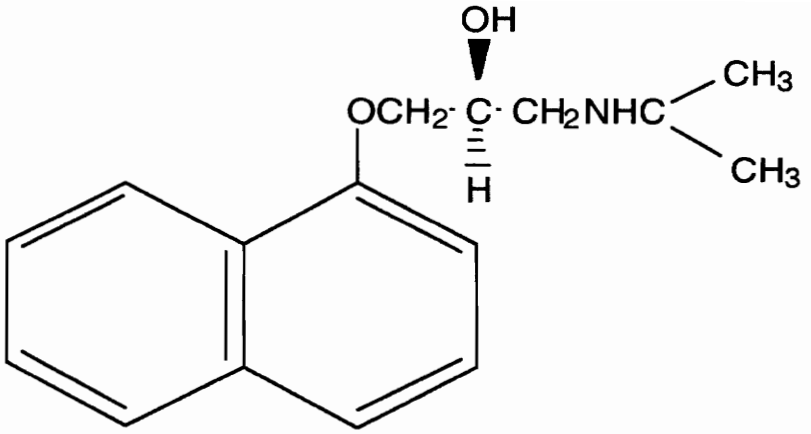

R-Propranolol

50 a.

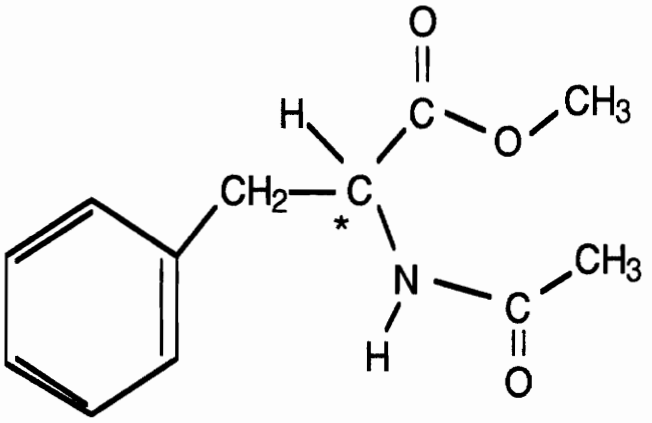

Acetylacetamide Cinnamic Acid Methyl Ester (AACA-ME)

50 b.

Figure 50. Structures of the two additional solutes in the mobile phase studies are shown.

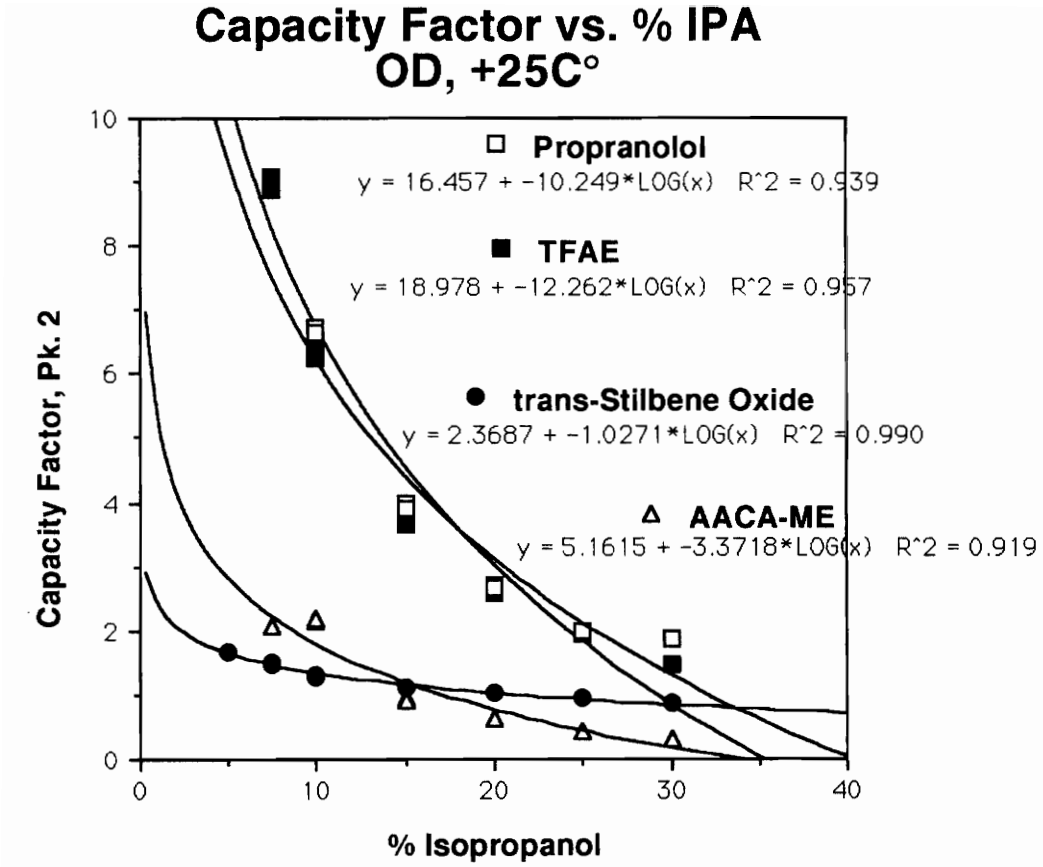

Figure 51. The capacity factor versus % IPA plots are shown for the four solutes separated on a Chiralcel OD column, at 25°C, with a 0.6 ml/min flow rate and three replicate injections per data point.

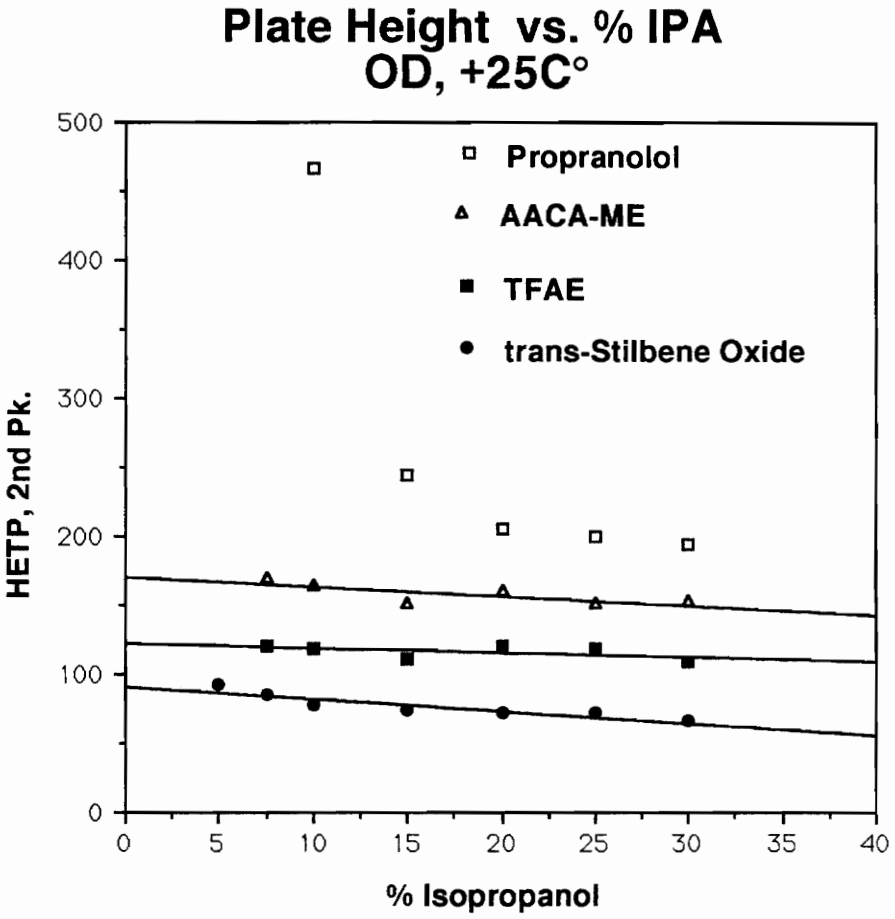

Figure 52. The plot of plate height versus alcohol concentration indicates a slight increase in HETP as the alcohol concentration increases, opposite to what was noted for TFAE separated on DNBPG.

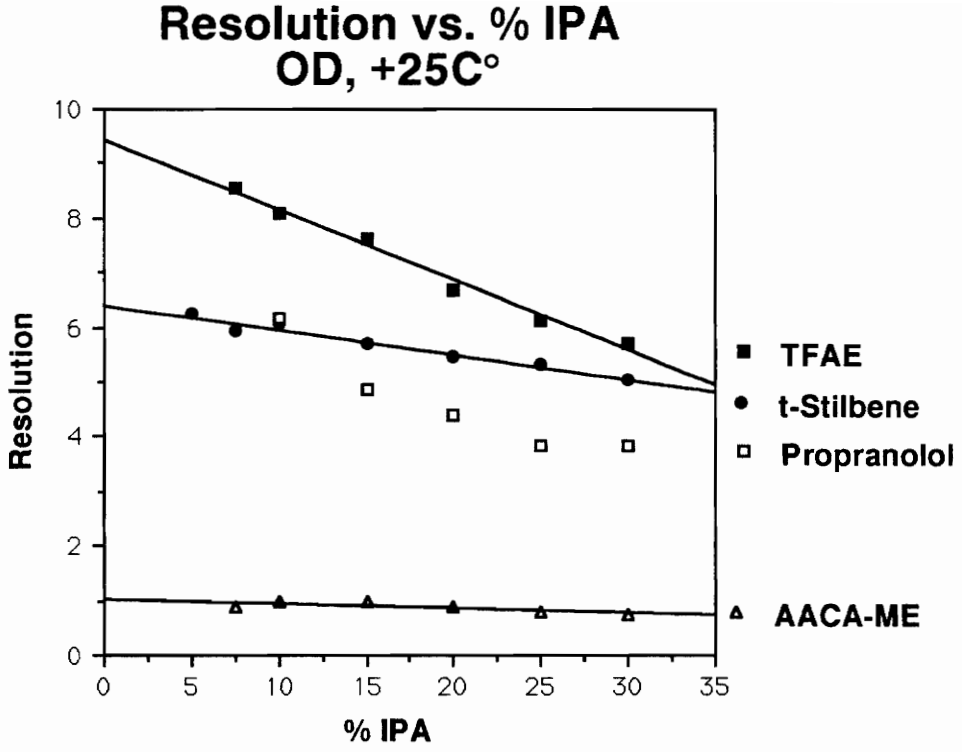

Figure 53. The resolution of four test solutes versus % isopropanol is plotted, with separation conditions as noted previously. The ranking of their resolution numbers is identical to the ranking for selectivity versus percent alcohol, and is indicative of the energy of their interactions with the cellulose CSP.

5.4 Quantitative Structure Retention Relationships: Evaluation of Structural Descriptors

The retention data from enantiomeric separations of TFAE, trans-stilbene oxide, propranolol and AACA-ME were plotted as the natural logarithm of the capacity factor of the second eluting peak versus percentage of 2-propanol in the mobile phase. All separations were performed at 25°C, 0.6 ml/min using the Chiralcel OD column. All solutes but the TFAE would have required derivatization to achieve enantiomeric resolution on the DNBPG column. Trans-stilbene oxide, propranolol and AACA-ME were tried on the Pirkle column, with the results of one peak appearing at approximately the void volume irrespective of the mobile phase composition. It was concluded that too few interactions are present between these underivatized compounds and the Pirkle CSP for adequate retention.

Figure 54 gives the linear regression results for plots of ln capacity factor versus percentage of 2-propanol in the mobile phase under the chromatographic conditions stated above. The objectives of these plots is to obtain a slope value, which is a measure of the sensitivity of the solute retention to modifier changes. The results of least squares linear regression models, including the slope determinations and the previously calculated structural constant s, are shown in Table XII.

Finally, in an attempt to correlate the structural descriptors with retention behavior, we plotted the Taft-Kamlett a and b values, as well as polarizability and molecular volume against the slopes determined by Figure 54. Only the Taft-Kamlett a descriptor, an index relating to the number of hydrogen bonding sites per molecule, could be correlated to retention. The results are shown in Figure 55, including a best-fit second degree polynomial equation. No conclusions can be drawn from this small amount of data, but the methodology is valid and

future work with a greater number of enantiomeric solutes, structural descriptors and other CSPs may help towards the ultimate goal of better column selection.

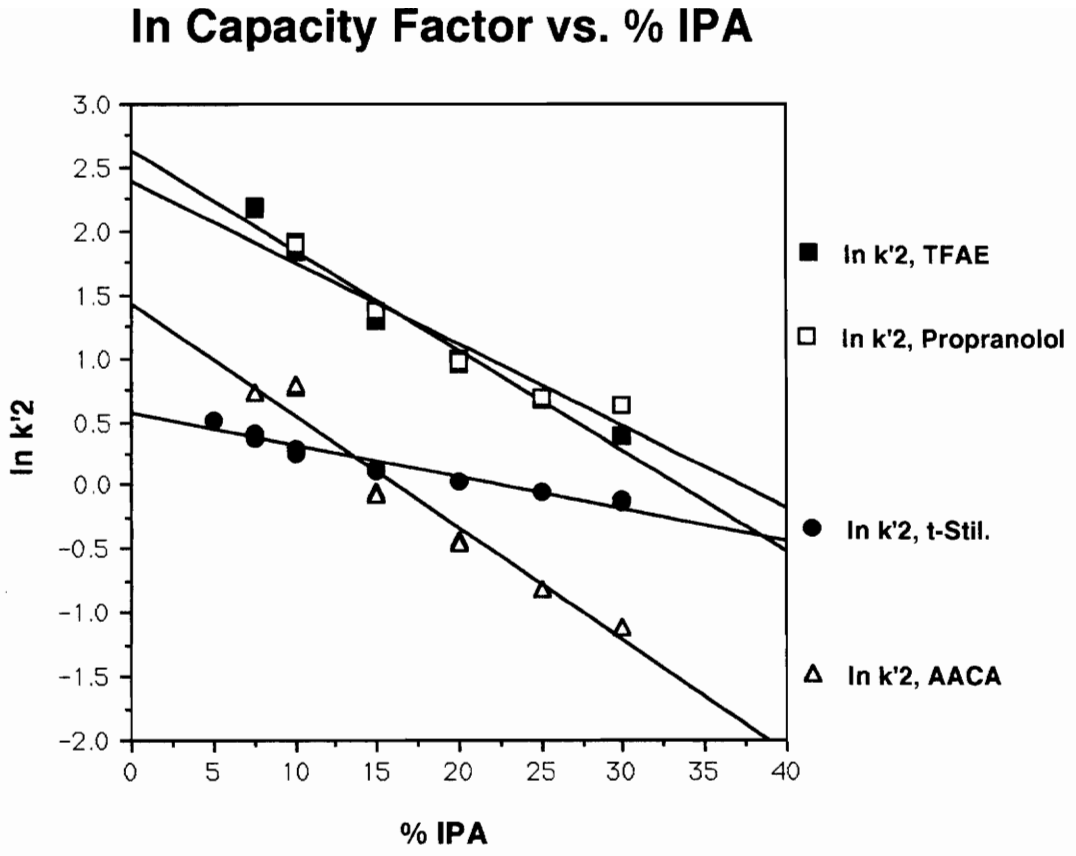

Figure 54. Plots of the ln of the second eluting enantiomer versus 2-propanol percentages are shown. Chromatographic conditions included a flow rate of 0.6 ml/min on a Chiralcel OD column, 25°C and detection at 230 nm.

Table XII. A summary of the experimentally determined slope values for ln k' vs. % IPA, and the computer-calculated structural descriptors for these test solutes.

Solute	Slope (x100)	Intercept	R2	T.-K. α	T.-K. β	Polariz.	Mol. Vol.
TFAE	-7.859	2.645	0.975	0.548	1.050	2.900	207.0
Propran-olol	-6.436	2.404	0.932	0.455	1.25	3.13	223.0
t-Stilbene	-2.494	0.5630	0.945	0.000	0.466	2.360	187.0
AACA-ME*	-8.857	1.432	0.965	NA	NA	NA	NA

* The SPARC program consistently "crashed" when this structure was input, and consequently no structural descriptors could be calculated.

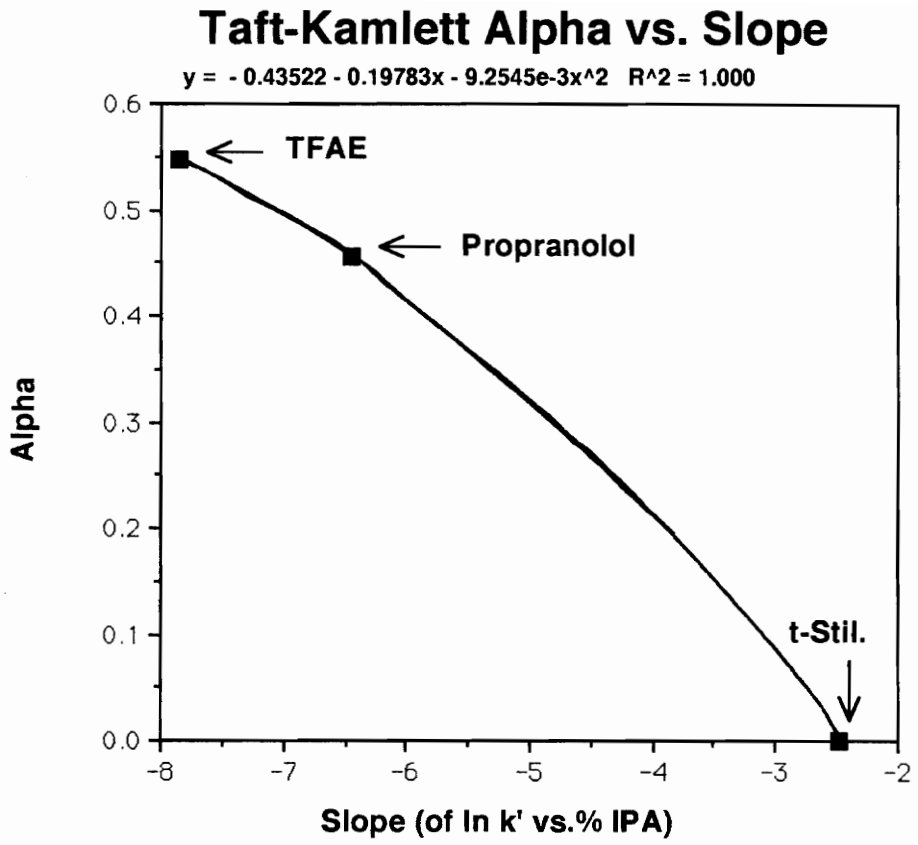

Figure 55. Shown above is the plot of Taft-Kamlett α versus the slope of a plot of ln k' vs. % IPA for the three solutes. A least squares fit of the second degree polynomial noted on the graph gave an R2 value of 1.000.

5.5 Application Studies

5.5.1 Acetylacetamide Cinnamic Acid Methyl Ester

This compound was synthesized by Dr. Brian Hanson of the VPI & SU faculty to explore the utility of a chiral catalyst. The task was to obtain the enantiomeric purity in a situation of very high concentration of one enantiomer. This required that the analysis be capable of quantitating a very small peak which elutes near a large one, sometimes a difficult job, especially for separations which exhibit moderate to large band broadening as many chiral analyses do.

The structure of AACA-ME is shown in Figure 50b. The first step in any method development is to examine the functional groups on the analyte, here looking for polar species and aromatic rings which can interact with a CSP. Solubility is also a question, and in this case AACA-ME is soluble at low concentrations in a mixture of 2-propanol and hexane. allowing the use of normal-phase type CSP, of which our lab had several.

The Daicel chiral application guide[277] was consulted, following the paper algorithm for a carbon chiral center with a secondary amine and a carbonyl group attached. Several similar structures were found, and the CSPs recommended were the cellulose types with a carbamate functional group (Chiralcel OD), and an carbonyl-linked phenyl (Chiralcel OB). Structures of these CSPs are shown in Table III.

Both the OB and OD were tired, but only the OD showed the minor peak, and then only as an unquantitatible hump (Figure 56a). The mobile phase was 90/10 hexane/2-propanol, at 0.3 ml/min, and detection was at 254 nm. The solid AACA-ME sample was dissolved in 80/20 hexane/2-propanol at a concentration of 200 ppm.

Figure 56b. shows the results after 1.0% acetonitrile was added to the mobile phase, sharpening up the minor peak considerably and allowing quantitation. The final analysis gave

a value of 2.09% ± 0.74 (calculated as per ref. 274, 95% CI) for Sample I, and 11.2% ± 1.54 for Sample II. Values are expressed in percentage of the total peak area, since no enantiomerically pure standards were available.

The acetonitrile has been recommended by many researchers as an additive in the 0.1 to 2.0% range which helps to reduce tailing and band spreading on cellulose-type columns. The mechanism may be analogous to a silica gel normal-phase column, which have active silanol groups. Upon the addition of a fixed percentage of a polar modifier to the mobile phase, peak shape and retention time reproducibility is improved as these active sites are occupied by the polar additive. A similar situation may be present on the silica-based cellulose columns, with exposed active silanol sites interacting strongly with more polar analytes, causing peak shape deformation.

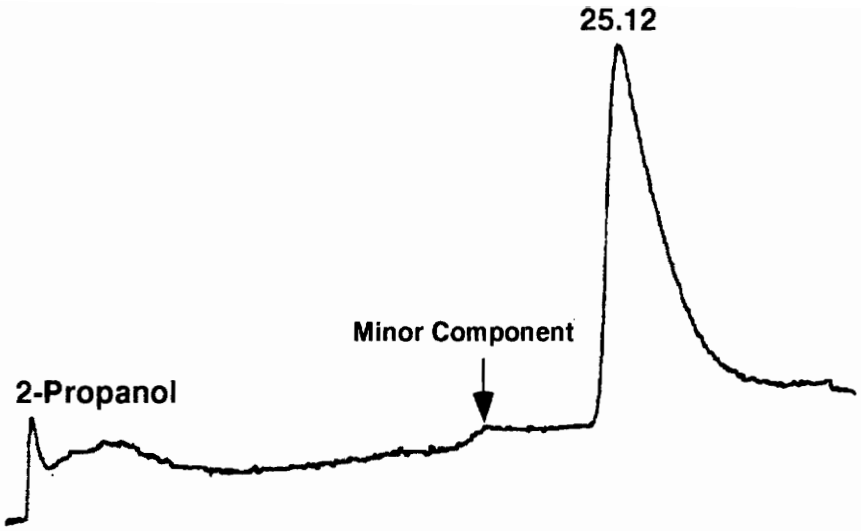

56a. Without acetonitrile

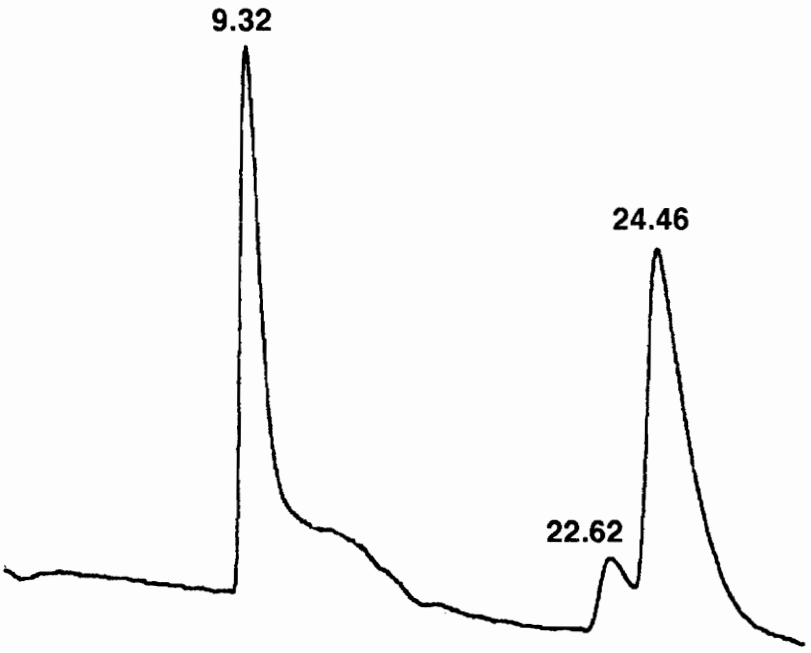

56b. With 1.0% acetonitrile

Figure 56. Method development results for AACA-ME; Chiralcel OD column, 0.3 ml/min of a 89/10/1 hexane/isopropanol/acetonitrile mobile phase, detection at 254 nm.

5.5.2 Method Development for 4-Fluoro-Glutamic Acid

A second chiral separation was undertaken for Dr. Milos Hudlicky, an internationally recognized expert in fluorine chemistry still active in research at VPI & SU.

The goal of this application was to provide additional data on enantiomeric purity of several new synthetic fluorinated glutamic acid molecules. Since sample quantity was not a problem, UV detection at 200 nm gave adequate signal strength for the 0.15% (w/v) solutions in water.

These compounds provided an ideal test environment for the 18-6 crown ether CSP from Daicel, the Crownpak CR+. The usual mobile phase consists of perchloric acid (valuable for its UV transparency) in water, with up to 15% methanol added if needed for very hydrophobic samples. The fluoroglutamic acid dissolved easily in a 1:1 mixture of the pH 1.1 perchloric acid mobile phase and water. Although resolution for some solutes has been increased by decreasing temperatures,[278] it was not needed for this application.

Flow rate was kept low at 0.3 ml/min, although higher rates were tried, resolution suffered above 0.7 ml/min.

The mechanism has been postulated to consist of both ionic-dipole interactions between the quaternary ammonium ion (a protonated primary amine group) and the oxygen atoms in the crown. An acidic mobile phase is usually necessary for adequate protonation, and a primary amine group is required on the analyte. These columns are specifically designed for underivatized amino acids. Further interactions can occur between the phenyl groups attached to the crown (see Figure 11c), which are staggered in such a way as to create a chiral axis.

Figures 57 and 58 show the chromatograms for L-threo and D-erythro-4-fluoro-glutamic acids. Note that these molecules have two chiral centers, and therefore have four possible isomeric forms. Pure standards were not avail able to identify the smaller peaks.

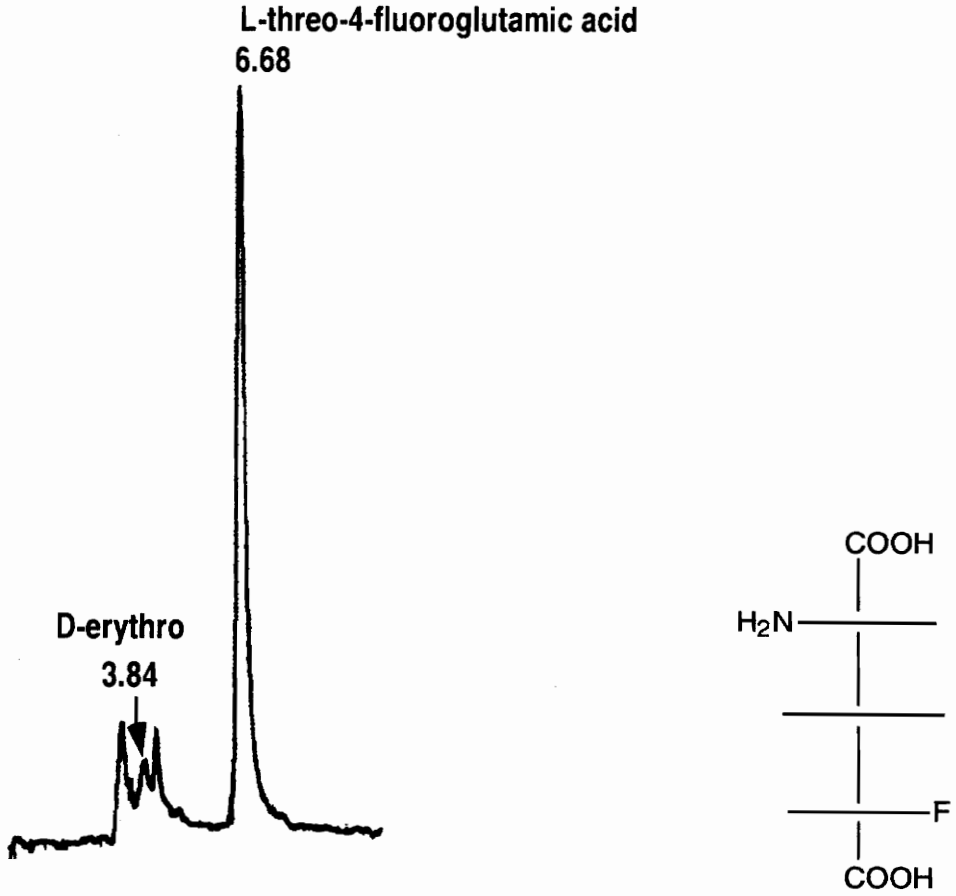

Figure 57. The separation of D-erythro and L-threo-4-fluoroglutamic acid is shown. The separation conditions are: Crownpak CR+ column (15 x 0.4 cm), perchloric acid mobile phase at.3 ml/min (pH 1.1), detection at 200 nm, temperature 25°C, samples 0.15% w/v in water (3.4 ug), injected volume 5 ul, detector cell volume 3 ul.

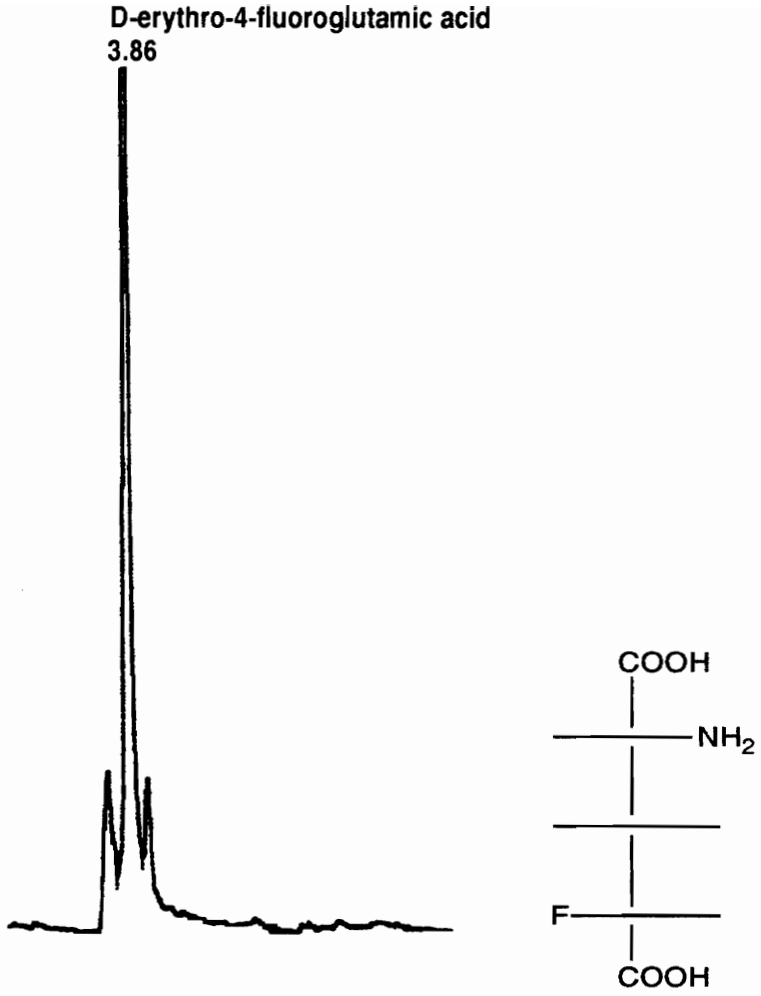

Figure 58. The injection of a nearly pure D-erythro-4-fluoroglutamic acid sample gave the above separation. Chromatographic conditions were identical to Figure 57.

5.6 Model Stationary Phase: Modification of Gold Surfaces

The various schemes which were tried in a effort to attach a chiral valine group to an oxidized gold surface were summarized in Chapter IV. The general strategy is presented in Figure 59.

The research time required to achieve the first step in this two-part experiment, attachment of a model CSP to the surface, far exceeded our original expectation of three to five months. Almost 10 months were spent first learning how to manipulate monolayer films and the analytical techniques required, then trying the various synthetic routes.

In the last month of work, a procedure which seems to yield a valine monolayer was discovered, but part two of the total experiment, *in situ* measurements of the model CSP-TFAE complex, has not yet been completed. Dr. Mark Anderson's research group at VPI &SU will continue with the experiment, developing the PM-FTIR *in situ* spectroscopic technique necessary for final results.

Results achieved for the surface modification experiments are novel and will be published, probably in a surface chemistry-oriented rather than chromatographic journal.

In this section we will summarize a surface modification technique which we believe was successful in attaching at least a partial monolayer of a (BOC)-L-Valine-functionalized 11-mercaptoundecanoic acid (MUA) chain to the surface via two separate synthetic schemes.

The first approach, outlined in Figure 22 in Chapter IV, reacted MUA in solution with the gold surface, then was itself reacted in the vapor phase with thionyl chloride in step 2. This moisture-sensitive layer was kept under vacuum in the manifold and immediately after purging excess thionyl chloride and HCL, the surface was flooded with a 300 mM solution of the (BOC)-L-Valine and allowed to react one hour. After rinsing and drying, IRRAS was

performed, yielding the spectrum seen in Figure 61. Compare this to Figure 60, the MUA spectrum before reaction with the acid chloride and amino acid.

Goal: Probe specific molecular interactions for diasteriomeric complexes between TFAE enantiomers and t-BOC-L-valine CSP, via FTIR of monolayers on gold surface

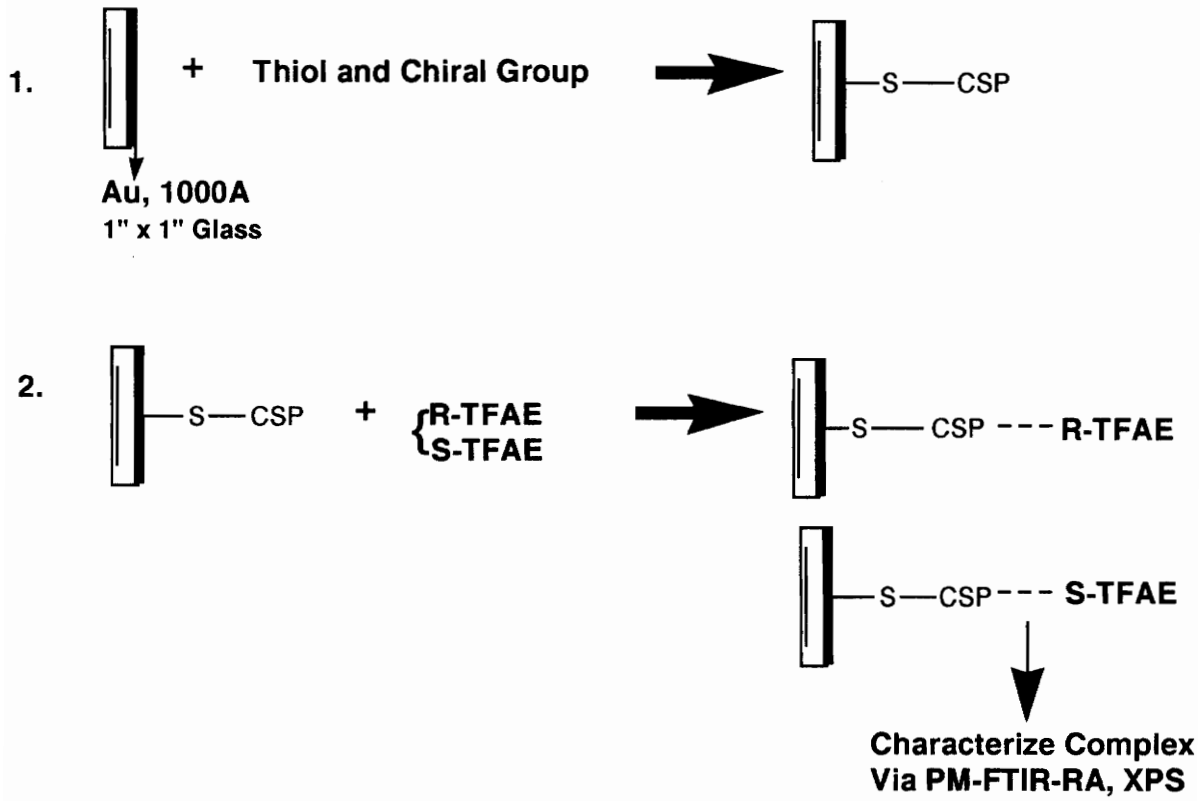

Figure 59. This is the overall experimental design for the model CSP work.

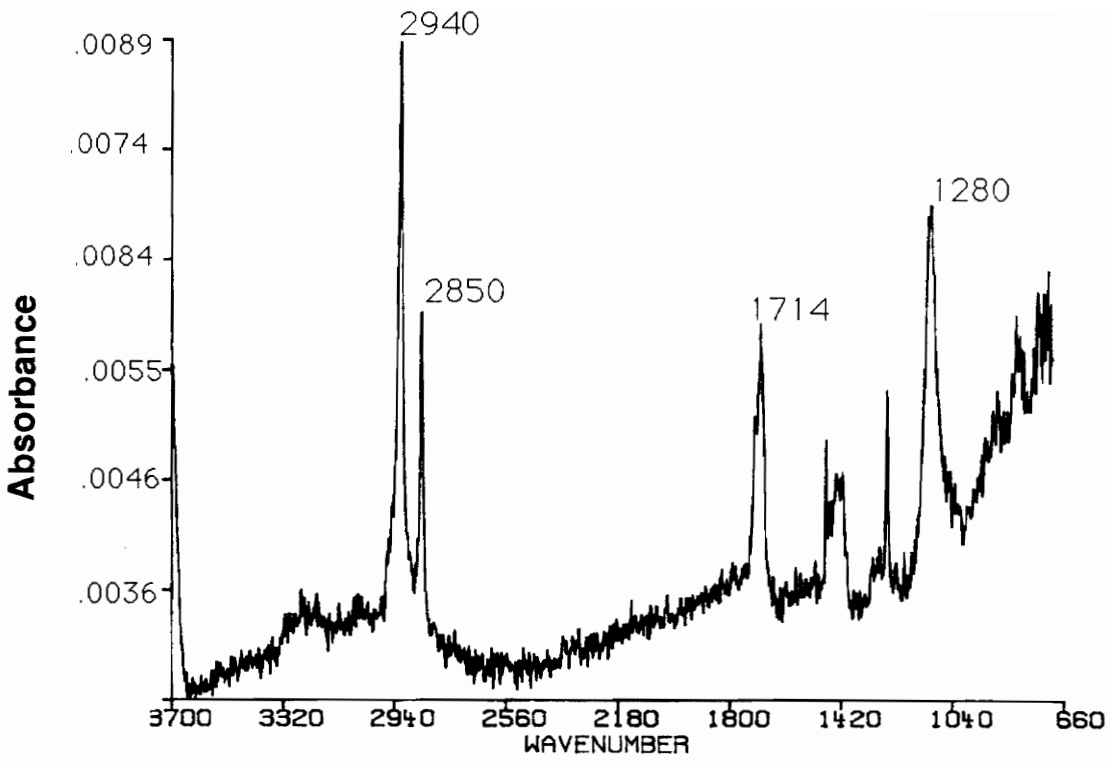

Figure 60. IRRAS spectrum of the 11-undecanoic acid-modified gold surface. Note the two bands for CH_2 symmetric and asymmetric stretching at 2940 and 2850 cm^{-1}.

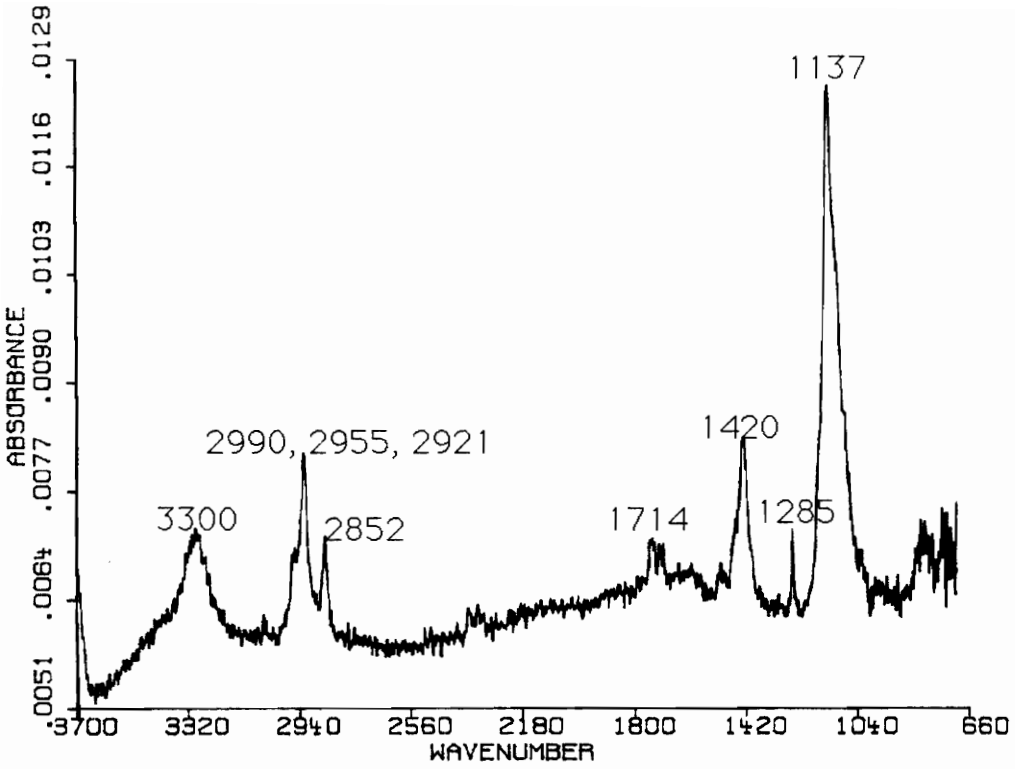

Figure 61. The IRRAS spectrum of a gold surface coated with a (BOC)-L-Valine group on the end of a undecanoic acid chain. Note the presence of the methyl group asymmetric stretching band at 2990, and the large anhydride band at 1137 cm^{-1}.

Figure 60 shows bands at 2940 and 2850 cm^{-1}, indicating methylene asymmetric and symmetric stretching, and at 1714, characteristic of the carbonyl stretching. The carbon-oxygen stretch shows up at about 1240. A very weak and broad O-H stretch is seen around 3250 cm^{-1}. Because of the very small amount of material absorbing the IR beam, the full scale range in absorbance units is only about 0.007 (0.003 to 0.009).

Figure 61 is the IRRAS spectrum of the same gold slide after reaction with thionyl chloride and the amino acid. No intermediate analysis of the acid chloride was attempted due to the reported lability toward atmospheric water.[279] The valine surface gives rise to bands for methyl and methylene stretching at 2990, 2955, 2921 and 2852 cm^{-1}, as well as a broad N-H stretch at 3300. The carbonyl peak is still evident at 1714, although diminished in amplitude, and the carbon-oxygen stretch is showing at 1285. A new, large band is now at 1137, indicating the anhydride (-CO-C-CO- stretch) formation..[280]

X-ray photoelectron spectroscopy was also conducted on the MUA and valine-surfaces, but with negative results. No trace of significant amounts of nitrogen, sulfur or even carbon could be obtained, although IRRAS results of these same surfaces before XPS work indicated at least some monolayer coverage compared to the freshly prepared blank slide. Our current explanation is that these polar carboxylic acid and amino acid surface may be present in a less even layer than typical hydrophobic C18-thiols and disulfides, and that the currently used vacuum and electron beam intensities are vaporizing the thin surface before data can be obtained.

A limited number of PM-IRRAS spectra were obtained recently, but they add little to the information obtained from the IRRAS spectrum of the same slide. The great usefulness of the PM technique lies in its ability to perform the in situ measurements of an enantiomeric solution in contact with the chiral surface. This work will be continuing in the months ahead.

CHAPTER VI
CONCLUSIONS

We have shown in depth the effects of lowered temperature on the enantiomeric separations of two common test solutes by two contrasting chiral stationary phases, a Pirkle-type (R)-dinitrobenzoylphenylglycine and a cellulose-based dimethylphenylcarbamate. carbamate. These CSPs differ in the variety of interaction possible between their chiral selector groups and functional groups, such as aromatic rings, carbonyls, hydroxyl and secondary amines attached to the solute.

The effects of temperature, flow rate and mobile phase changes on the three parts of the chromatographic resolution equation differ depending on the particular combination of stationary phase, solute and mobile phase. The basic retention mechanism is one of adsorption -desorption, as in liquid-solid "normal-phase" chromatography, but enantioselectivity occurs when diasteriomeric complexes, unequal in internal energy, form between the solute and CSP. The nature of these interactions is greatly affected by changes in separation conditions, as noted above. Unexpected changes in elution order and resolution can occur, and generalizations concerning optimization strategies are difficult to make unless some basic studies have been carried out on the CSP and a structurally similar solute to the analyte of interest.

A second goal of the this research has been to obtain quantitative data which, by inference, can support or refute some of the qualitative retention theories advanced for the two CSPs mentioned above. The DNBPG column was used as a benchmark, since it has a well-characterized retention mechanism. The newer and more complex cellulose CSP is capable of

several types of enantioselective interactions with a solute. We found quantitative thermodynamic evidence for multiple mechanisms when TFAE was separated on the cellulose column. Trans-stilbene oxide, capable of fewer interactions with the CSP, had much lower overall resolution values.

The final goal, to obtain *in situ* molecular level evidence via infrared spectroscopy concerning the nature and strength of interactions which make possible the diasteriomeric complex, was only partially achieved, but the research will continue. Our contribution to this promising methodology for retention mechanism investigation has been to devise a synthetic procedure for attaching a chiral valine molecule, using a carbon "brush", to a reflective gold surface. Although this surface seems more labile than more traditional hydrophobic monolayers, some IR evidence has been obtained. Several other procedures have also been developed for modifying gold surfaces.

In summary, this research has demonstrated the underlying complexity of chiral separation optimization, and has advanced some methodology with which practicing chromatographers might improve their enantiomeric separation work.

LITERATURE CITATIONS

1 Borman, Stu, *Chemistry and Engineering News*, **70** (1992) 5.

2 Stryer, Lubert, *Biochemistry*, W. H. Freeman and Co., San Francisco, (1975).

3 Mahler, Henry R and Cordes, Eugene H. *Biological Chemistry* Harper & Row, Inc., New York, N.Y. (1966).

4 Stinson, S. C. Chemical and Engineering News **70** (1992) 46.

5 ibid.

6 Taylor, D.R. and Maher, K. *J. Chrom Science* **30** (1992) 67.

7 Blaschke, G., Kraft, H. P., Fickentscher, K. and Kohler, F., *Arzeim.-Forsch.* **29** (1979) 1640.

8 Allenmark, Stig G., *Chromatographic Enantioseparation: Methods and Applications*, Ellis Horwood Lmtd, Chichester England (1988).

9 ibid.

10 Armstrong, D. W., *J. Liq. Chrom.*, **7** (1984) 353.

11 Dappen, R., Arm, H. and Meyer, V. *J. Chrom.* **373** (1986) 1.

12 Wainer, I. W., *Trends In Anal. Chem.* **6** (1987) 125.

13 Pirkle, W. H., and Welch, C. J., *J. Liq. Chrom.*, **14** (1991) 2027

14 ibid.

15 Taylor, ibid.

16 Armstrong, D.W., *Anal. Chem* **59** (1987) 84A.

17 Meyer, ibid.

18 Davankov, V.A.; Kurganov, A.A.; Bochkov, A.S., *Advances in Chromatography* **22** (1983) 71.

19 Lochmüller, C.H.; Ryal, R.R., *J. Chrom.* **150** (1978) 511.

20 Pirkle, W. H. and Pochapski, T.C. *Chem. Rev.* **89** (1989) 347

21 de Haseth, J.A., Lu, X-J. and Rogers, L.B., *Anal. Chem.*, **63** (1991) 2939.

22 Buffeteau, T., Desbat, B., Turlet, J., *Applied Spectroscopy* **45** (1991) 380.

23 Gatin, M. R., PhD. Dissertation, V.P.I. & S.U. (1992)

24 Mazzo, D. J. and Lindemann, C.J. Anal. Chem. 58 (1986) 636.

25 Akanya, J. N., and Taylor, D. R., *Chromatographia* **25** (1988) 639.

26 Weaner, L. E. and Hoerr, D. C., *J. Chromatog.* **437** (1988)109.

27 Rosset, R., Pecher, P., and M. Caude., *J. Chromatog.* **371** (1986) 159.

28 Macudiere, P.,Tambute, P., Caude, M., Rosset, R., Alembik, M. and Wainer, I. *J. Chrom.* **371** (1986) 177.

29 Meyer, V., Dappen, R., Arm, H., *J. Chrom.*, **373** (1986) 1.

30 Pirkle, W. H. and Pochapski, T.C., *Chem. Rev.* **89** (1989) 347.

31 Pirkle, W. H.; Hyun, M.H., *J. Chrom.* **316** (1984) 585 .

32 Pirkle, W. H., and Welch, C. J., J. Liq. Chrom., 14 (1991) 2027

33 Zief, M, Crane, L. J., Horvath, C., *J. Liq. Chrom.*, 7 (1984) 709

34 Zief, M. and Crane, L. J., ed., *Chromatographic Chiral Separations* , Marcel Dekker, Inc., New York (1988), Chp. 12.

35 Pirkle, W. H., and Welch, C. J., *J. Liq. Chrom.*, **14** (1991) 2027

36 Pirkle, W.H. and Burke, J.A., *J. of Chrom.* **557** (1991), 173.

37 Przybytek, J. T. *Solvent Guide* Burdick & Jackson Lab., Inc., Muskegon, MI (1982), pp. 64 and 102.

38 Synder, L. R., Kirkland, J. J., *Introduction to Modern Liquid Chromatography,* 2nd Ed., John Wiley & Sons, Inc., New York, NY (1979), Chp. 6.

39 Giddings, J. C., *Dynamics of Chromatography* Marcel Dekker, Inc., New York, NY (1965), pp. 27-35.

40 Lochmuller, C.H., Harris, J.M., and Souter, R.W., *J Chrom.*, **71** (1972), 405.

41 Lu, X-J. and Rogers, L.B.and de Haseth, J.A., *Anal. Chem.* **63** (1991) 2939

42 Kaliszan, R., *Quantitative Structure - Chromatographic Retention Relationships* Wiley-Interscience, NY, NY (1987)

43 Kaliszan, R., Noctor, T. A. G., Wainer, I. W., *Chromatographia* **33** (1992) 546.

44 Kaliszan, R., *Quantitative Structure - Chromatographic Retention Relationships* Wiley-Interscience, NY, NY (1987).

45 Kaliszan, R., Noctor, T. A. G., Wainer, I. W., *Chromatographia* **33** (1992) 546.

46 Norinder, U., Hermansson, J. *Chirality* **3** (1991) 422.

47 Berthod, A., Chang, S., and Armstrong, D.W., *Anal. Chem.* **64** (1992) 395.

48 Lu, X-J., Rogers, L.B.and de Haseth, J.A., *Anal. Chem.* **63** (1991) 2939.

49 Allenmark, Stig G., *Chromatographic Enantioseparation: Methods and Applications*, Ellis Horwood Lmtd, Chichester England (1988), p. 13.

50 Pasteur, L., *Ann. Chim. Phys.* **24** (1848) 442.

51 Richardson, G. M., ed., Scientific Memoirs. The Foundation of Stereochemistry, American Book Company, New York, NY (1901), p. 28.

52 Zief, M. and Crane,L. J., ed., *Chromatographic Chiral Separations*, Marcel Dekker, Inc., New York (1988), Chp. 1.

53 ibid.
54 Van't Hoff, J. H., *Arch. Neerl. Sci Exactes Natur.* **9** (1874) 445
55 Le Bel, J. A., *Bull. Soc. Chim. Paris* **22** (1874) 337.
56 Armstrong, D.W., *Anal. Chem* **59** (1987) 84A.
57 Henderson, G. M. and Rule, H. G. *J. Chem. Soc.* (1939) 1568.
58 Prelog, V., Weiland, P. *Helv. Chim. Acta* **27** (1944) 1127.
59 Kotake, M., Sakan, T., Nakamura, N. and Senon, S. *J. Am. Chem. Soc.* **73** (1951) 2973.
60 Dalgliesh, C. E. *J. Chem. Soc.* **47** (1952) 3940.
61 Pirkle, W. H. and Pochapski, T.C. *Chem. Rev.* **89** (1989) 347
62 Klemm, L. H. and Reed, D. *J. Chrom.* **3** (1960) 364.
63 Feibush, B. and Grinberg, N.,,"The History of Enantiomeric Resolution", Chp. 1 in Zief, M. and Crane, L. J., ed., *Chromatographic Chiral Separations* , Marcel Dekker, Inc., New York (1988).
64 Gil-Av, E., Feibush, B. and Charles-Sigler, R. *Tetrahedron Letters* (1966) 1099.
65 Taylor and Maher, op. cit., p. 68.
66 Allenmark, op. cit., Chp. 3.
67 Meinhand,C. and Bruneau *J. Chrom.* **450** (1988), 169.
68 Allenmark, op. cit., p. 28.
69 Turner, B. and Lloyd, D. *Lab Practice* **37** (1988) 80.
70 Purdie, Neil and Swallows, K. A. *Anal. Chem.* **61** (1989) 77A.
71 Mannschreck, A. *Chirality* **4** (1992) 163.
72 ibid.
73 Allenmark, op. cit., p. 35.
74 Lochmüller, op. cit., pp. 285, 287.
75 Taylor, op. cit., p. 68.
76 Armstrong, op. cit., p. 85A.
77 Lindner, W. "Indirect Separation of Enantiomers by Liquid Chromatography", chp. 4 of Zief, op. cit., p. 92.
78 Wainer, I. W.*Trends in Anal. Chem.* **6** (1987) 125.
79 Taylor, op. cit., p. 62.
80 Zief, op. cit., pp. 91-130.
81 Zief, op. cit., pp. 165-177.
82 Davankov, op. cit.

83 Briggs, D., Homer, R., Godfrey, R. in Stevenson, D and Wilson, I. *Chiral Separations* Plenum Press, New York, NY (1988), pp. 61-64.
84 Ishii, D., Takeuchi, T.; Asai, H. *J. Chrom* **235** (1982) 309.
85 Pettersson, C. and Josefsson, M. *Chromatographia* **21** (1986) 321.
86 Pettersson, C. *J. Chrom.* **316** (1984) 553.
87 Terabe, S., Miyashita, Y., Shibata, S. et al *J. Chrom.* **516** (1990) 23.
88 Guttman, A., Paulus, A., Grinberg, N., Cohen, A. and Karger, B. *J. Chrom.* **448** (1988) 41.
89 Kuhn, R., Erni, F., Bereuter, T., Haüsler, J. *Anal. Chem.* **64** (1992) 2815.
90 Birnbaum, S. and Nilsson, S. Anal. Chem. 64 (1992) 2872.
91 Wainer, I. W. *Trends in Anal. Chem.* **6** (1987) 125.
92 Dappen, op. cit.
93 Taylor, op. cit.
94 W. H. Pirkle, and M. H. Hyun. *J. Chrom.* **316** (1984) 585
95 Okamoto, Y., Aburatami, R., Miura, S., Hatada, K. *J. Liq. Chrom.* **10** (1987) 1613.
96 Pirkle, W. H. and Pochapsky, T.C. *Chem. Rev.* **89** (1989) 347.
97 Blaschke, G. *J. Liq. Chrom.* **9** (1986) 341.
98 Armstrong, D. W. and Stalcup, A. M. *Anal. Chem.* **62** (1990) 1610.
99 Davankov, op. cit.

100 Allenmark, Stig G. LC Magazine 3: 348-353 (1985)
101 Allenmark, Stig G. and Anderson, S. *Chirality* **4** (1992) 24.
102 Wainer, I. W. *A Practical Guide to the Selection and Use of HPLC* J. T. Baker, Phillipsburg, NJ (1988), p. 6.
103 Armstrong, D. W. and Stalcup, A. M. *Anal. Chem.* **62** (1990) 1610.
104 Caude, M., Lienne, M., Rosset, R. and Tambute, A. *J. Chrom.* **472** (1989) 265.
105 Gilpin, R.K., Ehtesham, S.E., Gregory, R.B. *Anal. Chem.* **63** (1991) 2825.
106 Neilson, K. L., McCombs, D. A., DeStefano, K. M. and Kirkland, J. J. *LC-GC* **10** (1992) 322.
107 Pirkle, W. H. and Pochapski, T.C., op. cit.
108 Akanya, J. N. and Taylor, D. R. *Chromatographia* **25** (1988) 639.
109 Hara, S. and Dobashi, A *J. Chrom.* **186** (1979) 543.
110 Pirkle and Pochapski, op. cit.
111 Pirkle, W. H.; Hyun, M.H. *J. Chrom.* **316** (1984) 585.

112 Wainer, I. W. *Trends in Anal. Chem.* **6** (1987) 125.
113 Zief, M, Crane, L. J. and Horvath, C. *J. Liq. Chrom.* 7 (1984) 709.
114 Ichida, A., Chibata, T., Okamoto, Yuki, Y., Namikashi, H., Toga, Y *Chromatographia* **19** (1984) 280.
115 Okamoto, Y., Aburatami, R., Miura, S., Hatada, K. *J. Liq. Chrom.* **10** (1987) 1613.
116 Voet, D. and Voet, J. G. *Biochemistry* John Wiley & Sons, New York, NY (1990), pp. 254-257.
117 Taylor and Maher, op. cit., p. 27.
118 Wainer, op. cit., p. 129.
119 Daicel Chemical Industries *Crownpak Chiralpak Chiralcel* Daicel USA, Los Angeles, CA (1991).
120 (J. T. Baker 1992 catalog, p.)
121 M. Henry, J. T. Baker, Inc., Phillipsburg, NJ, personal communication.
122 House, H. O. *Modern Synthetic Reactions*, W. A. Benjamin, Inc., Menlo Park, CA (1972).
123 Blaschke, G., Chp 7 in *Chromatographic Chiral Separations,* Zief, M. and Crane,L. J., ed., Marcel Dekker, Inc., New York (1988), p. 179.
124 Taylor, op. cit., p. 75.
125 Armstrong and Stalcup, op. cit.
126 Armstrong, D. W., Berthold, A., Li, W. *Anal. Chem.*. **64** (1992) 873.
127 Ward, T. J. and Armstrong, D. W., Chp. 5 in Zief and Crane, op. cit.
128 Armstrong and Stalcup, op. cit.
129 Ward, T. J. and Armstrong, D. W. *J. Liq. Chrom.* **9** (1986), 407.
130 ibid.
131 Wainer, I. W. A Practical Guide to the Selection and Use of HPLC Chiral Stationary Phases J. T. Baker, Phillipsburg, NJ (1988), p. 18.
132 Blaschke, G. *J. Liq. Chromatog.* **9** (1986) 341.
133 Davankov, V.A., Kurganov, A.A., Bochkov, A.S. *Adv. in Chrom.* **22** (1983) 71
134 Feinbush, B., Cohen, M. J., Karger, B. L. *J. Chrom.* **282** (1983) 3.
135 Karger, B.L., Tapurhi, Y., Miller, N. *J. Chrom.* **205** (1981), 325.
136 Esquivel, B, Nicholson, L., Peerey, L.; Fazio, M. *J. of H.R.C.* **14** (1991) 816.
137 Allenmark, Stig G. and Anderson, S. *Chirality* **4** (1992) 24
138 Allenmark, S. G. and Bomgren, B. *J. Chrom.* **316** (1984) 617.
139 Wainer, I. W *Trends in Anal. Chem.* **6** (1987) 125.

140 Kirkland, K. M., Neilson, K. L.; McCombs, D. A.; DeStefano, J. J. *LC-GC* **10** (1992) 322.

141 Aubry, A.-F., Gimenez, F., Farinotti, R., Wainer, I. W. *Chirality* **4** (1992) 30.

142 Snyder, L. R. and Kirkland, J. J. *Introduction to Modern Liquid Chromatography* Second Edition, John Wilely & Sons, Inc., New York, NY (1979).

143 ibid, p. 36.

144 Melander, W., Campbell, D. E., Horvath, C. *J. Chrom.* **158** (1978) 215.

145 Melander, W. R., Chen, B. K. and Horvath, C. *J. Chrom.* **185** (1979) 99.

146 Gant, J. R., Dolan, J. W. and Snyder, L. R. *J. Chrom.* **185** (1979) 153

147 Vigh, G. and Varga-Puchony, Z. *J. Chrom.* **196** (1980) 1.

148 Hancock, W.S., Knighton, D.R., Napier, J.R. and Harding, D.R. *J. Chrom.* **367** (1986) 1.

149 Knox, J. H. and Vasvari, G. *J. Chrom.* **83** (1973) 181.

150 Melander, 1978, op. cit., p. 218.

151 Cole, L.A. and Dorsey, J.G. *Anal Chem.* **64** (1992) 1317.

152 ibid., p. 1324.

153 Feitsma, K. G., Bosman, J., Drenth, B.F.H., De Zeeuw, R.A. *J. Chrom.* **333** (1985) 59.

154 Mazzo, D. J., Lindemann, C.J. and Brenner, G. S. *Anal. Chem.* **58** (1986) 636

155 Sander, L. C. and Wise, S.A. *Anal. Chem.* **61** (1989) 1749

156 Galli, B., Gasparrini, F., Misiti, D., Pierini, M., Villiani, C., and Bronzetti, M. *Chirality* **4** (1992) 384.

157 Pescher, P., Caude, M., Rosset, R. and Tambute, A. *J. Chrom.* **371** (1986) 159

158 Weaner, L. E. and Hoerr, D.C. *J. Chrom.* **437** (1988) 109 .

159 Witte, D. T.; Franke, J.-P., Bruggeman, F. J. *Chirality* **4** (1992) 389

160 Akanya, J. N. and Taylor, D. R. Chromatographia **25** (1988) 639

161 Gilpin, R. K., Ehtesham, S. E., Gregory, R. B. *Anal. Chem.* **63** (1991) 2825.

162 Pirkle, W. H. and Burke, J. A. *J. Chrom.* **557** (1991) 173.

163 Berthold, A., Li, W. and Armstrong, D. W. *Anal. Chem.* **64** (1992) 873.

164 Pescher, op. cit. p. 160.

165 Snyder and Kirkland, op. cit., chp. 9.

166 Synder, L. R. *J. Chrom.* **255** (1983) 3.

167 Zief, op. cit., chp. 12.

168 ibid.

169 Zief, M, Crane, L. J. and Horvath, C. J. *Liq. Chrom.* **7** (1984) 709.

170 Synder and Kirkland, op. cit., p. 263.

171 Taft, R. W., et al *J. Am Chem. Soc.* **91** (1969) 4801.

172 Synder and Kirkland, op. cit., p. 260.

173 Pescher, op. cit.

174 Pirkle, W. H. and Welch, C. J. *J. Liq. Chrom.* **14** (1991) 2027

175 Esquivel, B, Nicholson, L., Peerey, L.; Fazio, M. *J. of H.R.C.* **14** (1991) 816.

176 Kaliszan, R. Quantitative *Structure - Chromatographic Retention Relationships* Wiley-Interscience, NY, NY (1987).

177 Kaliszan, R., Osmialowski, K. and Hartwick, R. A. et al *J. Chrom.* **352** (1986) 141.

178 Jandera, P. *J. Chrom.* **314** (1984) 13.

179 Jinno, K., Kawasaki, K *Chromatographia* **18** (1984) 90.

180 Jinno, K., Kawasaki, K. *J. Chrom.* **316** (1984) 1.

181 Kaliszan and Osmialowski, op. cit.

182 Pirkle, W. H., House, D.W., and Finn. J. M. *J. Chrom.* **192** (1980) 143 .

183 Pirkle, W. H., Hyun, M.H. and Bank, B. *J. Chrom.* **316** (1984) 585.

184 Armstrong, D. W., Stalcup, A. M., et al *Anal. Chem.* **62** (1990) 1610.

185 Berthod, A., Chang, S., and Armstrong, D.W. *Anal. Chem.* **64** (1992) 395.

186 Pirkle, W. H. and Pochapsky, T.C. *Chem. Rev.* **89** (1989) 347

187 Galli, op. cit.

188 de Vries, N. K., Coussens, B., Meier, R. J. *J. H.R.C.* **15** (1992) 499.

189 Kaliszan, R., Noctor, T. A. G., Wainer, I. W. *Chromatographia* **33** (1992) 546.

190 Norinder, U. and Hermansson, *J. Chirality* **3** (1991) 422.

191 Lochmuller, C. H., Harris, J. M., and Souter, R. W. *J. Chrom.* **71** (1972) 405.

192 Li, S. and Purdy, W. C. Anal. Chem 64 (1992) 1405.

193 Lu, X-J., Rogers, L.B.and de Haseth, J.A. *Anal. Chem.* **63** (1991) 2939.

194 Rogers, L. B. and Still, M. G. *Talanta* **36** (1989) 35

195 Lipkowitz, K., Landwer, J. M., Darden, T. *Anal. Chem.* **58** (1986) 1611.

196 Lipkowitz, K. B., Demeter, D. A., Parish, C. A. *Anal. Chem.* **59** (1987) 1731 .

197 Lipkowitz, K. B., Demeter, D.A., Zegarra, R., Larter, R. and Darden, T. *J. Am. Chem. Soc.* **110** (1988) 3446.

198 Lipkowitz, K. B., Baker, B. *Anal. Chem.* **62** (1990) 770.

199 Allenmark, 1988, op. cit., p. 25.

200 Pirkle and Pochapsky, op. cit.

201 Allenmark, op. cit., 19.

202 ibid.

203 Taylor and Maher, op. cit.

204 Pirkle and Pochapsky, op. cit.

205 Melander, W., Campbell, D. E., Horvath, C. *J. Chrom.* **158** (1978) 215.

206 Cole, L.A. and Dorsey, J.G. *Anal Chem.* **64** (1992) 1317.

207 Atkins, P. W. Physical Chemistry W. H. Freeman & Co., San Francisco, CA (1978) p. 78.

208 Kaliszan, R. *Quantitative Structure - Chromatographic Retention Relationships* Wiley-Interscience, NY, NY (1987) p. 3.

209 ibid.

210 Atkins, op. cit., p. 746.

211 ibid., p. 761.

212 ibid., p. 751.

213 Huheey, J. E. Inorganic Chemistry Principles of Structure and Reactivity, Second Edition Harper & Row, Publishers, New York (1978), p. 242.

214 ibid, p. 240.

215 ibid, p. 241.

216 Pirkle and Welch 1991, op. cit., p. 2028-2030.

217 Pirkle and Burke (1991), op. cit.

218 Galli, op. cit.

219 Synder and Kirkland, op. cit., p. 271.

220 ibid., p. 237.

221 Shaw, D. J. *Introduction to Colloid and Surface Chemistry* Butterworths and Co. (Publishers), London (1986), p. 215.

222 Synder and Kirkland, op. cit., p. 171.

223 Zief, M, Crane, L. J. and Horvath, C. *J. Liq. Chrom* **7** (1984) 709

224 Soczewinski, E., Wachtmeister, C. A. *J. Chrom.* **7** (1962) 311.

225 Okamoto, Y., Aburatami, R., Miura, S., Hatada, K. *J. Liq. Chrom.* **10** (1987) 1613.

226 Okamoto, M. and Nukuzawa, H. *J. Chrom.* **588** (1991) 177.

227 Witte, D. T.; Franke, J.-P., Bruggeman, F. J. *Chirality* **4** (1992) 389.

228 Lipkowitz (1988) op.cit.

229 Burkert, U. and Allinger, N. L. *Molecular Mechanics* A.C.S., Washington DC (1982).

230 Netzer, L., Iscovici, R., Sagiv *J. Thin Solid Films* **99** (1983) 235.

231 Bigelow, W. C., Pickett, D. L., Zisman, W. A. *J. Colloid. Sci.* **1** (1946) 513.

232 Gatin, op. cit., p. 3.

233 Atkins, op. cit., p. 939.

234 ibid.

235 Duevel, R.V. and Corn, R. M. *Anal. Chem.* **64** (1992) 337.

236 Atkins op. cit., p. 943.

237 Bain, C. D., Evall, J., Whitesides, G. M. *J. Am. Chem. Soc.* **111** (1989) 7155.

238 Shaw, op. cit., pp. 145-147.

239 Rogers, L. B., Hsu, T. B.; Shah, P. A *J. Chrom.* **391** (1987) 145.

240 Klausner, Y. S.; Bodansky, M. *Synthesis* Sept. (1972) 453.

241 Fieser, M and Fieser, L. *Reagents for Organic Synthesis* Wiley-Interscience, New York (1974), Vol. **2**, 191; Vol. **3**, 137; Vol. **4**, 222.

242 Belleau, B., Martel, R., Lacasse, G., Ménard, M., Weinberg, N. L., Perron, Y. G. *J. Am. Chem. Soc* **90** (1968) 823.

243 Vollhardt, K. P. C. *Organic Chemistry* W.H. Freeman and Company, New York (1987), p. 748.

244 Fieser and Fieser, op. cit, Vol. **1** 158.

245 Gatin op. cit., pp. 11-13.

246 Griffiths, P. R. and de Haseth, J. A. *Fourier Transform Infrared Spectrometry* J. Wiley & Sons, New York (1986), chp. 5.

247 Porter, M. D. *Anal. Chem.* **60** (1988) 1143A.

248 Gatin op. cit., p. 17.

249 Buffeteau, T., Desbat, B., Turlet, J. *Applied Spectroscopy* **45** (1991) 380.

250 Barner, B., Green, M., Saez, E., and Corn, R. *Anal. Chem.* **63** (1991) 55.

251 Pirkle, W. H. and Welch, C. J. *J. Liq. Chrom.* **14** (1991) 1

252 Snyder, L. R. and Kirkland, J. J. op. cit., p. 240.

253 J. T. Baker 1992/1993 Catalog, J. T. Baker, Phillipsburg, NJ, p. 281.

254 Bidlingmeyer, B. A. and Warren, F. V. Jr. *Anal. Chem.* **56** (1984) 1583A.

255 Meyer, V. R. *J. Chrom.* **334** (1985) 197.

256 M. Henry, J. T. Baker Inc., Phillipsburg, N.J., personal communication.

257 Borman, S. *Chemistry & Engineering News* 2/19/90, 20.

258 McDaniel, V. K. *SPARC Users Manual, Prototype Version 1.0* (Performs Automated Reasoning In Chemistry) Environmental Research Lab, US EPA, Athens, GA (1990).

259 Karickhoff, S. W. *Predicting Chemical Reactivity by Computer, Parts 1, 2 and 3*, US EPA, Athens, GA 1989.

260 Stauffer, S. C., Doctoral Dissertation, VPI & SU, 1993.

261 Karickhoff, op. cit.

262 Kaliszan, R., Osmialowski, K. and Hartwick, R. A. et al *J. Chrom.* **352** (1986) 141.

263 Jinno, K., Kawasaki, K. *Chromatographia* **18** (1984) 103.

264 Finklea, H. O., Robinson, L.R., Blackburn, A., Richter, B., Allara, D. and Bright, T. *Langmuir* **2** (1986) 239.

265 Troughton, E. B., Bain, C. D., Whitesides, G. M.,Nuzzo, R. G., Allara, D. L., and Porter, M. D. *Langmuir* **4** (1988) 365.

266 Troughton, op. cit., p. 379.

267 Wolfe, R. W., Noll, K. M., Dennelly, M. I. *The J. of Bio. Chem.* **262** (1987) 513.

268 *Handbook of Chromatography, Vol. II,* CRC Press, Boca Raton, FL (1979), p. 151.

269 Griffiths, P. R. and de Haseth, J. A. *Fourier Transform Infrared Spectroscopy* John Wilely & Sons, New York, NY (1986), p. 550.

270 ibid., p. 552.

271 Gatin, op. cit.

272 (Pirkle? Attract.-Rep. Interaction weaker, more affected by temp. than h-bond.)

273 McGuffin, V.L.; Evans, C.E. *J. Microcol. Sep.* **3** (1991) 513.

274 McGuffin, V. L., Evans, C. E. and Chen, S.-H *J. Microcol. Sep.* **5** (1993) 3.

275 Miller, J. C. and Miller, J. N. Statistics for Analytical Chemistry Ellis Horwood Limited, Chichester, UK (1986), p. 43, Equation 2.9.

276 Zief, Crane and Horvath (1984) op. cit.

277 Daicel Chemical Industries. *1989 Applications Guide for Chiral Column Selection.* Daicel, Los Angeles, CA (1989).

278 Esquivel, B, Nicholson, L., Peerey, L.; Fazio, M.*J. of H.R.C.* **14** (1991) 816.

279 Duevel and Corn, op. cit.

280 Silverstein, R., Bassler, G., Morrill, T., *Spectrometric Identification of Organic Compounds* Third Ed., J. Wiley and Sons, New York (1974), p. 105.

VITA

Robert Cragg Klute was born in a Richmond, Indiana blizzard on November 18, 1950 and has not been fond of snow since. After taking two high school chemistry courses and serving as a laboratory assistant to Mr. Ivan Whitesel, he graduated from Richmond Senior High School in June of 1970. He initially entered Indiana University as a chemistry major, but was temporarily swept away by the times and graduated with a B.A in sociology, with Japanese language and culture as minor studies, in May of 1975. He spent part of 1973-1974 studying Japanese in Tokyo, Japan. Chemistry called and in 1978 he re-entered Indiana University to finish a B.A. in chemistry, after working as a journalist in Beaumont, Texas. The second Bachelors degree was granted in August of 1982, alternating academics with analytical chemistry work experience at St. Louis Testing Laboratories, St. Louis, Missouri. Until August of 1989, he was employed by the Monsanto Company of St. Louis, Missouri as an analytical chemist in the Bovine Somatotropin project, gaining valuable laboratory skills and a working knowledge of protein chemistry. From 1989 until March of 1993 he studied under Dr. Harold McNair at VPI & SU, helping teach many American Chemical Society gas and liquid chromatography short courses and acting as a teaching assistant for the quantitative chemical analysis course. In addition to chiral HPLC research, he participated in a project with Dr. Harry Dorn involving preparative HPLC of high molecular weight Buckminsterfullerene compounds. Upon graduation, Robert Klute accepted a position in the R&D Analytical Services group, under the direction of Dr. Norman Jamieson, at Mallinckrodt Specialty Chemicals Company in St. Louis, Missouri.

Robert C. Klute
3/29/93